Doctoral theses at NTNU, 2020:99

Yihan Cao

Statistical methods for estimating fluctuating selection

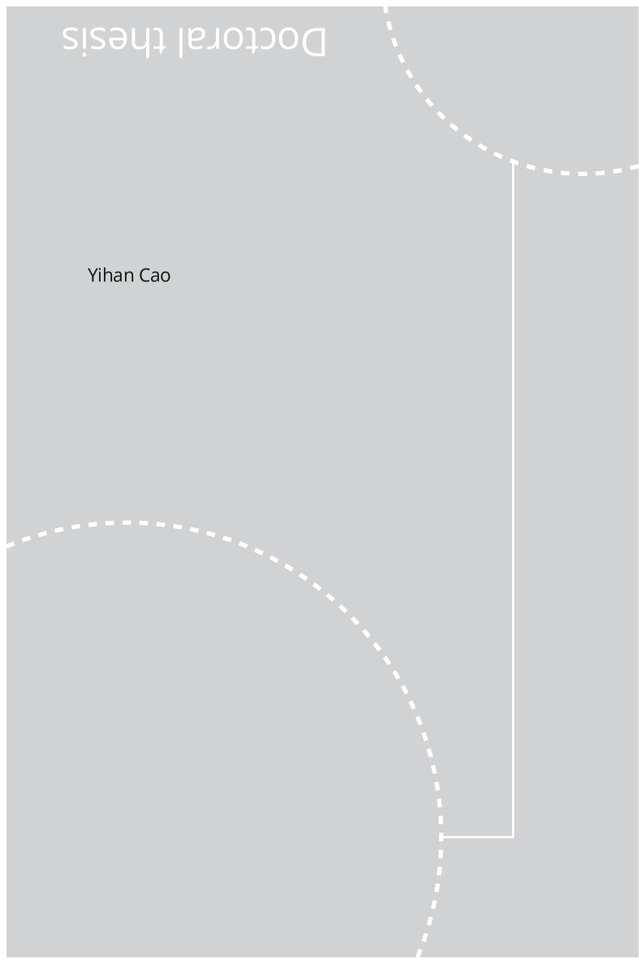

ISBN 978-82-326-4550-3 (printed ver.)
ISBN 978-82-326-4551-0 (electronic ver.)
ISSN 1503-8181

NTNU
Norwegian University of
Science and Technology

NTNU
Norwegian University of Science and Technology
Thesis for the Degree of
Philosophiae Doctor
Faculty of Information Technology and Electrical
Engineering
Department of Mathematical Sciences

Doctoral theses at NTNU, 2020:99

NTNU
Norwegian University of
Science and Technology

Yihan Cao

Statistical methods for estimating fluctuating selection

Thesis for the Degree of Philosophiae Doctor

Trondheim, April 2020

Norwegian University of Science and Technology
Faculty of Information Technology and Electrical Engineering
Department of Mathematical Sciences

NTNU
Norwegian University of
Science and Technology

NTNU
Norwegian University of Science and Technology

Thesis for the Degree of Philosophiae Doctor

Faculty of Information Technology and Electrical Engineering
Department of Mathematical Sciences

ISBN 978-82-326-4550-3 (printed ver.)
ISBN 978-82-326-4551-0 (electronic ver.)
ISSN 1503-8181

Doctoral theses at NTNU, 2020:99

Printed by NTNU Grafisk senter

Preface

This thesis is submitted in partial fulfillment of the requirements for the degree Philosophiae Doctor (Ph.D) at the Department of Mathematical Sciences at the Norwegian University of Science and Technology (NTNU). The whole work was financially supported by the Research Council of Norway through its Centres of Excellence funding scheme (project number 223257 to Centre for Biodiversity Dynamics (CBD)).

I would like to express my gratitude to my main supervisor, Professor Jarle Tufto at NTNU, for allowing me to do Ph.D in Norway and for his tireless guidance on my papers and thesis. I also would like to thank my co-supervisor, Professor Marcel E. Visser at NIOO-KNAW, for his guidance, encouragement, and consideration along my way to Ph.D. I thank my office mates and colleagues around me at CBD for sharing me with their research and knowledge, which helps me a lot with the study on evolutionary biology. I am also grateful to the colleagues in the statistics group at the Department of Mathematical Sciences for the talks, discussions, seminars over these three years.

Finally, I would thank my friends in Trondheim for their company and support through times good and bad in daily life during these years. I also thank my family for their understanding of my choices, their spiritual support, and encouragement in everything I do in life.

Contents

List of papers

I **Y. Cao**, M. E. Visser, and J. Tufto, 2019. A time-series model for estimating temporal variation in phenotypic selection on laying dates in a dutch great tit population. *Methods in Ecology and Evolution 10*(9), 1401–1411.

II J. Tufto, **Y. Cao**, M. E. Visser. Evolution of double brooding. In revision.

III **Y. Cao**, M. E. Visser, and J. Tufto. Multi-episodic fluctuating selection via fertility and viability in a great tit (*Parus major*) population. Manuscript.

IV **Y. Cao**, M. E. Visser, and J. Tufto. Bayesian inference with tmbstan for a state-space model with VAR(1) state equation. Manuscript.

Declaration of contributions

Paper I: M.E.V. provided the data; J.T. conceived the idea and initiated the statistical model; Y.C. analyzed the data and conducted the analyses; Y.C. wrote the initial draft with input from J.T.; all authors contributed to revisions on later manuscript versions and gave final approval for publication.

Paper II: J.T. conceived the idea and initiated the basic genetic model; J.T. derived analytical expression of the genetic model under different scenarios with input from Y.C.; J.T. conducted the numerical analyses with the theoretical models; M.E.V. provided the data for empirical study; J.T. and Y.C. conducted the empirical study with the data; J.T. wrote the initial draft with input from Y.C.; the final version was reviewed and commented by all co-authors.

Paper III: M.E.V. provided the data; J.T. conceived the idea; Y.C. initiated the statistical model, analyzed the data and conducted the analyses; Y.C. wrote the initial draft with input from J.T.; all authors contributed to revisions on later manuscript versions and gave final approval for publication.

Paper IV: J.T. conceived the idea; Y.C. set up the simulation studies with input from J.T.; Y.C. conducted simulations and analyzed simulation results; Y.C. conducted the empirical study with the data provided by M.E.V.; Y.C. wrote the manuscript and it was reviewed and commented by all co-authors.

All authors gave final consent for the use of listed work above in this thesis.

Introduction

Natural selection is a key mechanism of evolution and the central process in nature. It occurs when there is a difference between phenotypical traits in expected relative fitness (Gardner and Grafen, 2009; Hansen, 2017). It also plays a role in shaping life cycles in ways that optimize reproductive fitness (Charnov, 1993; Stearns, 2000) and the mechanism of which has been studied in the framework of life history theory. In population biology, one of the fundamental questions is which selection, under which circumstances and to what extent, can have an appreciable impact on population dynamics (Charlesworth, 1971; Saccheri and Hanski, 2006). Understanding the genetic basis of the traits that selection operates on and the signatures of past and present selection in patterns of variation in the genome remain as a priority in the research agenda for evolutionary biologists (Stinchcombe et al., 2017). Even though the interplay between selection and life history evolution, selection and population dynamics has been approached from various perspectives in each study area over the past years, to obtain a better understanding of the role of natural selection in driving evolutionary changes, accurate estimates of the strength of selection acting in the wild is an essential prerequisite (Linnen and Hoekstra, 2009).

Most of the previous work attempting to measure natural selection within populations drew on the seminal studies of Price (1970); Lande (1979); Lande and Arnold (1983), in which the selection is characterized by the relationship between traits and relative fitness. Building on their foundational work, Schluter (1988) provides a non-parametric estimate of the fitness function and uses it to suggest an appropriate parametric model. Thomson and Hadfield (2017) shows that using offspring fitness components as part of parental fitness ("mixed fitness" in their terms) is common in studies of birds and mammals, but will only lead to correct estimates of selection and evolutionary change under very restrictive conditions. Among many others, the enormous literature contains conceptual, methodological and statistical recommendations to estimating the phenotypic covariances between traits and some aspect of relative fitness (Stinchcombe et al., 2017). In empirical studies, the mode and intensity of natural selection are estimated by regressing relative fitness onto phenotypic values. The selection gradient (β) analysis has now been applied to a wide range of plant and animal taxa (reviewed by Kingsolver et al., 2001; Siepielski et al., 2009).

Fluctuating and auto-correlated selection

The publication of synthetic reviews of form and strength of selection (Kingsolver et al., 2001; Siepielski et al., 2009) confirms that phenotypic selection commonly fluctuates in strength and frequently changes in direction among years. The variance in phenotypic selection was usually estimated by computing the variance of the strength of selection using selection gradients estimated separately at each time point which reflects both random sampling error and real variation in selection (Morrissey and Hadfield, 2012). Since temporal variation in natural selection is a fundamental determinant of evolutionary outcomes and an appealing hypothesis to explain evolutionary stasis (Price and Liou, 1989; Merilä et al., 2001; Siepielski et al., 2010), more accurate models with a detailed look at the extent of variation in selection, accounting for sampling error, are desirable. Among the previous empirical studies accounting for the sampling error of variation, Calsbeek (2011) presents a non-parametric analysis in exploring the variation of fitness surfaces over time or space. In contrast, using a log-quadratic generalized linear mixed model

with a random effect on the regression slope implemented using Integrated Nested Laplace Approximations (INLA, Rue et al., 2009), Chevin et al. (2015) estimated yearly fluctuations and autocorrelation in optima of a Gaussian fitness function. Using instead the more flexible framework of Template Model Builder (TMB, Kristensen et al., 2016), Gamelon et al. (2018) fitted a model of fluctuating selection via several non-overlapping selection episodes with non-linear random effects added directly on the location of the fitness optima and on the peak of the fitness function. The latter two identify the pattern of temporal dynamics in the selection not only by its variance but also by its temporal auto-correlation. Previous theory has shown that the auto-correlation of selection strongly affects whether (and how much) genetic responses to selection optimize long-term fitness and population growth in a fluctuating environment (Charlesworth, 1993; Lande and Shannon, 1996; Bürger and Gimelfarb, 2002; Chevin, 2013; Tufto, 2015). The empirical estimate of auto-correlation in the location of the fitness optima turned out to be significant in Chevin et al. (2015); Gamelon et al. (2018); Cao et al. (2019). The generality of this finding, however, needs to be confirmed across a wider range of species, populations, and traits, using the same, statistically robust approach. As of yet, estimating auto-correlation in selection may require a large sample size with many time points (Chevin and Haller, 2014).

A straightforward extension of previous models with temporally varying selection strength for stabilizing selection is to allow all the properties (height, location of maximum and width) of a Gaussian fitness function at population level to be temporally fluctuating and even cross-correlated. Such a statistical model including all these possibilities into one framework can be as complex as that powerful enough model-fitting techniques are required for statistical inference. Cao et al. (2019) is among the few to have done this with an R package named Template Model Builder (TMB, Kristensen et al., 2016), which is developed for fast-fitting complex, linear or nonlinear statistical models. The temporal fluctuation in the strength and even the direction of selection can be captured by using appropriate statistical approaches. However, changes in the form of selection, which are likely common, are harder to quantify (Siepielski et al., 2009).

Selection on correlated traits

The target trait that selection acts on can be correlated with fitness either because they impact fitness directly (direct selection) or because they are correlated with other traits that affect fitness (indirect selection) (Linnen and Hoekstra, 2009). For the great tits, the brood size is correlated with the egg-laying date and the early breeders tend to lay bigger clutches (Perrins and McCleery, 1989; Barba et al., 1995). In a black-throated blue warbler population, the egg-laying date of the first brood is positively correlated with the propensity a second brood to be laid from a given female (Townsend et al., 2013). We tend to focus on traits that we have a priori reasons to believe are targets of selection. In fact, strong indirect selection can overcome direct selection in an opposing direction (Linnen and Hoekstra, 2009). How can we determine the actual target of selection? Lande and Arnold (1983) shows elegantly how total selection can be partitioned into direct selection on a trait and indirect selection through correlated traits, in which selection gradients (β) are calculated using multiple regression to control for indirect selection, thereby estimating direct selection on a trait. The famous Darwin's finches also illustrate the importance of measuring multiple traits and estimating both direct and total selection.

The correlated characters that selection is acting simultaneously on might likely be genetically

correlated, so selection on one trait can result in a change in the other. The total response to selection will be a combination of direct selection on a particular trait, plus indirect selection resulting from a correlated response to selection on some other traits, and therefore leads to an accurate picture of adaptation and evolutionary constraint in natural populations. In reality, the data on genetic structure of correlated traits are not always available, it is thus necessary to conduct simulations with various genetic and phenotypic covariance structures for correlated traits, explore the evolutionary trajectories under different scenarios and compare them with the reality, to gain a better understanding of the mechanism behind the correlational selection on the traits. Alternatively, Reed et al. (2016) uses an animal model to obtain the genetic covariance matrix of clutch size and laying date and then calculates predicted response to selection based on the Robertson–Price Identity and the multivariate breeder's equation (MVBE). It finally concludes that the similar prediction indicates that unmeasured covarying traits were not missing from the analysis.

Selection via multiple fitness components

Most studies estimating natural selection focus on a specific component. For short-lived hole-nested species, pre-breeding mortality is one of the major sources of individual variation in lifetime reproductive success (Clutton-Brock, 1988; Newton et al., 1989), which implies that the fate of individual fledglings is completely altered after recruiting to the population. This phenomenon can be recognized as a straightforward reason of different selection patterns estimated with the same populations since either number of fledglings or recruits is taken as the fitness component (for example Verboven and Visser, 1998; Reed et al., 2013a; Chevin et al., 2015), but rarely both (except for Gamelon et al., 2018). How the temporal dynamics of phenotypic selection may vary among fitness components (e.g. fecundity and survival) is poorly understood thus (Siepielski et al., 2010). Furthermore, many previous studies (for example Siikamäki, 1998; Verboven and Visser, 1998) have demonstrated that the date of fledgling affects post-fledgling survival, the usual pattern being early fledglings experienced higher survival. An advancement of mean annual egg-laying date is thus expected to be observed to maximize offspring fitness, however, the reality contradicting the expectation is that an enlarging mistiming between the egg-laying date and food peak date over the course of study is observed (Visser et al., 1998; Chevin et al., 2015; Cao et al., 2019). One potential explanation is that the adaptive evolutionary change is determined by relative form and strength of selection acting among different fitness components (Schluter et al., 1991; Hoekstra et al., 2001). Besides, integrating multiple fitness components into one modeling framework is a start point to explore the evolution of life history traits (e.g. size at birth, number, size, and sex of offspring, lifespan) and the dynamic interaction between them, which is research objectives in life history theory.

Even though the importance of measuring selection through separate episodes of selection over the reproductive cycle was pointed out by Arnold and Wade (1984), the empirical measurements on selection have rarely done this. The exceptions include Engen et al. (2011), in which selection is estimated separately with fitness components (fecundity and survival) in different age classes. Gamelon et al. (2018) proposes a multi-episodic approach where different reproductive stages (clutch size, survival from egg to fledgling, from fledgling to recruit and breeding mothers) are included in one statistical model. Potential ecological drivers of selection on both laying dates

and clutch sizes were accounted and the method was applied to a dipper population.

Partial and complete brood failure

In altricial birds, the nestlings are brooded for 1 to 2 weeks after hatching and typically obtain extensive parental care from both parents before independence (Liker et al., 2015). Partial and complete brood failure is common in this period and this is a key determinant of variation in reproductive success in such species (Santema and Kempenaers, 2018). The underlying causes of nestling mortality are usually unknown unless the nest predation is identified (Martin and Briskie, 2009). In some bird species, complete brood failure is found associated with nest predation, (McCleery et al., 1996) which might be related to nest-site security (Wesołowski, 2002) and to the sudden and permanent disappearance of one of the parents (Santema and Kempenaers, 2018). It is often hypothesized that offspring mortality results from a particular factor such as breeding timing that determines brood success through its effect again on parental care. Even though it is plausible that a particular factor influences both partial and complete brood mortality, the effect sizes of the factor on them likely differ. Moreover, if partial and complete brood mortality has different proximate causes, it might give misleading results on the effects of biological factors on offspring mortality when they are lumped together. Therefore, it is biologically and statistically necessary to separate complete brood failure from partial brood failure when exploring the proximate mechanism of offspring mortality.

Ecological selective agents

Changes in ecological conditions driven by climatic fluctuations appear to be common and important. Natural selection on wild populations is driven by such changes in biotic and abiotic conditions (Bell, 2010). Despite of increasing interests in the environmental sensitivity of phenotypic selection, few studies have identified causal mechanisms underlying temporal variation in the form, direction, and strength of selection (Siepielski et al., 2009). Several studies have linked temporal variation in natural selection through survival or fecundity to variation in ecological factors such as density, temperature, precipitation, predation, competition, and many other factors. These factors are heterogeneous at both temporal and spatial scales. For example, the survival of juveniles is identified to be strongly density-dependent (Reed et al., 2013a,b) and density is shown to be a varying selective agent in a dutch great tit population (Sæther et al., 2016). The temporal variation in optimal phenotypic maximizing yearly fitness subjects to fluctuating spring temperature (Chevin et al., 2015; Gamelon et al., 2018). Predation is a selective pressure leading to fledglings hatched early in the season suffering lower probability of complete brood failure in great tits (Sæther and Bakke, 2000). In turn, the changing climate conditions lead phenotypic distribution to be constantly shaped and reshaped by various agents of natural selection (Endler, 1986). Even though these studies have accumulated our understanding of environmental sensitivity in natural selection, incorporating abiotic and biotic factors as potential selective agents into the big picture of estimating varying selective selection on various traits throughout the life cycle has remained challenging.

Double brooding evolution

Multiple breeding (more than one reproductive attempt in a breeding season) is a common reproductive strategy in short-lived species (Verhulst et al. 1997 and references therein). The frequency of double brooding is an important factor determining the productivity of a population, as Nagy and Holmes (2004) shows that 19% of the annual variance in fecundity is explained by double brooding in a black-throated blue warbler population in America. Since annual fecundity plays a major role in determining population growth (Sæther and Bakke, 2000), understanding the mechanism of multi-brooding in short-lived species has implications on the future viability of a population. Several studies of birds have investigated the intra-seasonal costs (Mulvihill et al., 2009) or determinants (Jacobs et al., 2013) of multiple-breeding, either experimentally (Parejo and Danchin, 2006) or using longitudinal studies (Townsend et al., 2013) or combination of them (Evans Ogden and Stutchbury, 1996; Verboven and Verhulst, 1996). These studies find that delaying hatching date, as well as increasing clutch size and/or brood size, commonly lead to a lower probability of initiating a second clutch (Lindén, 1988; Geupel and DeSante, 1990; Evans Ogden and Stutchbury, 1996; Verboven and Verhulst, 1996; Verboven et al., 2001; Parejo and Danchin, 2006; Townsend et al., 2013). The study species include wren tit, hooded warbler, black-throated blue warbler, great tit, and many others. Husby et al. (2009) shows that in four long-term study populations of great tits in the Netherlands, the proportion of females that double brood has declined in all populations. They stated that the decline has two-fold reasons. The first is the increase in the mistime to the food peak experienced by the population over the study years and thus birds are less likely to attempt a second clutch. The second is the temporal decline in the number of recruits produced from the second clutch. They concluded that changing environmental conditions are important in determining the number of clutches a female lays and therefore potentially alter important life-history traits in the species.

These studies no doubt give us a better understanding of the mechanism of multiple brooding and provide promising explanations for the observational temporal fluctuations in the frequency of double-brooding. However, little theoretical and mechanical hypotheses for the double-brooding evolution exists. It is unclear if there is a genetic basis of the liability of multiple brooding and how the genetic structure interacts with different climate scenarios to produce different evolutionary consequences of double brooding. Due to the lack of genetic data on these reproductive traits of natural bird populations, investigating the mechanism of double brooding evolution is probably feasible only through theoretical genetic models.

Bayesian analysis of ecological processes

Both frequentist and Bayesian inferences are powerful tools for a better understanding of ecological processes in population and community ecology. In the frequentist framework, the most state-of-the-art model fitting technique, an R package named Template Model Builder (TMB, Kristensen et al., 2016) is gaining popularity recently due to its power and efficiency in fitting complex nonlinear mixed models, which are common when modelling complicated ecological processes (for example Cadigan, 2015; Albertsen et al., 2016; Auger-Méthé et al., 2017). One worth mentioning feature of TMB is that it enables Laplace approximation of the marginal likelihood where the random effects are automatically integrated out. Maximum marginal likelihood estimation with the Laplace approximation tends to be orders of magnitude faster but poten-

tially leads to biased inference (Monnahan and Kristensen, 2018). In spite of the flexibility and efficiency of TMB, however, the lack of capability of working in the Bayesian framework has hindered the adoption of it for Bayesians. In the Bayesian framework, Bayesian statistical inference is used extensively to model dynamics of single species, population dispersal, growth, and extinction (Ellison, 2004). The software package *Stan* (Gelman et al., 2015), a probabilistic programming language for Bayesian statistical inference written in C++ is attracting people's attention in many fields as an alternative to BUGS (Lunn et al., 2000) and recommended to be widely applied in ecology due to its improved efficiency (Monnahan et al., 2017).

To best utilize the merits of both TMB and Stan, a new R package *tmbstan* (Kristensen, 2018) was developed to allow users to make Bayesian statistical analysis with TMB models. It provides MCMC sampling for TMB models while the integration of randoms effects can be calculated either with Laplace Approximation (by specifying *laplace=TRUE*) or with Stan. Monnahan and Kristensen (2018) conducts simulation studies and real case studies to compare the computational efficiency of tmbstan with and without Laplace approximation and check the validity of Laplace approximation. They found that enabling the Laplace approximation was less efficient than full MCMC integration, but it is unclear whether this will typically be true. The case studies also showed the Laplace approximation is not always met. Even though it is intuitive to apply tmbstan to estimating fluctuating natural selection especially when prior knowledge on some parameters is available, this has not been done to date. Therefore, there exists no guideline on whether Laplace approximation should be used to achieve better efficiency especially when the statistical model for estimating selection is extremely complicated. To answer this question, simulation studies under different scenarios in different statistical frameworks are necessary.

Aims

Linking the sources of natural selection to the dynamics of evolution has been a major goal of evolutionary biology, however, the lack of a unified framework to quantify the fluctuations in selection accurately has hampered this progress. Previous empirical findings show that fitness landscapes are not constant over time, and populations are evolving towards a continuously changing fitness optimum. A more statistically robust approach, however, is needed to be applied to a wider range of species, populations, and traits. This thesis contributes to this end by showing how current methods for estimating fluctuations in selection can be extended using a more flexible statistical framework. Due to the flexibility of the method equipped with state-space models and TMB, it can be extended to estimating fluctuating selection of life history for different life cycle segments while identifying biotic and abiotic factors exerting selective pressures and identifying which traits (egg-laying date or clutch size in our study), or combinations of traits (potentially correlated), will be targets of the selection. The method can be alternatively implemented in the Bayesian framework by taking prior information into account and using the Bayesian inference tool tmbstan. Using long-term brood-based data from a great tit population in the Netherlands, we hope to be able to answer the questions below:

1. Is there temporal variation, auto-correlation, and cross-correlation in phenotypic selection on the egg-laying date? (paper I, III)

2. What is the possible explanation for the observed decline in the frequency of double brooding? (paper I, II)

3. How selection operates on phenotypes differently in different selective episodes? (paper III)

4. Which ecological variables drive the temporal variation in the phenotypic selection? (paper III)

5. Is Bayesian inference made by ”tmbstan” comparable with frequentist inference for estimating phenotypic selection and should Laplace approximation be used? (paper IV)

The diagram in Fig. 1 shows the connection and transition of the papers in my dissertation. To be specific, paper II, III and IV are extended from paper I by asking specific questions listed above that are not addressed in paper I. According to the modeling approach used in the study, paper I, III and IV are grouped into ”statistical model” and for paper II, it is ”theoretical genetic model”. Furthermore, Paper I and III are classified in the frequentist framework, while paper IV in the Bayesian framework, as illustrated by different colors of the blocks in the last row of the diagram.

Figure 1: A diagram showing how the papers in this dissertation are connected. Paper II, III and IV are extended from paper I by asking specific questions listed above. Generally, paper I, III and IV involve statistical modeling approaches and paper II theoretical genetic modeling approach, as illustrated by the last row. Furthermore, the studies in paper I and paper III were carried out in the frequentist framework, while paper IV in the Bayesian framework, as indicated by the different colors of the blocks.

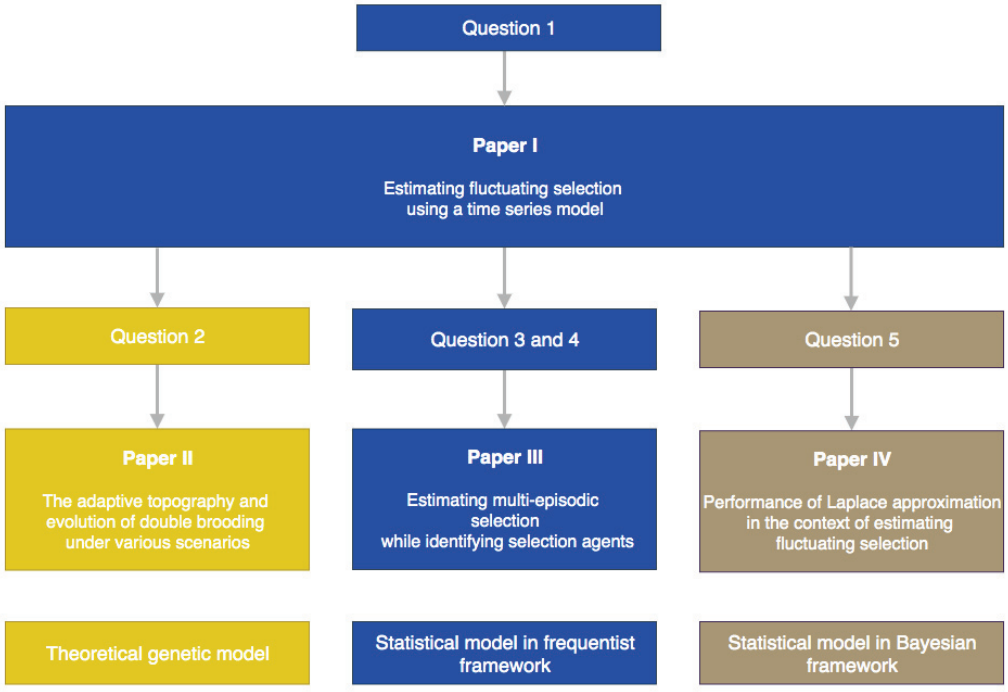

Methods

The central elements of our statistical methods are great tit data (paper I, II, III and IV), state-space models (paper I, III, and IV), vector autoregression (paper I, III, and IV), zero-inflated models (paper I, III), Template Model Builder (paper I, III, and IV), tmbstan (paper IV), and evolution of double brooding (paper II).

The great tit study system

Figure 2: Map of the park (National Park of Hoge Veluwe in the Netherlands) where the great tit data have been collected.

Figure 3: A great tit.

The great tit (*Parus major*, Fig 3) is 18-20g small passerine bird species widespread throughout European woodlands and gardens. As a cavity nester, it readily accepts nest-boxes for breeding, which allows monitoring of the whole population if a surplus of nest-boxes is provided (Harvey et al., 1979). The study area (52°02' - 52°07'N, 5°51' - 5°32'E in The Netherlands, Fig 2) consists of mixed pine-deciduous woodland on poor sandy soils. From 1955 to 2015, more nest boxes than needed were placed in the study area at approximately constant availability. On average the ratio of nest boxes to breeding females was around 3:1 in a typical year. A surplus of nest boxes is supplied so that the actual number of individuals that survive is generally determined by selection and not by external limiting factors such as the number of nest sites. During the breeding season from April to June/July, nest boxes were visited once per week. At each visit, the number of eggs or nestlings was counted and nestlings were given metal leg rings on day 7 and the parents caught on the nest using a spring trap. For some years, clutch or brood size manipulation experiments were carried out, which possibly affected fledgling production or recruitment probability, therefore, manipulated broods were excluded from our studies.

State-space models

A State-Space Model (SSM) is a time series model where observations are regarded as made up of distinct components such as trend, seasonal, regression elements and disturbance terms (Durbin and Koopman, 2012). A typical SSM consists of two equations:

$$\mathbf{x}_t = g(\mathbf{x}_{t-1}, \mathbf{c}); \tag{1}$$

$$\mathbf{y}_t = h(\mathbf{x}_t, \nu), \tag{2}$$

where equation (1) is a process model describing the relationship between unobserved states with function g and parameter $\mathbf{c}$ and $\mathbf{x}_t$ denotes the state at time t. The observation model in equation (2) links the observation or measurement $\mathbf{y}_t$ with state $\mathbf{x}_t$ at time t through function h and parameter ν.

State-space models are often used for analyzing complex ecological processes that can not be observed directly, such as marine animal movement (Albertsen et al., 2015), population dynamics (Wang, 2007) and animal behavior (Morales et al., 2004). It provides a natural paradigm for ecosystem modeling (Pedersen et al., 2011). In spite of the flexibility of SSMs for estimating the unobserved states while simultaneously relating them to various environmental (and other) covariates of interest, these models and their implementations still have limitations arising from underlying difficulties of likelihood computation and maximization for non-Gaussian and nonlinear models. Johnson et al. (2008) utilized the computationally efficient Kalman filter to compute the model likelihood but it is applicable only to linear Gaussian SSM formulations. Jonsen et al. (2005) and McClintock et al. (2012) relied on Markov Chain Monte Carlo (MCMC) techniques performed by sampling from the posterior likelihood of the parameters and the unobserved states, but it is computationally expensive and comparatively slow. Pedersen et al. (2011) examines and compares the estimation performance of three methods for fit of a theta logistic model for population dynamics with simulated data, namely Hidden Markov Model (HMM), AD Model Builder (ADMB) and the popular Bayesian framework of BUGS. It concludes that estimation performance for all three methods are largely identical, while ADMB establishes computing time superiority. The most state-of-the-art statistical tool named Template Model Builder (TMB) that can be used for fitting state-space models will be introduced later.

Vector autoregression

Vector autoregression (VAR) is a stochastic process model used to capture the linear interdependencies among multiple time series. It is an extension of the univariate autoregression model to multivariate time series data and consists of a list of models that can be hypothesized to affect each other intertemporally. All variables in a VAR enter the model in the same way: each variable has an equation explaining its evolution based on its own lagged values, the lagged values of the other model variables, and an error term.

The basic p-lag vector autoregressive (VAR(p)) model has the form:

$$\mathbf{y}_t = \mathbf{c} + \mathbf{A}_1\mathbf{y}_{t-1} + \mathbf{A}_2\mathbf{y}_{t-2} + \cdots + \mathbf{A}_p\mathbf{y}_{t-p} + \mathbf{e}_t, t = 1, \ldots, T, \tag{3}$$

where each $\mathbf{y}_i$ is a vector of length k, each $\mathbf{A}_i$ is a $k \times k$ coefficient matrix and $\mathbf{e}_i$ is a $k \times 1$ unobservable zero mean white noise vector. Here I write a first-order VAR (VAR(1)) in a large

matrix notation as

$$\begin{bmatrix} y_{1,t} \\ y_{2,t} \\ \vdots \\ y_{k,t} \end{bmatrix} = \begin{bmatrix} c_1 \\ c_2 \\ \vdots \\ c_k \end{bmatrix} + \begin{bmatrix} a^1_{1,1} & a^1_{1,2} & \cdots & a^1_{1,k} \\ a^1_{2,1} & a^1_{2,2} & \cdots & a^1_{2,k} \\ \vdots & \vdots & \ddots & \vdots \\ a^1_{k,1} & a^1_{k,2} & \cdots & a^1_{k,k} \end{bmatrix} \begin{bmatrix} y_{1,t-1} \\ y_{2,t-1} \\ \vdots \\ y_{k,t-1} \end{bmatrix} + \begin{bmatrix} e_{1,t} \\ e_{2,t} \\ \vdots \\ e_{k,t} \end{bmatrix}. \tag{4}$$

Each variable $(y_{1,t}, y_{2,t}, \cdots, y_{k,t})$ in the model has one equation. The current (time t) observation of each variable depends on its own lagged values as well as on the lagged values of each other variable in the VAR(1). Vector $(c_1, c_2, \cdots, c_k)$ is a k-vector of constants (intercepts). The matrix consisting of $a^1_{1,1}$ and so on is called transition matrix or autoregressive matrix. Vector $(e_{1,t}, e_{2,t}, \cdots, e_{k,t})$ is errors that are usually assumed to be multivariate normal distributed. Variables $(y_{1,t}, y_{2,t}, \cdots, y_{k,t})$ are cross-correlated either through the transition matrix or variance-covariance matrix of $(e_{1,t}, e_{2,t}, \cdots, e_{k,t})$. To guarantee this VAR(1) process to be stationary, it is sufficient to ensure that the eigenvalues of the transition matrix lie in unit circle (Lütkepohl, 2005; Wei, 2006).

Zero-inflated models

In ecological research, most count data are zero-inflated. In our analyzed data set, for example, the response variable (number of chicks, number of fledglings, number of recruits) contain more zeros than expected based on the Poisson or negative binomial distribution. A zero-inflated model is a statistical model based on a zero-inflated probability distribution that can deal with the excessive number of zeros. The common used zero-inflated models for count data include zero-inflated Poisson (ZIP), zero-inflated negative binomial (ZINB), zero-altered Poisson (ZAP) and zero-altered negative binomial (ZANB) models. The latter two differ from ZIP and ZINB in terms of the nature of zeros. ZAP and ZANB are two-part models that can deal with false zeros (see Zuur et al. (2009) for the definition of false zeros). The negative binomial models (ZINB and ZANB) can cope with overdispersion not only due to excessive numbers of zeros but also due to extra variation in the count data. The main R packages for modeling zero-inflated data include pscl, INLA, MCMCglmm, glmmADMB, mgcv, brms, gamlss and glmmTMB (Zeileis et al., 2008; Rue et al., 2009; Hadfield et al., 2010; Skaug et al., 2013; Wood et al., 2016; Bürkner et al., 2017; Stasinopoulos et al., 2017; Magnusson et al., 2017). Brooks et al. (2017) makes a comparison between the packages and claims that glmmTMB is most appealing to users in terms of the combination of speed and flexibility.

In our analysis, zero-inflated Poisson (ZIP) model was used to deal with the excessive number of zeros in the number of fledglings and zero-inflated Beta-Binomial (ZIBB) was used to model the offspring viability (in our study offspring viability is defined as non-zero inflation probability$\times$offspring survival probability), in which there are excess zeros and the remaining component (offspring survival probability) can be modeled with predictors instead of being a fixed parameter. To be specific, a ZIP model consists of two components (equations (5) and (6)) corresponding to two zero generating processes. The first is governed by a binary distribution and second by a Poisson distribution, which also generates zero counts. The two model components

are described as follows with probability mass functions f:

$$f(y=0) = \pi + (1-\pi)e^{-\lambda}; \tag{5}$$

$$f(y|y \geq 1) = (1-\pi)\frac{\lambda^y e^{-\lambda}}{y}, \tag{6}$$

where the outcome variable y has any non-negative integer value. The expected Poisson count is denoted as λ and π is the probability of extra zeros.

A ZIBB model (see Hu et al. (2018) for more details) also consists of two zero-generating processes. One is again governed by a binary distribution and the other one by a Beta-binomial distribution in which the probability p is a random variable drawn from a beta distribution parameterized by α and β. The two components are given below:

$$f(y=0) = \pi + (1-\pi)f_{\text{beta-bino}}(0|n,\alpha,\beta); \tag{7}$$

$$f(y|y \geq 1) = (1-\pi)f_{\text{beta-bino}}(y|n,\alpha,\beta), \tag{8}$$

where n is the total number of events with any non-negative integer value and y is the number of successes. π is again the probability of extra zeros. The probability mass function of a Beta-binomial distribution $f_{\text{beta-bino}}$ is given by:

$$f_{\text{beta-bino}}(y \mid n,\alpha,\beta) = \binom{n}{y}\frac{B(y+\alpha, n-y+\beta)}{B(\alpha,\beta)}, \tag{9}$$

which consists of a binomial function and a beta function B.

Laplace approximation to deal with random effects

Consider a hierarchical model where the data y depend on a parameter vector θ and random effects u, then maximum likelihood inference requires maximization of

$$L(\theta) = P_\theta(y) = \int P_\theta(y \mid u)P_\theta(u)du. \tag{10}$$

The evaluation of this integral proves often difficult. Various numerical or analytical approaches were proposed to calculate the approximation of the integral. Among them, Laplace's method has been widely used to approximate likelihoods (Raudenbush et al., 2000). In standard Laplace approximation, the natural log of the integrand is expanded in a second-order Taylor series and higher order terms diminish with big sample size, the approximation to the likelihood is thus given as

$$L^*(\theta) \propto \det(|H(\theta)|)^{-\frac{1}{2}} \times P_\theta\left\{y \mid \hat{u}(\theta)\right\} P_\theta\left\{\hat{u}(\theta)\right\}, \tag{11}$$

where

$$\hat{u}(\theta) = \underset{u}{\operatorname{argmax}}\, P_\theta(y)P_\theta(u)$$

and

$$H(\theta) = \frac{\partial^2 L}{\partial u^2} \ln \{P_\theta(y) P_\theta(\hat{u}(\theta))\}$$

(see Kristensen et al. (2016) for the review of Laplace approximation).

I mentioned glmmTMB as an R package that can deal with zero-inflated models. In our analyses, however, I used another R package named Template Model Builder (TMB, Kristensen et al., 2016) instead of glmmTMB as a model fitting technique to benefit from the flexibility in model formulation in TMB. The relationship between them is that glmmTMB is built on TMB and provides a user-friendly interface similar to lme4 for researchers who have difficulties with TMB since TMB requires users to formulate models with C++. The core feature of TMB is that it evaluates the integral with Laplace approximation. The procedure of using TMB to fit a statistical model can be summarized into three steps. Firstly, the joint likelihood for the data, the fixed effects, and the random effects are defined by the user as a C++ template function. Then the package evaluates and maximizes the Laplace approximation of the marginal likelihood where the random effects are automatically integrated out. This approximation and calculation of its derivatives are achieved by using reverse-mode automatic differentiation (up to order three) of the joint likelihood. At last, the approximated likelihood function and its derivatives are passed to optimizers in R such as nlminb and optim.

The combination of reverse-mode automatic differentiation and Laplace approximation for high-dimension integrals allows for the efficient fitting of complex (nonlinear, non-Gaussian, and hierarchical) models with large multivariate data sets to perform parameter estimation (Fournier et al., 2012). The performance of TMB is superior to ADMB (Kristensen et al., 2016) and thus is gaining researchers to use it instead of ADMB to fit state-space models (for example Albertsen et al., 2015; Cadigan, 2015; Albertsen et al., 2016; Berg and Nielsen, 2016). Another model fitting tool that uses the Laplace approximation and is known to be computationally efficient is INLA (Rue et al., 2009), but it is restricted to fit a class of models where the random effects are Gauss-Markov random fields (Kristensen et al., 2016).

MCMC sampling from a TMB model

I mentioned in the introduction that tmbstan (Kristensen, 2018) as an R package developed for MCMC Sampling from TMB model objects using Stan (Team, 2017; Carpenter et al., 2017), is able to make efficient Markov chain Monte Carlo (MCMC) sampling for a broad range of Bayesian models. It is worth noting that tmbstan not only provides TMB users with a possibility of making Bayesian statistical analysis with Stan, but also takes advantage of the features of both TMB and Stan by utilizing the flexibility of TMB in the model specification as well as the high computational efficiency of Stan.

I have introduced that TMB uses the Laplace approximation to integrate random effects. However, Laplace approximation is not always accurate especially when the random effects u are not Gaussian distributed. In addition, the higher-order terms in the Taylor series not necessarily diminish as sample size increases in some special model classes (Raudenbush et al., 2000). In a Bayesian analysis, MCMC integrates all parameters and this allows us to check the accuracy of Laplace approximation in TMB. tmbstan is featured with an argument 'laplace'. When this

argument is enabled, TMB would integrate random effects and Stan integrates the rest fixed effects. The accuracy of the Laplace approximation thus can be tested by comparing the posterior distributions of the fixed effects with and without Laplace approximation enabled in tmbstan (Monnahan and Kristensen, 2018).

The evolution of double brooding

For a great tit population, consider reproductive traits z_1 and z_2, for example, z_1 is the laying date of first brood and z_2 is the liability of initializing a second brood. The phenotypic values z_1 and z_2 are assumed to be jointly multivariate normal. I also assume the genetic and phenotypic variance-covariance matrix $\mathbf{G}$ and $\mathbf{P}$ of z_1 and z_2, as well as the age-specific fecundity and mortality rates for each phenotype, remain nearly constant for a few generations.

With above assumptions and let $\bar{z}_1$ and $\bar{z}_2$ be the mean phenotypic values in a given generation, then the change in mean phenotypic values from one generation to the next is given by

$$\Delta \bar{\mathbf{z}} = \mathbf{G} \nabla \ln \bar{w}(\bar{z}_1, \bar{z}_2), \tag{12}$$

where $\nabla = (\frac{\partial}{\partial \bar{z}_1}, \frac{\partial}{\partial \bar{z}_2})^\top$is the gradient operator, $\mathbf{G}$ is the additive genetic variance and covariance matrix and $\bar{w}(\bar{z}_1, \bar{z}_2)$ is the mean of individual fitness taken over the phenotype distribution of the population (Lande, 1982; Lande and Arnold, 1983; Caswell, 2006). The population responds to selection by moving uphill in the steepest direction that the selection gradient points at, $\ln \bar{w}(\bar{z}_1, \bar{z}_2)$, which is a vector of directional selection pressures (Lande, 1982).

Main results and discussion

Zero-inflated observations

In our analyzed great tit dataset, the proportion of zero observations in the number of chicks, fledglings, and recruits is 6.56%, 15.5%, 74.91% respectively. A zero-inflated Poisson model is used by Chevin et al. (2015) to estimate selection for the same population and the number of fledglings is taken as a fitness component. In the study, the zero-inflation probability is treated as a parameter instead of a separate selective episode. From a biological viewpoint, it is reasonable to assume that the complete brood failure is going though a selective process different from the expected number of fledglings. Our statistical results in paper I and III also indicate that the model where the zero-inflated observations were regarded as a separate selective episode acting on laying dates report much better model fit than the models where zero-inflated probability is taken as a model parameter.

Directional selection via complete brood failure

In paper I, the number of fledglings was partitioned into two fitness components, namely, the expected number of fledglings and the brood failure probability. The expected number of fledglings can be recognized as a straightforward extension of the conceptualization of propensity fitness, which is measured as expected rather than actual numbers of offspring (Brandon, 1978; Mills and Beatty, 1979). The best model suggested directional selection through complete brood failure and stabilizing selection via the expected number of fledglings. The direction and strength of selection via complete brood failure fluctuated over the course of study, but in most of the study years (78%) the selection favors early broods implying that females that bred late relative to the food peak were more likely to fail to raise any fledglings. Similarly, the offspring viability at each reproductive stage, from egg to chick, chick to fledgling, fledgling to recruit was split into offspring survival probability and the brood failure probability in paper III. The complete brood failure was assumed to go through directional selection in the study. The results show that selection favors early broods from stage egg to chick and implies again that early broods suffered lower probability of complete brood failure, while laying dates show no effect on complete brood failure probability from neither chick to fledgling nor from fledgling to recruit. Altogether, even though there is a much higher proportion of zero observations in number of recruit than the other episodes, directional selection operates on laying dates through complete brood failure only in the early stage of a brood, from egg to fledgling.

Stabilizing selection via expected number of fledgling (and offspring survival)

The offspring mortality is the result of malnutrition due to the mismatch between the rearing and the abundance of caterpillar peak, the main food of great tit chicks (Visser et al., 1998). Therefore, in theory, the broods laid either too early or too late relative to the peak of food resource would suffer high offspring mortality, which leads to stabilizing selection favoring the laying dates that can synchronize the chicks rearing with a narrow window of food peak. Indeed,

the analyzed great tit data set supports the best model in paper I with stabilizing selection against the model with directional selection through the expected number of fledglings on laying dates. It is thus reasonable in paper III to assume that the offspring mortality in consecutive reproductive cycle segments from egg to chick, chick to fledgling and fledgling to recruit all experienced stabilizing selection on laying dates. The properties in stabilizing fitness function (the height, location, and width) turn out to fluctuate over the course of study. The episode from chick to fledgling experienced the strongest selection implied by the smallest estimate of the width of the fitness function, compared to the other two selective episodes. Even though these three properties are assumed to be a VAR(1) process, it turns out that only the optimal laying date and width of fitness function are temporally auto-correlated and no significant cross-correlation between the fitness properties are found. It is thus safe to conclude that the annual optimal laying date and width of fitness function follow an AR(1) process respectively. The auto-correlation of optimal laying dates is estimated to as large as 0.49 and for the width of the fitness function, it is 0.64. Even though with such strong auto-correlation estimated, the simulation studies in paper I and IV suggest that the auto-correlation is probably underestimated. The temporal variation in the optimal laying dates for the different selective episodes from egg to recruit is estimated to be the same, while the variation in the width of fitness function from egg to chick is almost four times larger than the other selective episodes. In addition, the episode from fledgling to recruit estimates a much early mean optimal laying date (18.7 ± 3.1) compared to episode from egg to chick (40.7 ± 2.6) and chick to fledgling (33.5 ± 2.4). The annual overall optimal laying date calculated by maximizing the multiplication of the fitness (only for offspring survival) for the three episodes shows a close track with the optimal laying date for the third episode, from fledgling to recruit. The offspring viability (multiplication of offspring survival and non-zero inflation probability) from fledgling to recruit is also the determinant of recruit value for a specific brood and dominating the other episodes for annual reproductive success contribution. All of these imply that the cue used for timing of breeding is only available in the early breeding season, this might result from that climate change is not at constant pace through the entire breeding season, or other factors than climate have larger effects on the population outside the breeding season.

Ecological drivers of selection

One of the study aims of paper III is to identify causal mechanisms underlying temporal variation in the strength and direction of phenotypic selection on laying dates and compare the effect sizes of selective agents between the life cycle segments. We found no correlational selection on laying date and clutch size. Clutch size and laying date are negatively correlated but the correlation is weak. We found neither adult survival cost to lay broods early nor to lay big broods. The beech crop index (BCI) have lager effects on offspring survival from fledgling to recruit than from egg to fledgling, where BCI shows almost no effect. Higher BCI level is found to be positively correlated with higher female survival. Bigger clutch size is associated with higher offspring survival from egg to chick, while negatively affects offspring survival from chick to recruit. The size of the effect reduced along with the life cycle segments from egg to recruit. We also found that bigger clutches suffered a lower probability of complete brood loss from egg to chick and chick to fledgling, the effect is much stronger for the former. Not surprisingly, clutch size is negatively correlated with population density. Higher population density is found

also linked to higher offspring survival from chick to fledgling. As expected, higher population density is linked to earlier optimal laying date for offspring survival, the effect is especially strong for the episode from fledgling to recruit. The food resource peak is positively correlated with optimal laying date for each episode. In an average environment and year, the stabilizing selection strength is strongest for the episode from chick to fledgling. Higher spring temperate is associated with the wider fitness function, which suggests a weaker strength of selection. Early laying date is also linked to lower risk of complete brood loss from egg to chick but early caterpillar peak date is linked to a higher risk of complete brood loss from chick to fledgling. Breeding females differ to each in the clutch size they lay, also in the ability to survive, the ability to rear offspring successfully, and the ability to protect their broods against complete loss from egg to chick. The difference is relatively more significant for the episode from chick to fledgling.

Decreasing probability of double-brooding

The double-brooding behavior reported in our study population has been less common over the study years and the probability that a female breeds twice in a breeding season is related to the timing of her first clutch relative to the peak in caterpillar abundance (Husby et al., 2009). Indeed, we estimated the phenotypic correlation between the breeding time of first brood and liability of producing a second brood to be -0.302. Using a genetic model with parameter values estimated from the study population and a large cost of double-brooding, we show that the adaptive topography of mean population fitness exhibits two peaks at a location where there is no double-brooding or there is 100% double-brooding and the observed mean reproductive traits are overall moving towards the adaptive peak where there is no double-brooding. As long as there is no strong negative genetic correlation between the breeding time of first brood and liability of producing a second brood, the genetic model provides another possible explanation for the observed decline in the frequency of double brooding in this population in addition to the empirical study.

Laplace approximation in tmbstan

When using R package tmbstan for Bayesian inference, the built-in feature Laplace approximation to the marginal likelihood with random effects integrated out can be switched on and off. Both the simulation results and case study result in paper IV show that the Laplace approximation is accurate. In addition, turning on Laplace approximation in tmbstan would probably lower the computational efficiency. I conclude that only when there is a good amount of data, both tmbstan with and without Laplace approximation are worth trying since in this case, Laplace approximation is more likely to be accurate and may also lead to slightly higher computational efficiency. The transition parameters and scale parameters in a VAR(1) process are hard to be estimated accurately and increasing the sample size at each time point does not help in estimation, only more time points in the data contain more information on these parameters and make the likelihood dominate the posterior likelihood, thus lead to accurate estimates for them.

Conclusions and perspectives

In this thesis, we have built a statistical framework to measure fluctuating and potentially temporally auto-correlated selection, extended the framework to include more life cycle segments while taking selective forces of variation in selection into account. A simpler statistical model for estimating fluctuating selection has also been implemented in the Bayesian framework and by which we conducted simulation studies to evaluate the performance of Laplace approximation, one core feature of the Bayesian inference tool tmbstan. We also developed quantitative genetic models to provide a possible explanation for observed decreasing double-brooding frequency in the study population.

Either from a biological point of view or the result of statistical analysis, we found that offspring viability in the Dutch great tit population is ongoing two separate selective processes, both of which produce zero chicks/fledglings/recruits for a given brood. The nest failure experienced temporally varied directional selection and the selection generally favors early broods. The expected number of fledglings, as well as offspring survival given that the brood is successful, experienced stabilizing selection. The maximum value, optimal laying date, and width of the fitness function tend to fluctuate and auto-correlate temporally. Mother survival cost of laying eggs early is not detected. Clutch size increased along with a shift towards earlier laying date, but the effect is too small (one day earlier the laying date is, 0.0635 bigger the clutch would be) to produce a noticeable increase in clutch size even though the mean laying date has advanced around 19 days in past 50 years. We find no evidence of correlational selection on laying date and clutch size. The ecological variables, including beech crop index (BCI), population density, food peak date tend to affect one selective episode and another, in different sizes and directions. The recruit probability is the determinant of recruit value and reproductive success. The seasonal reproductive success contributed by second broods is diminishing when the first brood is laid too late provided there is no strong negative genetic correlation between the laying date of first brood and liability of attempt second brood, which provides a possible explanation for the observed decreasing frequency of double-brooding. In the state-space model, the parameters in the transition matrix and variance-covariance matrix of unobserved states are of our main interest, which are also the most difficult parameters to estimate. The simulation study in the Bayesian analysis shows that to estimate these parameters accurately, it is necessary to increase the time points in the data instead of the sample size at each time point. Laplace approximation would probably slow down the computational efficiency of MCMC especially when there is a small sample size in the data. The rule of thumb might be using Laplace approximation when you have more than 50 time points in the data.

Thanks to the new model-fitting techniques TMB and tmbstan, using state-space models to estimate a large number of parameters and random effects in complicated biological processes or ecological systems become possible even in cases where the state-space equations are highly nonlinear or non-Gaussian. By treating the phenotypical selection process as a time series and allowing a flexible covariance structure for the Gaussian fitness parameters, our method is capable of modeling different forms of variation and autocorrelation in phenotypic selection. Besides VAR(1), it can also accommodate other autoregressive structures, such as VAR(p) (p-order vector autoregressive process) and vector ARMA(p,q) processes. Within species, there is substantial geographic variation in the response to climate change, therefore, another direction of extending our studies could be estimating the temporal-spatial variation and correlation in fluctuating se-

lection and investigating the causes of geographic variation in selection within species to get a better understanding of avian responses at a broader geographic scale.

Although our studies have developed applicable statistical tools for the measurement of natural selection on reproductive traits (breeding time and clutch size) through life cycle segments, however, the relationship between the timing of breeding and breeding performance is still unclear. In our studies, the clutch size has no noticeable increase in the population with a temporal shift towards earlier egg-laying. We also found no evidence of adult survival cost being laying early and selection through complete brood failure favors early broods. The probability of initializing second brood is also decreasing with delayed first brood. Take all these together, there seems no reason not to advance laying date of first brood to match the seasonal breeding time with food abundance, which is not happening in reality. One explanation could be that the timing of laying is adapted to other factors besides the timing of food supply for the chicks, or the birds are just not capable enough to track the cues of climate change. Another missing piece in our analysis is the social interaction between the phenotype (the laying date) of breeding females and males and the phenotypes of the species they associate with. At last, developing a mechanistic and theoretical understanding of the relationship between reproductive decisions and breeding performance as well as the physiological basis for these relationships are beyond the scope of our studies, but should be top priorities in extended studies since they are essential for linking the responses of birds to climate models and predicting long-term change in populations.

Bibliography

Albertsen, C. M., Nielsen, A., and Thygesen, U. H. (2016). Choosing the observational likelihood in state-space stock assessment models. *Canadian Journal of Fisheries and Aquatic Sciences*, 74(5):779–789.

Albertsen, C. M., Whoriskey, K., Yurkowski, D., Nielsen, A., and Flemming, J. M. (2015). Fast fitting of non-gaussian state-space models to animal movement data via template model builder. *Ecology*, 96(10):2598–2604.

Arnold, S. J. and Wade, M. J. (1984). On the measurement of natural and sexual selection: theory. *Evolution*, 38(4):709–719.

Auger-Méthé, M., Albertsen, C. M., Jonsen, I. D., Derocher, A. E., Lidgard, D. C., Studholme, K. R., Bowen, W. D., Crossin, G. T., and Flemming, J. M. (2017). Spatiotemporal modelling of marine movement data using Template Model Builder (TMB). *Marine Ecology Progress Series*, 565:237–249.

Barba, E., Gil-Delgado, J. A., and Monros, J. S. (1995). The costs of being late: consequences of delaying great tit parus major first clutches. *Journal of Animal Ecology*, pages 642–651.

Bell, G. (2010). Fluctuating selection: the perpetual renewal of adaptation in variable environments. *Philosophical Transactions of the Royal Society B: Biological Sciences*, 365(1537):87–97.

Berg, C. W. and Nielsen, A. (2016). Accounting for correlated observations in an age-based state-space stock assessment model. *ICES Journal of Marine Science*, 73(7):1788–1797.

Brandon, R. N. (1978). *Adaptation and evolutionary theory*. Wiley-Blackwell.

Brooks, M. E., Kristensen, K., van Benthem, K. J., Magnusson, A., Berg, C. W., Nielsen, A., Skaug, H. J., Machler, M., and Bolker, B. M. (2017). glmmTMB balances speed and flexibility among packages for zero-inflated generalized linear mixed modeling. *The R journal*, 9(2):378–400.

Bürger, R. and Gimelfarb, A. (2002). Fluctuating environments and the role of mutation in maintaining quantitative genetic variation. *Genetics Research*, 80(1):31–46.

Bürkner, P.-C. et al. (2017). brms: An R package for Bayesian multilevel models using Stan. *Journal of Statistical Software*, 80(1):1–28.

Cadigan, N. G. (2015). A state-space stock assessment model for northern cod, including underreported catches and variable natural mortality rates. *Canadian Journal of Fisheries and Aquatic Sciences*, 73(2):296–308.

Calsbeek, B. (2011). Exploring variation in fitness surfaces over time or space. *Evolution*, 66(4):1126–1137.

Cao, Y., Visser, M. E., and Tufto, J. (2019). A time-series model for estimating temporal variation in phenotypic selection on laying dates in a dutch great tit population. *Methods in Ecology and Evolution*, 10(9):1401–1411.

Carpenter, B., Gelman, A., Hoffman, M. D., Lee, D., Goodrich, B., Betancourt, M., Brubaker, M., Guo, J., Li, P., and Riddell, A. (2017). Stan: A probabilistic programming language. *Journal of statistical software*, 76(1).

Caswell, H. (2006). Matrix population models. *Encyclopedia of Environmetrics*, 3.

Charlesworth, B. (1971). Selection in density-regulated populations. *Ecology*, 52(3):469–474.

Charlesworth, B. (1993). The evolution of sex and recombination in a varying environment. *Journal of Heredity*, 84(5):345–350.

Charnov, E. L. (1993). *Life history invariants: some explorations of symmetry in evolutionary ecology*, volume 6. Oxford University Press, USA.

Chevin, L.-M. (2013). Genetic constraints on adaptation to a changing environment. *Evolution: International Journal of Organic Evolution*, 67(3):708–721.

Chevin, L.-M. and Haller, B. C. (2014). The temporal distribution of directional gradients under selection for an optimum. *Evolution*, 68(12):3381–3394.

Chevin, L.-M., Visser, M. E., and Tufto, J. (2015). Estimating the variation, autocorrelation, and environmental sensitivity of phenotypic selection. *Evolution*, 69(9):2319–2332.

Clutton-Brock, T. H. (1988). *Reproductive success: studies of individual variation in contrasting breeding systems*. University of Chicago Press.

Durbin, J. and Koopman, S. J. (2012). *Time series analysis by state space methods*. Oxford university press.

Ellison, A. M. (2004). Bayesian inference in ecology. *Ecology letters*, 7(6):509–520.

Endler, J. A. (1986). *Natural selection in the wild*. Princeton University Press.

Engen, S., Lande, R., and Sæther, B.-E. (2011). Evolution of a plastic quantitative trait in an age-structured population in a fluctuating environment. *Evolution: International Journal of Organic Evolution*, 65(10):2893–2906.

Evans Ogden, L. J. and Stutchbury, B. J. (1996). Constraints on double brooding in a neotropical migrant, the hooded warbler. *The Condor*, 98(4):736–744.

Fournier, D. A., Skaug, H. J., Ancheta, J., Ianelli, J., Magnusson, A., Maunder, M. N., Nielsen, A., and Sibert, J. (2012). AD Model Builder: using automatic differentiation for statistical inference of highly parameterized complex nonlinear models. *Optimization Methods and Software*, 27(2):233–249.

Gamelon, M., Tufto, J., Nilsson, A. L. K., Jerstad, K., Røstad, O. W., Stenseth, N. C., and Sæther, B.-E. (2018). Environmental drivers of varying selective optima in a small passerine: A multivariate, multiepisodic approach. *Evolution*.

Gardner, A. and Grafen, A. (2009). Capturing the superorganism: a formal theory of group adaptation. *Journal of evolutionary biology*, 22(4):659–671.

Gelman, A., Lee, D., and Guo, J. (2015). Stan: A probabilistic programming language for Bayesian inference and optimization. *Journal of Educational and Behavioral Statistics*, 40(5):530–543.

Geupel, G. R. and DeSante, D. F. (1990). Incidence and determinants of double brooding in wrentits. *The Condor*, 92(1):67–75.

Hadfield, J. D. et al. (2010). MCMC methods for multi-response generalized linear mixed models: the MCMCglmm R package. *Journal of Statistical Software*, 33(2):1–22.

Hansen, T. F. (2017). On the definition and measurement of fitness in finite populations. *Journal of theoretical biology*, 419:36–43.

Harvey, P. H., Greenwood, P. J., and Perrins, C. M. (1979). Breeding area fidelity of great tits (parus major). *The Journal of Animal Ecology*, 48(1):305.

Hoekstra, H. E., Hoekstra, J. M., Berrigan, D., Vignieri, S. N., Hoang, A., Hill, C. E., Beerli,

P., and Kingsolver, J. G. (2001). Strength and tempo of directional selection in the wild. *Proceedings of the National Academy of Sciences*, 98(16):9157–9160.

Hu, T., Gallins, P., and Zhou, Y.-H. (2018). A zero-inflated beta-binomial model for microbiome data analysis. *Stat*, 7(1):e185.

Husby, A., Kruuk, L. E., and Visser, M. E. (2009). Decline in the frequency and benefits of multiple brooding in great tits as a consequence of a changing environment. *Proceedings of the Royal Society B: Biological Sciences*, 276(1663):1845–1854.

Jacobs, A. C., Reader, L. L., and Fair, J. M. (2013). What determines the rates of double brooding in the western bluebird? ¿ qué determina las tasas de nidada doble en sialia mexicana? *The Condor*, 115(2):386–393.

Johnson, D. S., London, J. M., Lea, M.-A., and Durban, J. W. (2008). Continuous-time correlated random walk model for animal telemetry data. *Ecology*, 89(5):1208–1215.

Jonsen, I. D., Flemming, J. M., and Myers, R. A. (2005). Robust state–space modeling of animal movement data. *Ecology*, 86(11):2874–2880.

Kingsolver, J. G., Hoekstra, H. E., Hoekstra, J. M., Berrigan, D., Vignieri, S. N., Hill, C., Hoang, A., Gibert, P., and Beerli, P. (2001). The strength of phenotypic selection in natural populations. *The American Naturalist*, 157(3):245–261.

Kristensen, K. (2018). *MCMC Sampling from 'TMB' Model Object using 'Stan'*. R package version 1.0.1.

Kristensen, K., Nielsen, A., Berg, C. W., Skaug, H. J., and Bell, B. (2016). TMB: Automatic differentiation and Laplace approximation. *Journal of Statistical Software*, 70(5):1–21.

Lande, R. (1979). Quantitative genetic analysis of multivariate evolution, applied to brain: body size allometry. *Evolution*, 33(1Part2):402–416.

Lande, R. (1982). A quantitative genetic theory of life history evolution. *Ecology*, 63(3):607–615.

Lande, R. and Arnold, S. J. (1983). The measurement of selection on correlated characters. *Evolution*, 37(6):1210–1226.

Lande, R. and Shannon, S. (1996). The role of genetic variation in adaptation and population persistence in a changing environment. *Evolution*, 50(1):434–437.

Liker, A., Freckleton, R. P., Remeš, V., and Székely, T. (2015). Sex differences in parental care: Gametic investment, sexual selection, and social environment. *Evolution*, 69(11):2862–2875.

Lindén, M. (1988). Reproductive trade-off between first and second clutches in the great tit parus major: an experimental study. *Oikos*, pages 285–290.

Linnen, C. R. and Hoekstra, H. E. (2009). Measuring natural selection on genotypes and phenotypes in the wild. In *Cold Spring Harbor Symposia on Quantitative Biology*, volume 74, pages 155–168. Cold Spring Harbor Laboratory Press.

Lunn, D. J., Thomas, A., Best, N., and Spiegelhalter, D. (2000). WinBUGS-a Bayesian modelling framework: concepts, structure, and extensibility. *Statistics and computing*, 10(4):325–337.

Lütkepohl, H. (2005). *New introduction to multiple time series analysis*. Springer Science & Business Media.

Magnusson, A., Skaug, H., Nielsen, A., Berg, C., Kristensen, K., Maechler, M., van Bentham, K., Bolker, B., Brooks, M., and Brooks, M. M. (2017). Package 'glmmtmb'. *R Package Version 0.2. 0*.

Martin, T. E. and Briskie, J. V. (2009). Predation on dependent offspring: a review of the consequences for mean expression and phenotypic plasticity in avian life history traits. *Annals of the New York Academy of Sciences*, 1168(1):201–217.

McCleery, R., Clobert, J., Julliard, R., and Perrins, C. (1996). Nest predation and delayed cost of reproduction in the great tit. *Journal of Animal Ecology*, pages 96–104.

McClintock, B. T., King, R., Thomas, L., Matthiopoulos, J., McConnell, B. J., and Morales, J. M. (2012). A general discrete-time modeling framework for animal movement using multistate random walks. *Ecological Monographs*, 82(3):335–349.

Merilä, J., Sheldon, B., and Kruuk, L. (2001). Explaining stasis: microevolutionary studies in natural populations. *Genetica*, 112(1):199–222.

Mills, S. K. and Beatty, J. H. (1979). The propensity interpretation of fitness. *Philosophy of Science*, 46(2):263–286.

Monnahan, C. C. and Kristensen, K. (2018). No-U-turn sampling for fast Bayesian inference in ADMB and TMB: Introducing the adnuts and tmbstan R packages. *PloS one*, 13(5):e0197954.

Monnahan, C. C., Thorson, J. T., and Branch, T. A. (2017). Faster estimation of Bayesian models in ecology using Hamiltonian Monte Carlo. *Methods in Ecology and Evolution*, 8(3):339–348.

Morales, J. M., Haydon, D. T., Frair, J., Holsinger, K. E., and Fryxell, J. M. (2004). Extracting more out of relocation data: building movement models as mixtures of random walks. *Ecology*, 85(9):2436–2445.

Morrissey, M. B. and Hadfield, J. D. (2012). Directional selection in temporally replicated studies is remarkably consistent. *Evolution: International Journal of Organic Evolution*, 66(2):435–442.

Mulvihill, R. S., Latta, S. C., and Newell, F. L. (2009). Temporal constraints on the incidence of double brooding in the louisiana waterthrush. *The Condor*, 111(2):341–348.

Nagy, L. R. and Holmes, R. T. (2004). Factors influencing fecundity in migratory songbirds: is nest predation the most important? *Journal of Avian Biology*, 35(6):487–491.

Newton, I. et al. (1989). *Lifetime reproduction in birds*. Academic Press.

Parejo, D. and Danchin, E. (2006). Brood size manipulation affects frequency of second clutches in the blue tit. *Behavioral ecology and sociobiology*, 60(2):184–194.

Pedersen, M. W., Berg, C. W., Thygesen, U. H., Nielsen, A., and Madsen, H. (2011). Estimation methods for nonlinear state-space models in ecology. *Ecological Modelling*, 222(8):1394–1400.

Perrins, C. M. and McCleery, R. H. (1989). Laying dates and clutch size in the great tit. *The Wilson Bulletin*, pages 236–253.

Price, G. R. (1970). Selection and covariance. *Nature*, 227(5257):520–521.

Price, T. and Liou, L. (1989). Selection on clutch size in birds. *The American Naturalist*, 134(6):950–959.

Raudenbush, S. W., Yang, M.-L., and Yosef, M. (2000). Maximum likelihood for generalized linear models with nested random effects via high-order, multivariate Laplace approximation. *Journal of computational and Graphical Statistics*, 9(1):141–157.

Reed, T. E., Gienapp, P., and Visser, M. E. (2016). Testing for biases in selection on avian reproductive traits and partitioning direct and indirect selection using quantitative genetic models. *Evolution*, 70(10):2211–2225.

Reed, T. E., Grøtan, V., Jenouvrier, S., Sæther, B.-E., and Visser, M. E. (2013a). Population growth in a wild bird is buffered against phenological mismatch. *Science*, 340(6131):488–491.

Reed, T. E., Jenouvrier, S., and Visser, M. E. (2013b). Phenological mismatch strongly affects individual fitness but not population demography in a woodland passerine. *Journal of Animal Ecology*, 82(1):131–144.

Rue, H., Martino, S., and Chopin, N. (2009). Approximate Bayesian inference for latent gaussian models by using integrated nested Laplace approximations. *Journal of the royal statistical society: Series b (statistical methodology)*, 71(2):319–392.

Saccheri, I. and Hanski, I. (2006). Natural selection and population dynamics. *Trends in Ecology & Evolution*, 21(6):341–347.

Sæther, B.-E. and Bakke, Ø. (2000). Avian life history variation and contribution of demographic traits to the population growth rate. *Ecology*, 81(3):642–653.

Sæther, B.-E., Visser, M. E., Grøtan, V., and Engen, S. (2016). Evidence for r-and k-selection in a wild bird population: a reciprocal link between ecology and evolution. *Proceedings of the Royal Society B: Biological Sciences*, 283(1829):20152411.

Santema, P. and Kempenaers, B. (2018). Complete brood failure in an altricial bird is almost always associated with the sudden and permanent disappearance of a parent. *Journal of Animal Ecology*, 87(5):1239–1250.

Schluter, D. (1988). Estimating the form of natural selection on a quantitative trait. *Evolution*, 42(5):849–861.

Schluter, D., Price, T. D., and Rowe, L. (1991). Conflicting selection pressures and life history trade-offs. *Proceedings of the Royal Society of London. Series B: Biological Sciences*, 246(1315):11–17.

Siepielski, A. M., DiBattista, J. D., and Carlson, S. M. (2009). It's about time: the temporal dynamics of phenotypic selection in the wild. *Ecology letters*, 12(11):1261–1276.

Siepielski, A. M., DiBattista, J. D., Evans, J. A., and Carlson, S. M. (2010). Differences in the temporal dynamics of phenotypic selection among fitness components in the wild. *Proceedings of the Royal Society B: Biological Sciences*, 278(1711):1572–1580.

Siikamäki, P. (1998). Limitation of reproductive success by food availability and breeding time in pied flycatchers. *Ecology*, 79(5):1789–1796.

Skaug, H., Fournier, D., and Nielsen, A. (2013). glmmADMB: generalized linear mixed models using AD Model Builder–R Package.

Stasinopoulos, M. D., Rigby, R. A., Heller, G. Z., Voudouris, V., and De Bastiani, F. (2017). *Flexible regression and smoothing: using GAMLSS in R*. Chapman and Hall/CRC.

Stearns, S. C. (2000). Life history evolution: successes, limitations, and prospects. *Naturwissenschaften*, 87(11):476–486.

Stinchcombe, J. R., Kelley, J. L., Conner, J. K., and Freckleton, R. (2017). How to measure natural selection. *Methods in Ecology and Evolution*, 8(6).

Team, S. D. (2017). Stan modeling language: User's guide and reference manual. *Version 2.17.0*.

Thomson, C. E. and Hadfield, J. D. (2017). Measuring selection when parents and offspring interact. *Methods in Ecology and Evolution*, 8(6):678–687.

Townsend, A. K., Sillett, T. S., Lany, N. K., Kaiser, S. A., Rodenhouse, N. L., Webster, M. S.,

and Holmes, R. T. (2013). Warm springs, early lay dates, and double brooding in a north american migratory songbird, the black-throated blue warbler. *PLoS One*, 8(4):e59467.

Tufto, J. (2015). Genetic evolution, plasticity, and bet-hedging as adaptive responses to temporally autocorrelated fluctuating selection: a quantitative genetic model. *Evolution*, 69(8):2034–2049.

Verboven, N., Tinbergen, J. M., and Verhulst, S. (2001). Food, reproductive success and multiple breeding in the great tit parus major. *Ardea*, 89(2):387–406.

Verboven, N. and Verhulst, S. (1996). Seasonal variation in the incidence of double broods: the date hypothesis fits better than the quality hypothesis. *Journal of Animal Ecology*, pages 264–273.

Verboven, N. and Visser, M. E. (1998). Seasonal variation in local recruitment of great tits: the importance of being early. *Oikos*, pages 511–524.

Visser, M., Van Noordwijk, A., Tinbergen, J., and Lessells, C. (1998). Warmer springs lead to mistimed reproduction in great tits (parus major). *Proceedings of the Royal Society of London B: Biological Sciences*, 265(1408):1867–1870.

Wang, G. (2007). On the latent state estimation of nonlinear population dynamics using Bayesian and non-Bayesian state-space models. *Ecological Modelling*, 200(3):521–528.

Wei, W. (2006). *Time Series Analysis: Univariate and Multivariate Methods*. Pearson Addison Wesley, 2nd edition.

Wesołowski, T. (2002). Anti-predator adaptations in nesting marsh tits parus palustris: the role of nest-site security. *Ibis*, 144(4):593–601.

Wood, S. N., Pya, N., and Säfken, B. (2016). Smoothing parameter and model selection for general smooth models. *Journal of the American Statistical Association*, 111(516):1548–1563.

Zeileis, A., Kleiber, C., and Jackman, S. (2008). Regression models for count data in R. *Journal of statistical software*, 27(8):1–25.

Zuur, A., Ieno, E. N., Walker, N., Saveliev, A. A., and Smith, G. M. (2009). *Mixed effects models and extensions in ecology with R*. Springer Science & Business Media.

Paper I

Received: 22 January 2019 | Accepted: 21 June 2019

DOI: 10.1111/2041-210X.13249

RESEARCH ARTICLE

Methods in Ecology and Evolution BRITISH ECOLOGICAL SOCIETY

A time-series model for estimating temporal variation in phenotypic selection on laying dates in a Dutch great tit population

Yihan Cao[1] | Marcel E. Visser[2] | Jarle Tufto[1]

[1]Centre for Biodiversity Dynamics, Department of Mathematical Sciences, Norwegian University of Science and Technology, Trondheim, Norway

[2]Department of Animal Ecology, Netherlands Institute of Ecology (NIOO-KNAW), Wageningen, Netherlands

Correspondence
Yihan Cao
Email: yihan.cao@ntnu.no

Handling Editor: Thomas Hansen

Abstract

1. Temporal and spatial variation in phenotypic selection due to changing environmental conditions is of great interest to evolutionary biologists, but few existing methods estimating its magnitude take into account the temporal autocorrelation.
2. We use state-space models (SSMs) to analyse phenotypic selection processes that cannot be observed directly and use Template Model builder (TMB), an R package for computing and maximizing the Laplace approximation of the marginal likelihood for SSM and other complex, nonlinear latent variable model via automatic differentiation. Using a long-term great tit (*Parus major*) dataset, we fit several SSMs and conduct model selection based on Akaike information criterion (AIC) to assess the support for fluctuated directional or autocorrelated stabilizing selection on breeding time of the great tit population.
3. Our results show that there is directional selection on the probability of breeding failure, and stabilizing selection on the mean number of fledglings. This selection for early laying date is consistent with a previous study of the same population. We also estimate the variation and autocorrelation in other parameters of the fitness functions, including the width and height, and found the height and location of annual fitness function are autocorrelated with significant variation, while the width can be assumed to constant over time.
4. Using TMB to fit SSMs, we are able to estimate additional parameters compared to previous methods, all without requiring a substantial increase in computational resources. Furthermore, our specification of complex nonlinear model structure benefits greatly from the flexibility of model formulation with TMB. Therefore, our approach could be directly applied to estimating even more complicated phenotypic selection processes induced by environmental change for other species.

KEYWORDS

fluctuating selection, Gaussian fitness function, generalized linear mixed model, state-space model, template model builder, zero-inflated Poisson regression

1 | INTRODUCTION

Fluctuating selection resulting from environmental variation has been of long-lasting interest. Empirical and theoretical research have documented that natural populations respond to varying selection through various mechanism including conventional Darwinian genetic evolution (Lande & Shannon, 1996), evolution of phenotypic plasticity (Scheiner, 1993; Van Tienderen & Koelewijn, 1994), evolution of genetic polymorphism (reviewed by Hedrick, 2006; Bell, 2010), genetic variance (Barton & Keightley, 2002), evolution of the phenotypic variance (Zhang & Hill, 2005) including diversifying bet-hedging (Bull, 1987; Cohen, 1966; Svardal, Rueffler & Hermisson, 2011) or combinations of these response modes (Tufto, 2015). Importantly, the relative magnitudes of these different responses depend on the temporal autocorrelation in selective optima. Even though the phenotypic traits typically evolve through natural selection to match the environmental conditions to maximize fitness (Futuyma, 2006), phenotypic adaptation through genetic evolution is limited by the amount of genetic variance in the trait under selection, which might lead to mistiming between the mean phenotype and the phenotypic optimum (Lande & Shannon, 1996). Adaptive tracking through phenotypic plasticity acting in conjunction with genetic evolution may also be limited by factors such as imperfect cue reliability (Post & Forchhammer, 2007; Gienapp, Reed & Visser, 2014) or parental energetic costs (Visser, Marvelde & Lof, 2012; Visser et al., 2015).

There are few studies estimating the temporal variability and autocorrelation of phenotypic selection in spite of the importance. The variance in phenotypic selection in previous studies was usually estimated by computing the variance of the strength of selection using selection gradients estimated separately at each time point (reviewed by Siepielski, DiBattista & Carlson, 2009), which reflects both sampling error and real variation in selection (Morrissey & Hadfield, 2012). Among the previous empirical studies accounting for the sampling error of variation, Calsbeek (2011) presented a nonparametric analysis in exploring the variation of fitness surfaces over time or space, but such nonparametric estimates are difficult to relate to parameters appearing in theoretical models. In contrast, using a log-quadratic generalized linear mixed model (GLMM) with a random effect on the regression slope implemented using integrated nested Laplace approximations (INLA) (Rue, Martino & Chopin, 2009), Chevin, Visser and Tufto (2015) estimated yearly fluctuations and autocorrelation in optima of a Gaussian fitness function. However, INLA and GLMMs in general are restricted to cases where the predictor is linear in parameters and random effects. Using instead the more flexible framework of Template Model Builder (TMB) (Kristensen, Nielsen, Berg, Skaug & Bell, 2015), Gamelon et al. (2018) fitted a model of fluctuating selection via several non-overlapping selection episodes with nonlinear random effects added directly on the location of the fitness optima and on the peak of the fitness function. This model form is not feasible within the framework of INLA or GLMMs (see Gamelon et al., 2018, Appendix A for a technical discussion).

Here, we extend the approach taken in Chevin et al. (2015) and Gamelon et al. (2018) in several new ways. First, instead of assuming a fixed zero-inflation parameter for modelling the number of fledglings as in Chevin et al. (2015), we model the zero-inflation probability using a separate linear (or nonlinear) predictor. This leads to a model with selection via zero-inflation and via the Poisson mean, although occurring during the same interval. As with multi-episodic selection more generally (Gamelon et al., 2018), selection through two episodes can involve the same or different biological processes. Second, in addition to random effects on the peak and location of the fitness optimum as in Gamelon et al. (2018), we also allow the width of the fitness function to vary between years, with all three properties of the Gaussian fitness function jointly following a vector autoregressive process. Such variation in the width is of theoretical importance for the evolution of the phenotypic variance (Zhang & Hill, 2005) and for the evolutionary stability of the additive genetic variance-covariance matrix (Revell, 2007). Third, instead of treating the total number of fledglings from all broods laid by a female in a particular year as the sample unit and estimating stabilizing selection on onset of breeding via its effect on the sum of number of fledglings from all broods as in Chevin et al. (2015), we treat the number of fledglings from each brood as the sample unit and fit the model under the assumption that the expected number of fledglings depend on the laying date according to the same Gaussian fitness function for all broods. In addition to increased statistical power, this has the advantage that the parameters relate directly to theoretical models for the joint evolution of multiple brooding and onset of breeding (Tufto, Cao and Visser, submitted manuscript). Fourth, as an alternative to stabilizing selection, we allow each episode (here selection via zero-inflation and via the Poisson mean) to instead involve directional selection. As in Gamelon et al. (2018), we implement our method using TMB (Kristensen et al., 2015), an R package providing a comprehensive framework for fast fitting nonlinear, complex, latent variable models.

2 | MATERIALS AND METHODS

2.1 | Study population

The data analysed come from a natural population of great tits (*Parus major*) at the Hoge Veluwe National Park in the Netherlands (52°02′ – 52°07′N, 5°51′ – 5°32′ E). Female great tits usually start reproduction in the second calendar year of life (Perrins, 1979) and are capable of producing a second and very rarely, a third brood in a season. The analysed dataset consists of 5892 records of 3257 females breeding in 61 years from 1955 to 2015. Unlike the previous studies on the same population (e.g. Reed, Jenouvrier & Visser, 2013), we kept the data from the 1991 breeding season when a late frost led to a very late caterpillar food peak (Visser, Noordwijk, Tinbergen, & Lessells 1998) and we expected a very late optimum estimate for this breeding season. Laying dates are presented as the number of days after March 31 (day 1 = April 1, day 31 = May 1). The number of fledglings for each visited brood

was counted and the mother of each brood was identified (3257 breeding mothers in our analysed data). The average number of breeding records per known female was 1.81. See Supporting Information for more details on study population and fieldwork procedures.

2.2 | Model formulation

We formulated a statistical model that takes into account temporally fluctuated stabilizing selection and used laying date as the focal trait that selection operates on. We also considered alternative models assuming fluctuated directional selection. We take the number of individuals surviving to fledglings as the measure of fecundity component of fitness and it is assumed to follow a zero-inflated Poisson distribution instead of a Poisson distribution due to the high probability of clutch failure (around 15.7% in our analysed dataset, clutch failure in this study means that no single chick survived to fledgling). In addition, previous studies showed (e.g. Reed et al., 2013; Townsend et al., 2013) that the relative contribution to fitness from each brood, at individual level, is determined by the food abundance at the time each brood is raised. We therefore assume that the expected number of fledglings and the probability of clutch failure potentially depends on laying dates in the same way for first, replacement (first broods failed) and second (first broods succeeded) broods via the same Gaussian fitness function. We present our approach using selection on the number of fledglings, but it can be applied to any selection episodes, such as viability, fertility selection or overall selection through lifetime fitness for species with non-overlapping generations.

We assume that the number of fledglings Y_i (i = 1,2,...,n) from the ith brood follow a zero-inflated Poisson (ZIP) distribution. Such random variables can be represented as a product $Y_i = I_i X_i$ where

$$\begin{aligned} I_i|p_i &\sim \text{Bernoulli}(1-p_i),\\ X_i|I_i = 1, w_i &\sim \text{Poisson}(w_i). \end{aligned} \tag{1}$$

Here, p_i is the probability of zero-inflation (complete brood failure), w_i is the Poisson mean and i is the index for all of the broods in our analysed dataset, i = 1,2,...,5892. Using the law of total expectation, the overall fitness contribution from brood i is then

$$\begin{aligned} E(Y_i|p_i, w_i) &= E(X_i I_i|p_i, w_i)\\ &= E(X_i I_i|p_i, w_i, I_i = 1)P(I_i = 1) + E(X_i I_i|p_i, w_i, I_i = 0)P(I_i = 0)\\ &= E(X_i|I_i = 1, w_i)E(I_i|p_i). \end{aligned} \tag{2}$$

The decomposition of the left-hand side into the two factors on the right-hand side shows that the zero-inflation part I_i can be interpreted as a separate selection episode, which we refer to as episode P for short in this study. Similarly, the Poisson part X_i is referred to as episode W in the rest of this paper.

We consider two selection modes: fluctuating stabilizing selection and fluctuating directional selection. In the fluctuating stabilizing selection model, the zero-inflation probability p_i and the Poisson mean w_i are determined by the same process, driven by deviation from the optimal onset of breeding. In addition, we assume that p_i is linked to covariates of interest via a logit link function while for w_i via a log link function. Therefore, $\text{logit}(1-p_i)$ and $\ln w_i$ are given by models of the same form:

$$\text{logit}(1-p_i) = \eta_{p,t}^{(\alpha)} - \frac{(z_i - \eta_{p,t}^{(\theta)})^2}{2(e^{\eta_{p,t}^{(\omega)}})^2} + \tau_p^m \epsilon_{j(i)}; \tag{3}$$

and

$$\ln w_i = \eta_{w,t}^{(\alpha)} - \frac{(z_i - \eta_{w,t}^{(\theta)})^2}{2(e^{\eta_{w,t}^{(\omega)}})^2} + \tau_w^m \epsilon_{j(i)}. \tag{4}$$

Here, $\eta_{p,t}^{(\alpha)}$, $\eta_{p,t}^{(\theta)}$ and $\eta_{p,t}^{(\omega)}$, t = 1,2,...,61 are parameters determining maximum fitness (indicated by superscript α), optimal laying dates (indicated by θ) and widths of fitness function (indicated by ω) of brood i in year t respectively for $\text{logit}(1-p_i)$. Similar explanations apply to the equation of $\ln w_i$. The variable z_i is the laying date of the ith brood. The term $\epsilon_{j(i)} \sim N(0,1)$, j = 1,2,...,J (where J is total number of unique females) is a random effect included to model extra variation between the mothers and assumed to be same for the two episodes, but the magnitude of the effects on the two episodes are potentially different, subscript p,w thereby allow standard deviations of mother effect τ_p^m, τ_w^m to differ between episode P and W.

The maximum fitness, optimal laying date and width of fitness function in the two episodes are assumed to have a constant difference c_α, c_θ and c_ω ($\eta_{w,t}^{(\alpha)} = \eta_{p,t}^{(\alpha)} + c_\alpha$, $\eta_{w,t}^{(\theta)} = \eta_{p,t}^{(\theta)} + c_\theta$ and $\eta_{w,t}^{(\omega)} = \eta_{p,t}^{(\omega)} + c_\omega$) and we therefore model $\eta_{p,t}^{(\alpha)}$, $\eta_{p,t}^{(\theta)}$ and $\eta_{p,t}^{(\omega)}$ by the three stochastic processes

$$\begin{aligned} \eta_{s,t}^{(\alpha)} &= \bar{\alpha}_s + \alpha_t,\\ \eta_{s,t}^{(\theta)} &= \bar{\theta}_s + \theta_t,\\ \eta_{s,t}^{(\omega)} &= \bar{\omega}_s + \omega_t, \end{aligned} \tag{5}$$

where index s takes values from (P,W) indicating the two episodes respectively. Parameters $\bar{\alpha}_s$, $\bar{\theta}_s$, $\bar{\omega}_s$ are the means of the three processes. More assumptions in terms of stochastic processes α_t, θ_t, ω_t are made. They are assumed to follow a first-order vector autoregressive VAR(1) process

$$\begin{bmatrix} \alpha_t \\ \theta_t \\ \omega_t \end{bmatrix} = \mathbf{\Phi} \begin{bmatrix} \alpha_{t-1} \\ \theta_{t-1} \\ \omega_{t-1} \end{bmatrix} + \mathbf{w}_t, \tag{6}$$

where $\mathbf{\Phi}$ is a 3 × 3 matrix of autoregressive coefficients and $\mathbf{w}_t$ is multivariate normal zero-mean white noise with variance-covariance matrix $\mathbf{\Sigma}$. Correlation between α_t, θ_t and ω_t are determined through off-diagonal entries in both $\mathbf{\Sigma}$ and $\mathbf{\Phi}$. Possible model alternatives are obtained by making $\mathbf{\Phi}$ and $\mathbf{\Sigma}$ both diagonal, such that α_t, θ_t and ω_t simplify to independent AR(1) processes. If all entries of $\mathbf{\Phi}$ are zero, α_t, θ_t and ω_t are independent and identically distributed white noise processes. Alternatively, we model each episode as fluctuating directional selection, which can be described by a GLMM with annual random intercept and slope:

$$\begin{aligned} \text{logit}(1-p_i) &= \beta_p^{(0)} + u_{p,t}^{(0)} + (\beta_p^{(1)} + u_{p,t}^{(1)})z_i + \tau_p^m \epsilon_{j(i)};\\ \ln w_i &= \beta_w^{(0)} + u_{w,t}^{(0)} + (\beta_w^{(1)} + u_{w,t}^{(1)})z_i + \tau_w^m \epsilon_{j(i)}. \end{aligned} \tag{7}$$

In this model, $\beta_p^{(0)}$ and $\beta_p^{(1)}$ are fixed intercept and slope respectively for episode *P*, random intercepts and slopes are denoted by $u_{p,t}^{(0)}$ and $u_{p,t}^{(1)}$, which account for the variation among years. These random effects are assumed to be multivariate normal:

$$\begin{pmatrix} u_{p,t}^{(0)} \\ u_{p,t}^{(1)} \end{pmatrix} \sim N\left(\mathbf{0}, \begin{pmatrix} (\sigma_{0,p})^2 & \rho_p\sigma_{0,p}\sigma_{1,p} \\ \rho_p\sigma_{0,p}\sigma_{1,p} & (\sigma_{1,p})^2 \end{pmatrix}\right).$$

Similar explanation applies to the alternative model for episode *W* ($\ln w_i$). As before, z_i, τ_p^m, τ_w^m and $\epsilon_{j(i)}$ have same interpretations as that in Equations 3 and 4.

Since our statistical method relies on model selection, the candidate models we tested include different assumptions for α_t, θ_t and ω_t, or different selection patterns for episode *P* and *W*, among many others.

2.3 | Model selection and inference

All model alternatives were implemented using R package TMB. Briefly, based on a C++ function computing the joint density of the observed data and unobserved random effects, TMB computes the Laplace approximation of the marginal likelihood of the observed data. This is then maximized numerically to obtain maximum likelihood estimates of model parameters and approximate standard errors based on information theory.

We fitted in total 43 different alternative models. Among the candidate models, each selection episode *P* and *W* maybe equipped with either directional selection or stabilizing selection. For the directional selection mode, we tested models with only fixed effects, with random intercepts and with both random intercepts and random slopes. For the stabilizing selection mode, the fitness parameters α_t, θ_t and ω_t were either considered as constant, as three independent AR(1) processes, as jointly following a VAR(1) process, or combinations of them.

Our model selection relies on the measurement of data support for the different models which vary in degree of complexity. We use Akaike information criterion (AIC; Akaike, 1973) based on the observed Fisher information as a model selection criterion (see Burnham & Anderson, 2003 for more details about AIC). The model with lowest AIC value was selected as the best model and the estimates of all parameters together with their approximate standard errors were obtained. All the source code of this study are archived and accessible online.

3 | CASE STUDY RESULTS AND DISCUSSION

3.1 | Model selection procedure

As introduced in section 2.3, in total, 43 candidate models were tested. For brevity, only the selected model and its neighbour models are listed in Table 1. The model numbering is consistent with the model updating sequence in our R code. Updating procedure from model 1 to model 8b can be found in Supporting Information. Based on the best model selected (model 9), the differences of AIC value for each model from the selected model are calculated and listed in column ΔAIC, along with the difference in the number of parameters (Δp). Model 9 with directional selection in episode *P* and stabilizing selection in episode *W* is the best model.

Model 10 with directional selection via both episode *P* and *W* does not improve the model fit. To guarantee that model 9 is indeed the best one among all the candidate models, model 11 to model 14i are neighbour models updated around model 9 for comparison purpose, but none of them improves the model fit. It is worth noting that the performance of model 14g with fixed ω_t is only slightly worse than our selected model, implying a constant ω_t assumption in our study would be reasonable. The estimates of parameters from the selected model (model 9) and from model 14g with constant ω_t are listed in the Supporting Information for comparison.

We also carried out a simulation study (see Supporting Information) to explore the power of our model selection technique in identifying our best model especially against model 14g and 14i. We concluded from the simulation study that our model selection technique has around 80% probability to distinguish the model with fixed ω_t from the one with random ω_t when the variation scale of ω_t being 0.2. This further implies that model 14g might be as good as our selected model. The simulation study also showed that a weak mother effect (e.g. the standard deviation of random mother effects is 0.05) is hard to detect. However, since our selected model reports 6.44 lower AIC values with the estimate of standard deviation of mother effects being 0.041 in episode *W*, we have confidence in the mother effects in the underlying 'true' model. The remaining challenge is that there is no strong evidence for model 9 outperforms model 13, we thus should be cautious when interpreting estimates of correlations between the errors for α_t, θ_t and ω_t.

The selected model (model 9) has stabilizing selection via episode *W*, directional selection via *P* with annual correlated random intercepts and slopes given by

$$\begin{aligned} \text{logit}(1-p_i) &= \beta_p^{(0)} + u_{p,t}^{(0)} + \left(\beta_p^{(1)} + u_{p,t}^{(1)}\right) z_i + \tau_p^m \epsilon_{j(i)}, \\ \ln w_i &= \eta_{w,t(i)}^{(\alpha)} - \frac{\left(z_i - \eta_{w,t(i)}^{(\theta)}\right)^2}{2\left(e^{\eta_{w,t(i)}^{(\omega)}}\right)^2} + \tau_w^m \epsilon_{j(i)}. \end{aligned} \tag{8}$$

Furthermore, the selected model supports VAR(1) process of α_t, θ_t and ω_t in the episode *W*. However, the three processes are correlated through errors instead of the transition matrix $\mathbf{\Phi}$. Mother effects are significant in both episodes. More details about the parameter estimates are given in next section 3.2.

3.2 | Directional selection via probability of clutch failure

Our selected model (Equation 8) indicates directional selection via episode *P* with annual random intercept ($u_{p,t}^{(0)}$) and slope ($u_{p,t}^{(1)}$). The estimates

TABLE 1 A part of model selection procedure of phenotypic selection on breeding time of great tits. The order of models listed below is accordance with the order of models fitting, from model 9 to 14i. ΔAIC and Δp is the difference in AIC and number of parameters p between each model and the best model (model 9). The column of description gives the details of the updated model based on the previous ones. For simplification, the probability of successful brooding is denoted as episode *P* and the mean number of fledglings episode as *W*. The updating procedure from model 1 to model 8a can be found in Supporting Info

Model	ΔAIC	Δp	Description
Directional selection via episode *P* and stabilizing selection via episode *W*			
9	0	0	The selected model formulated as Equation 8
Directional selection for both episode *P* and *W*			
10	104.11	−5	The model formulated as Equation 7 with correlated random intercepts and slopes
Model 9 is the best model so far, test neighbour models with minor changes based on model 9			
11	4.075	7	Add all entries of Φ back
12	14.32	−3	Keep only significant entries in Φ and significant correlations between the errors for α_t, θ_t and ω_t
13	0.54	−2	Keep only significant correlations between the errors for α_t, θ_t and ω_t
Model 9 is still the best model so far, test models with all possible specifications for α_t, θ_t and ω_t, and remove mother effect from each episode			
14	210.47	−6	Change random α_t into fixed, θ_t and ω_t are random
14a	203.98	−4	Change random α_t into fixed, θ_t and ω_t are AR(1)
14b	96.99	−6	Change random θ_t into fixed, α_t and ω_t are random
14c	85.47	−4	Change random θ_t into fixed, α_t and ω_t are AR(1)
14d	24.84	−4	Change random ω_t into fixed, α_t and θ_t are AR(1)
14e	28.64	−2	Change random ω_t into fixed, VAR(1) α_t and θ_t
14f	7.1	−1	Change random ω_t into fixed, VAR(1) α_t and θ_t, add correlation to the errors of α_t and θ_t
14g	3.27	−3	Change random ω_t into fixed, VAR(1) α_t and θ_t with significant entries in Φ, add correlation to the errors of α_t and θ_t
14h	21.1	−1	Remove mother effect from episode *P*
14i	6.44	−1	Remove mother effect from episode *W*

TABLE 2 Estimates (standard errors) and corresponding 95% confidence intervals of model parameters from the selected model (i.e. model 9 of Table 1, only for selection via the probability of successful brooding)

Parameter	Meaning	Estimate (*SE*)	95% CI
$\beta_p^{(0)}$	Fixed intercept	2.946 (0.220)	(2.515, 3.377)
$\beta_p^{(1)}$	Fixed slope	−0.025 (0.005)	(−0.035, −0.015)
$\sigma_{1,p}$	*SD* of random slopes	0.032 (0.004)	(0.024, 0.040)
τ_p^m	*SD* of mother effect	0.701 (0.092)	(0.520, 0.881)
ρ_p	Correlation between random intercepts and slopes	−0.827 (0.054)	(−0.933, −0.720)

of parameters of our interest are listed in Table 2. We estimated the fixed slope, the mean of the annual selection gradient to $\hat{\beta}_p^{(1)} = -0.025$ (red dashed line on the right panel of Figure 1). Given a standard deviation of the random slopes estimated to $\hat{\sigma}_{1,p} = 0.032$, corresponding to selection for early laying 78% of the time, the distribution of selection gradients is shown with the black line in the right panel of Figure 1, which implies that over 22% of the study years experienced positive selection, therefore, favoured late broods. The left panel of Figure 1 shows the annual selection gradient together with error bars representing ± one standard error. The selection favoured early broods in 82% (note that the 78% is obtained with selection distribution while 82% with temporal estimated selection) of the study years, as can be seen from the left panel that most of the selection gradients fall below 0.

This result agrees with the finding from Reed et al. (2013) that females that breed late relative to the food peak (influenced by temperature, see Visser, Holleman and Gienapp (2006)) were more likely to fail to raise any fledglings. Perrins (1965) states that there is a higher proportion of predation in the later part of the season and the young of the later broods are more vulnerable to the predators since the young in the later broods are more noisy and lighter. Maziarz, Wesolowski, Hebda, Cholewa and Broughton (2016) shows that nest losses are mostly due to predation (69% nest failures of a great tit population in Poland) and the risk of nest failure varied with nest cavity attributes. To explore which biotic and abiotic factors best explain the sign and variation in annual directional selection via the probability of successful brooding, more data information concerning these factors are required and this would be one among other interesting expansions of this study. In this selection episode, mother effects contribute to explaining the variation of successful-brooding probabilities and the estimate of the standard deviation τ_p^m is 0.701, as shown in Table 2.

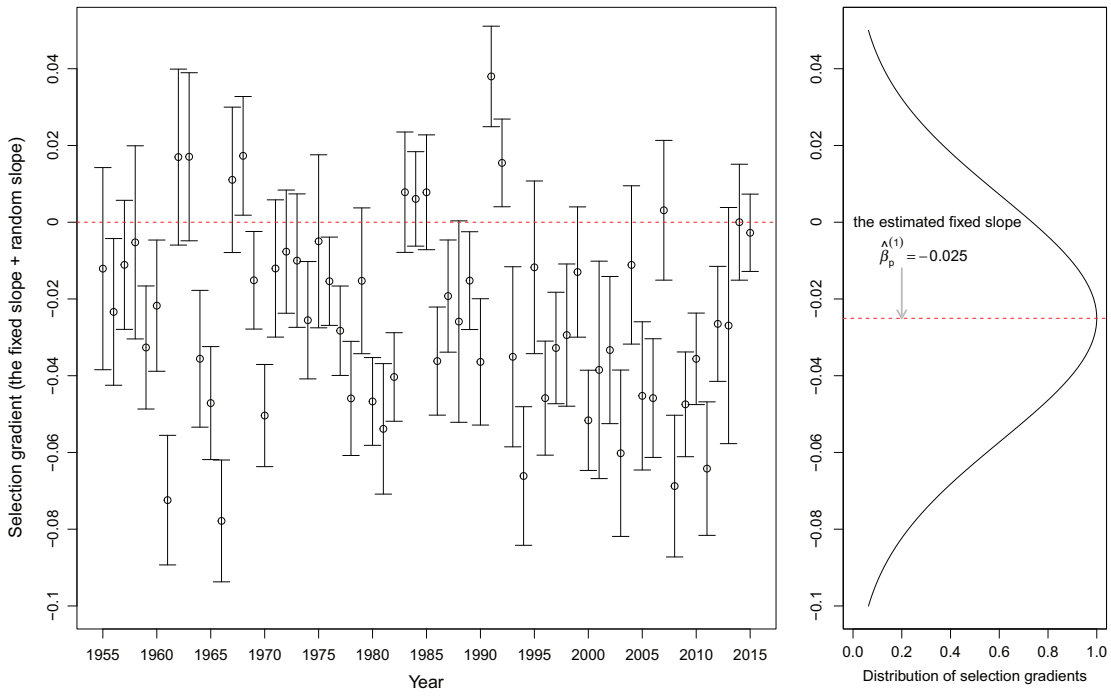

FIGURE 1 Annual directional selection gradient (left panel, defined as the sum of the fixed slope and annual random slope) associated with error bars representing one standard error and the distribution of it (right panel) for episode *P* (selection on laying date via the probability of successful brooding). The red dashed line on the left plot is an indication of 0 and on the right plot is estimated fixed slope (−0.025)

3.3 | Stabilizing selection via the mean number of fledglings

Our selected model indicates that stabilizing selection acts via the mean of the Poisson component. Parameter estimates of the Gaussian fitness function in Equation 4, and the estimates for the parameters involved in the VAR(1) α_t, θ_t and ω_t, along with their confidence intervals are shown in Table 3.

The estimates of the mean of maximum fitness ($\bar{\alpha}$) and optimum ($\bar{\theta}$) are 2 (exponent with base *e* approximates to 7 fledglings) and 18.227 (approximately 18th of April) respectively. Our estimate for the width of the fitness function is much wider than that from Chevin et al. (2015) (47.395 vs. 24.11 days), in which the sum of the fledglings from multiple broods instead of the single brood was treated as the sample unit and the lay dates of only first broods (with a much narrower range) were used. We doubt that the distribution of this summation of multiple broods is well approximated by a Gaussian function and therefore we modelled the number of fledglings from each brood separately, and the second broods were laid in the late breeding season and this might be the reason of a wider fitness function being estimated with our selected model.

The estimates of the standard deviation of α_t, θ_t and ω_t are 0.176, 21.180 and 0.205 respectively. The estimate of standard deviation for θ_t is slightly larger than that from Chevin et al. (2015) (21.18 vs. 11.3 days) and this might partly result from the different datasets we used. In Chevin et al. (2015), the data before 1973 were excluded from their analysis and we therefore also fit the selected model with data only after 1973 for a fairer comparison. It turned out that the estimates with both full and partial datasets are quite close, while the estimates with full data generally have less uncertainty (narrower %95 confidence intervals). The detailed comparison can be found in Supporting information. The estimated variance in ω_t (0.042) translates to a coefficient of variation for $e^{\eta_{\omega,t}^{(\omega)}}$ of $\sqrt{e^{0.042}-1} = 0.207$, that is, quite large fluctuation in the width of the fitness function. When conducting model selection we fitted a model with fixed ω_t (model 14g in Table 1) over study period, however, it turned out the model fit did not improve much when ω_t is taken random as in our selected model. In addition, by comparing the standard deviations of parameter estimates from the models with fixed and random ω_t reported in Supporting Information, we find that uncertainties of parameter estimates are comparable. These imply that the whole analysis would not change much if in our study the constant ω_t assumption was made.

The autocorrelation estimates of α_t ($\hat{\phi}_{\alpha,\alpha}$) and θ_t ($\hat{\phi}_{\theta,\theta}$) are 0.334 and 0.524, respectively, but ω_t is not autocorrelated in our selected model. The estimate of $\phi_{\theta,\theta}$ in Chevin et al. (2015) was 0.2472 with a wide 95% confidence interval (−0.1745, 0.626). While our selected

TABLE 3 Estimates(standard errors) and corresponding 95% confidence intervals of model parameters with the selected model (only for selection via the mean number of fledglings)

Parameter	Meaning	Estimate (*SE*)	95% CI
$\bar{\alpha}$	Mean of process $\eta_{w,t}^{(\alpha)}$	2.000 (0.036)	(1.929, 2.071)
$\bar{\theta}$	Mean of process $\eta_{w,t}^{(\theta)}$	18.227 (5.826)	(6.808, 29.647)
$e^{\bar{\omega}}$ (days)	Mean of process $e^{\eta_{w,t}^{(\omega)}}$	47.395 (3.234)	(41.056, 53.734)
$\gamma_{\alpha,\alpha}$	*SD* of α_t	0.176 (0.024)	(0.129, 0.224)
$\gamma_{\theta,\theta}$	*SD* of θ_t	21.180 (3.422)	(14.473, 27.888)
$\gamma_{\omega,\omega}$	*SD* of ω_t	0.205 (0.049)	(0.110, 0.300)
$\phi_{\alpha,\alpha}$	Autocorrelation of α_t	0.334 (0.122)	(0.094, 0.574)
$\phi_{\theta,\theta}$	Autocorrelation of θ_t	0.524 (0.110)	(0.310, 0.739)
σ_α	*SD* of errors of α_t	0.166 (0.023)	(0.120, 0.212)
σ_θ	*SD* of errors of θ_t	18.034 (2.808)	(12.531, 23.538)
σ_ω	*SD* of errors of ω_t	0.205 (0.049)	(0.110, 0.300)
$\rho_{\alpha,\theta}$	Correlation between the errors of α_t and θ_t	−0.592 (0.125)	(−0.837, −0.346)
$\rho_{\alpha,\omega}$	Correlation between the errors of α_t and ω_t	−0.357 (0.287)	(−0.920, 0.206)
$\rho_{\theta,\omega}$	Correlation between the errors of θ_t and ω_t	−0.307 (0.254)	(−0.806, 0.191)
τ_w^m	*SD* of mother effect	0.041 (0.013)	(0.015, 0.066)

model reported a significant and larger estimate of $\phi_{\theta,\theta}$ with narrower confidence interval (0.310, 0.739). With the result from the simulation study, even this larger estimate may be potentially underestimated. The estimates of the standard deviations of errors of VAR(1) α_t, θ_t and ω_t (σ_α, σ_θ, σ_ω) are also listed in Table 3, along with estimates of correlations of the correlated noises. Even though our result indicates that the VAR(1) stochastic processes α_t, θ_t and ω_t are correlated through errors $\mathbf{w}_t$ not through transition matrix $\mathbf{\Phi}$, we are conservative in interpreting the estimates of $\rho_{\alpha,\omega}$ and $\rho_{\theta,\omega}$ since the candidate model 13 with only $\rho_{\alpha,\theta}$ reported almost the same AIC value as our best model. The estimate of standard deviation of mother effect is 0.041, implying that the mean of X_i from broods produced by the same mother are weakly correlated to each other.

The estimated optimum phenotype is shown in Figure 2 with a solid blue line. It fluctuates over the study period with an obvious downward trend. The mean within-year laying dates (denoted with black dots) also show a downward trend but the advance is not as strong as the optimum, resulting in increasing mistiming between the optimal laying date and the mean within-year laying date, which is in line with the finding from previous study of the same population (e.g. Chevin et al., 2015; Reed et al., 2013; Visser & Both, 2005; Visser et al., 1998). Since the reproductive fitness of the great tits depends strongly on the mismatch with food phenology, mistiming in our case therefore equals mismatch, even though the food resource phenology is not considered in our study (see Visser and Gienapp (2019) for the difference between mistiming and mismatch). One explanation for the mismatch is that females might be unwilling to breed at the optimal date in terms of the offspring fitness because of higher energetic cost of producing and incubating earlier in harsh environment where it is cold and food is scarce, mismatching by a few days might therefore be optimal for the sake of parental fitness (Te Marvelde, Webber, Meijer & Visser, 2011). Beside this optimal mismatch hypothesis, another leading explanation (the cues hypothesis) is that the cues used for timing laying are no longer accurately predicting the phenology of the food peak (see Visser et al., 2012 for more details on these two hypotheses).

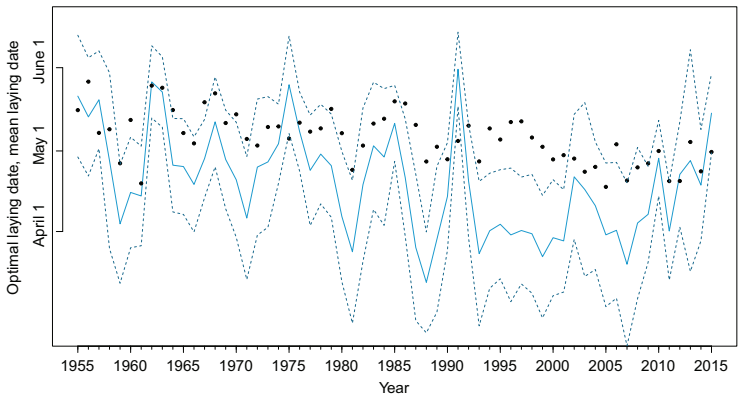

FIGURE 2 Position of optimal laying date over study period from 1955 to 2015. The estimated movement of optimal laying date from the selected model is shown with solid blue line, along with its 95% confidence interval (dashed blue lines). The black dots are the observed within-year mean laying dates

3.4 | Model evaluation

The performance of our selected model is evaluated by visualizing the observed and predicted number of fledglings for each year. Each panel in Figure 3 shows the observed (dots in the panels) and predicted number of fledglings (dark solid line) against laying date for a specified year (from 1955 to 2015). Our analysed data includes three brood types represented by three colours in the plots. The red, green and blue dots correspond to first, replacement and second broods respectively. The solid grey curve represents nonparametric loess regression through the points with the dashed grey lines being associated 95% confidence band. With our selected model,

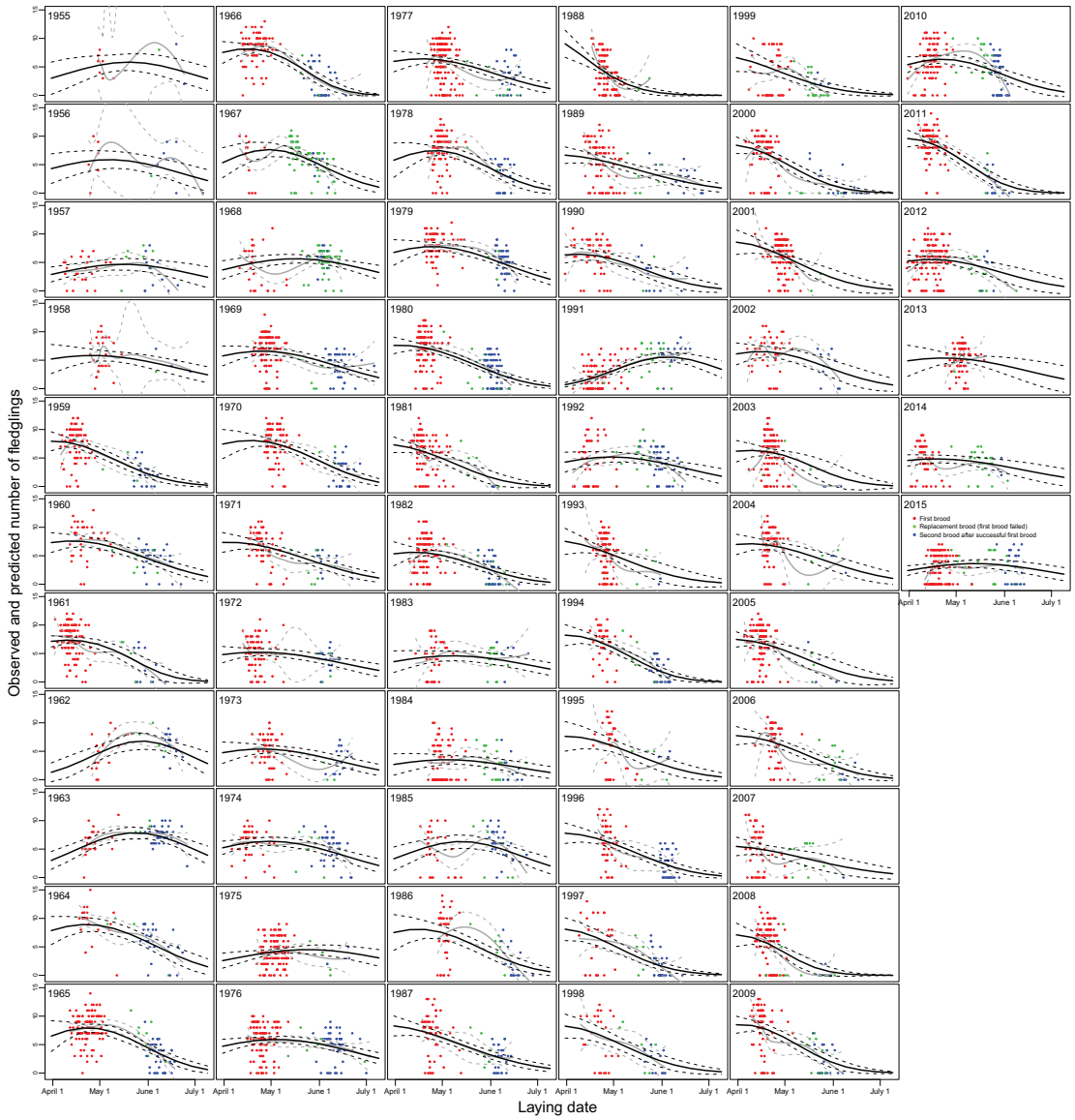

FIGURE 3 Observed and predicted number of fledglings ($E(Y_i|p_i, w_i)$) against the laying date for each year. The blue, red and green dots represent the observed number of fledglings from first, replacement and second broods respectively. The grey curve is loess regression (with default degree of smoothing = 0.75) through the scatter points with 95% confidence band (dashed grey lines). The black line indicates the number of fledglings predicted with our selected model conditional on zero mother random effects with dashed black lines representing its 95% confidence band. The 95% confidence band was calculated by multiplying the standard errors reported with TMB by the 2.5 and 97.5th percentiles of the normal distribution

the dark curve shows the predicted number of fledglings at laying dates conditional on zero mother effect over the whole breeding season, with the dashed dark lines representing associated 95% confidence band again. The figure indicates a good fit of our selected model to the data as we can see that the dark lines lie within the loess confidence bands for all the years. For most of the years, the prediction of number of fledglings peaked at early breeding season when the first broods were laid except year 1991, when a late frost hit the population and the plot validates our expectation of a very late optimum estimate.

4 | CONCLUSION AND POSSIBLE EXTENSIONS

Thanks to the new techniques such as TMB for fast likelihood computation for non-Gaussian and nonlinear models, the use of state-space models for analysing ecological systems is increasing (for example Cadigan, 2015; Albertsen, Nielsen & Thygesen, 2016; Auger-Méthé et al., 2017). The conditional independence structure in state-space models yield a sparse precision matrix for the joint distribution of the data and the random effects (Kristensen et al., 2015) and TMB takes maximal advantage of this sparseness structure (through automatic sparsity detection) in its computation of the Laplace approximation. Therefore, using state-spaces models coupled with TMB makes estimating a large number of parameters and random effects which is usually the case in modelling complicated biological processes or ecological systems, possible. Compared with the models and approaches adopted by previous studies on fluctuating selection, our method based on SSM, GLMM and TMB has several advantages. First, state-space models allow us to explore two correlated fitness components simultaneously, instead of measuring different fitness components independently. Second, due to the flexibility of SSMs, parameters can be estimated efficiently with little computational effort. Third, the formulation of our theoretical models turns out to be more realistic to account for directional selection and non-Gaussian fitness residual, as GLMMs. Our results from the great tit case study partly agree with the findings from previous studies on the same population, and due to the VAR(1) formulation for the fitness parameters we could gain more in terms of the underlying patterns of the fluctuating selection. For the researchers who are interested in applying our method to their data either for modelling fluctuating selection or general ecological systems with VAR(1) stochastic processes, it is worth to mention that TMB has no built-in probability function for modelling VAR(1). Our study can serve as a template for this as well as for conducting model selection with TMB.

In our study, we treated fluctuations in properties of the Gaussian fitness function as a vector autoregressive process. In principle, our approach can also accommodate other autocovariance structures, such as vector autoregressive moving-average (ARMA) models (see Wei, 2006 for the definition). Besides, in our statistical model, the random mother effect $\epsilon_{j(i)}$ is assumed to be same for the two episodes but vary in magnitude, which implies that a mother that is likely to have complete brood failure will be more likely to have a low number of fledglings (with correlation 1). To relax this assumption, the mother effects can be treated differently for the two episodes and assumed to be multivariate Gaussian distributed $(\epsilon_{p,j(i)}, \epsilon_{w,j(i)})^T \sim N(0,\Sigma)$ with Σ being a covariance matrix. Furthermore, the number of fledglings is chosen as the selection component so that the estimates could be compared to those from Chevin et al. (2015), which claims that using the number of recruits may cause more uncertainty in estimates of parameters due to the much larger coefficient of variation in the number of recruits. However, in some previous studies (e.g. Reed et al., 2013), the fecundity component of fitness is measured as the number of recruits surviving to the next breeding season instead of the number of individuals surviving to become fledglings. As claimed by Naef-Daenzer and Grüebler (2016), using the number of fledglings as a proxy for fitness may be misleading in inference of evolutionary significance since reproductive success can be completely altered by many causal factors driving the adaptations which operate during the post-fledgling period, and thereby change the juveniles' fate from fledgling to independence. Therefore, it would be interesting to expand our model to incorporate both pre- and post-fledgling period, such as chicks' survival and recruitment probability, as well as a female's survival, into a comprehensive life-history framework for the lifetime selection exploration.

Our study demonstrates a technique of estimating fluctuating selection in cases where ecological covariates are not available. To understand whether observed shift in selection are biologically meaningful, however, it is important to elucidate the ecological drivers of fluctuations in selection. Empirical investigations of the causal mechanisms driving such selection dynamism are needed before the development of novel analytical and statistical techniques. In our great tit case, for example, the peak movement might be affected by the height of the caterpillar peak, the mean breeding timing relative to the caterpillar peak and the breeding density. The width of the fitness function is likely being affected by the height and probably the width of the caterpillar peak (Visser et al., 2006). The location of optimum might be influenced by environmental variables (e.g. Chevin et al., 2015; Gienapp et al., 2013). However, the biotic interactions coupled with other abiotic factors playing a direct or indirect role in the selective process could likely make analysis much more complicated. Other extensions include analysis of correlational selection on multivariate traits and estimating the temporal-spatial variation and correlation in fluctuating selection.

ACKNOWLEDGEMENTS

This work was supported by the Research Council of Norway through its Centres of Excellence funding scheme (project number 223257 to CBD).

AUTHORS CONTRIBUTIONS

M.E.V. provided the data; J.T. conceived the idea and initiated the statistical model; Y.C. analysed the data and conducted the analyses;

Y.C. wrote the initial draft with input from J.T.; all authors contributed to revisions on later manuscript versions and gave final approval for publication.

DATA AVAILABILITY STATEMENT

All the necessary data and source code to carry out the analyses in this study are available in the Dryad Digital Repository https://doi.org/10.5061/dryad.q4q8r89 (Cao, Visser & Tufto, 2019).

REFERENCES

Akaike, H. (1973). Information theory and an extension of the maximum likelihood principle. In *2nd international symposium on information theory, Akademiai Kiado, Budapest, 1973* (pp. 267–281).

Albertsen, C. M., Nielsen, A., & Thygesen, U. H. (2016). Choosing the observational likelihood in state-space stock assessment models. *Canadian Journal of Fisheries and Aquatic Sciences*, *74*(5), 779–789.

Auger-Méthé, M., Albertsen, C. M., Jonsen, I. D., Derocher, A. E., Lidgard, D. C., Studholme, K. R., … Flemming, J. M. (2017). Spatiotemporal modelling of marine movement data using template model builder (TMB). *Marine Ecology Progress Series*, *565*, 237–249.

Barton, N. H., & Keightley, P. D. (2002). Multifactorial genetics: understanding quantitative genetic variation. *Nature Reviews Genetics*, *3*(1), 11.

Bell, G. (2010). Fluctuating selection: the perpetual renewal of adaptation in variable environments. *Philosophical Transactions of the Royal Society B: Biological Sciences*, *365*(1537), 87–97.

Bull, J. (1987). Evolution of phenotypic variance. *Evolution*, *41*(2), 303–315.

Burnham, K. P., & Anderson, D. R. (2003). *Model selection and multimodel inference: a practical information-theoretic approach*. Berlin: Springer Science & Business Media.

Cadigan, N. G. (2015). A state-space stock assessment model for northern cod, including under-reported catches and variable natural mortality rates. *Canadian Journal of Fisheries and Aquatic Sciences*, *73*(2), 296–308.

Calsbeek, B. (2011). Exploring variation in fitness surfaces over time or space. *Evolution*, *66*(4), 1126–1137.

Cao, Y. H., Visser, M. E., & Tufto, J. (2019). Data from: A time series model for estimating temporal variation in phenotypic selection on laying dates in a Dutch great tit population. *Dryad Digital Repository*. https://doi.org/10.5061/dryad.q4q8r89

Chevin, L.-M., Visser, M. E., & Tufto, J. (2015). Estimating the variation, autocorrelation, and environmental sensitivity of phenotypic selection. *Evolution*, *69*(9), 2319–2332.

Cohen, D. (1966). Optimizing reproduction in a randomly varying environment. *Journal of Theoretical Biology*, *12*(1), 119–129.

Futuyma, D. J. (2006). *Evolutionary biology* (3rd ed.). New York: W. H. Freeman; Basingstoke: Palgrave [distributor].

Gamelon, M., Tufto, J., Nilsson, A. L. K., Jerstad, K., Røstad, O. W., Stenseth, N. C., … Sæther, B. E. (2018). Environmental drivers of varying selective optima in a small passerine: a multivariate, multiepisodic approach. *Evolution*, *72*(11), 2325–2342

Gienapp, P., Lof, M., Reed, T. E., McNamara, J., Verhulst, S., & Visser, M. E. (2013). Predicting demographically sustainable rates of adaptation: can great tit breeding time keep pace with climate change? *Philosophical Transactions of the Royal Society B: Biological Sciences*, *368* (1610).

Gienapp, P., Reed, T. E., Visser, M. E. (2014). Why climate change will invariably alter selection pressures on phenology. *Proceedings of the Royal Society B: Biological Sciences 281*(1793), 20141611.

Hedrick, P. W. (2006). Genetic polymorphism in heterogeneous environments: the age of genomics. *Annual Review of Ecology, Evolution, and Systematics*, *37*(1), 67–93.

Kristensen, K., Nielsen, A., Berg, C. W., Skaug, H., & Bell, B. (2015). TMB: automatic differentiation and Laplace approximation. *arXiv preprint arXiv:1509.00660*.

Lande, R., & Shannon, S. (1996). The role of genetic variation in adaptation and population persistence in a changing environment. *Evolution*, *50*(1), 434–437.

Maziarz, M., Wesolowski, T., Hebda, G., Cholewa, M., & Broughton, R. K. (2016). Breeding success of the Great Tit Parus major in relation to attributes of natural nest cavities in a primeval forest. *Journal of Ornithology*, *157*(1), 343–354.

Morrissey, M. B., & Hadfield, J. D. (2012). Directional selection in temporally replicated studies is remarkably consistent. *Evolution*, *66*(2), 435–442.

Naef-Daenzer, B., & Grüebler, M. U. (2016). Post-fledging survival of altricial birds: ecological deter minants and adaptation. *Journal of Field Ornithology*, *87*(3), 227–250.

Perrins, C. M. (1965). Population fluctuations and clutch-size in the Great Tit, Parus major L. *The Journal of Animal Ecology*, 601–647.

Perrins, C. M. (1979). *British tits* (Vol. *62*). New York, NY: HarperCollins.

Post, E., & Forchhammer, M. C. (2007). Climate change reduces reproductive success of an arctic herbivore through trophic mismatch. *Philosophical Transactions of the Royal Society B: Biological Sciences*, *363*(1501), 2367–2373.

Reed, T. E., Jenouvrier, S., & Visser, M. E. (2013). Phenological mismatch strongly affects individual fitness but not population demography in a woodland passerine. *Journal of Animal Ecology*, *82*(1), 131–144.

Revell, L. J. (2007). The G matrix under fluctuating correlational mutation and selection. *Evolution: International Journal of Organic Evolution*, *61*(8), 1857–1872.

Rue, H., Martino, S., & Chopin, N. (2009). Approximate bayesian inference for latent gaussian models by using integrated nested laplace approximations. *Journal Of The Royal Statistical Society Series B: (Statistical Methodology)*, *71*(2), 319–392.

Scheiner, S. M. (1993). Genetics and evolution of phenotypic plasticity. *Annual Review of Ecology and Systematics*, *24*(1), 35–68.

Siepielski, A. M., DiBattista, J. D., & Carlson, S. M. (2009). It's about time: the temporal dynamics of phenotypic selection in the wild. *Ecology Letters*, *12*(11), 1261–1276.

Svardal, H., Rueffler, C., & Hermisson, J. (2011). Comparing environmental and genetic variance as adaptive response to fluctuating selection. *Evolution*, *65*(9), 2492–2513.

Te Marvelde, L., Webber, S. L., Meijer, H. A. J., & Visser, M. E. (2011). Mismatched reproduction is energetically costly for chick feeding female great tits. *Functional Ecology*, *25*(6), 1302–1308.

Townsend, A. K., Sillett, T. S., Lany, N. K., Kaiser, S. A., Rodenhouse, N. L., Webster, M. S., Holmes, R. T. (2013). Warm springs, early lay dates, and double brooding in a North American migratory songbird, the black-throated blue warbler. *PLoS ONE*, *8*(4), 59467.

Tufto, J. (2015). Genetic evolution, plasticity, and bet-hedging as adaptive responses to temporally autocorrelated fluctuating selection: a quantitative genetic model. *Evolution*, *69*(8), 2034–2049.

Van Tienderen, P. H., & Koelewijn, H. P. (1994). Selection on reaction norms, genetic correlations and constraints. *Genetics Research*, *64* (2), 115–125.

Visser, M. E., & Both, C. (2005). Shifts in phenology due to global climate change: the need for a yardstick. *Proceedings of the Royal Society B: Biological Sciences*, *272*(1581), 2561–2569.

Visser, M. E., & Gienapp, P. (2019). Evolutionary and demographic consequences of phenological mismatches. *Nature Ecology and Evolution*, *3*, 879–885.

Visser, M. E., Gienapp, P., Husby, A., Morrisey, M., de la Hera, I., Pulido, F., Both, C. (2015). Effects of spring temperatures on the strength of

selection on timing of reproduction in a long-distance migratory bird. *PLoS Biology*, *13* (4), 1–17.
Visser, M. E., Holleman, L. J., & Gienapp, P. (2006). Shifts in caterpillar biomass phenology due to climate change and its impact on the breeding biology of an insectivorous bird. *Oecologia*, *147* (1), 164–172.
Visser, M. E., Marvelde, L. te, & Lof, M. E. (2012). Adaptive phenological mismatches of birds and their food in a warming world. *Journal of Ornithology*, *153*, 75–84.
Visser, M. E., Noordwijk, A.V., Tinbergen, J. M., Lessells, C. M. (1998). Warmer springs lead to mistimes reproduction in Great Tits (Parus major). *Proceedings of the Royal Society B*, *265*(1408), 1867–1870.
Wei, W. (2006). Time series analysis: Univariate and multivariate methods. (2 ed.,). Boston, MA: Pearson Addison Wesley.
Zhang, X. S., & Hill, W. G. (2005). Evolution of the environmental component of the phenotypic variance: stabilizing selection in changing environments and the cost of homogeneity. *Evolution*, *59*(6), 1237–1244.

SUPPORTING INFORMATION

Additional supporting information may be found online in the Supporting Information section at the end of the article.

How to cite this article: Cao Y, Visser ME, Tufto J. A time series model for estimating temporal variation in phenotypic selection on laying dates in a Dutch great tit population. *Methods Ecol Evol*. 2019;10:1401–1411. https://doi.org/10.1111/2041-210X.13249

Supporting Information (SI) for

A time series model for estimating temporal variation in phenotypic selection on laying dates in a Dutch great tit population

About TMB

Template Model Builder (TMB; Kristensen, Nielsen, Berg, Skaug, & Bell, 2015)) is an R package for fitting statistical latent variable models. It is functionally similar to ADMB (Fournier et al., 2012). The joint likelihood for the data and the random effects are defined by the user as a C++ template function. Then the package evaluates and maximizes the Laplace approximation of the marginal likelihood where the random effects are automatically integrated out. This approximation is achieved by using reverse-mode automatic differentiation (up to order three) of the joint likelihood. The combination of reverse-mode automatic differentiation and the Laplace approximation for high-dimension integrals allows for the efficient fitting of complex (nonlinear, non-Gaussian, and hierarchical) models with large multivariate data sets to perform parameter estimation (Fournier et al., 2012). TMB takes maximal advantage of sparseness structure (Kristensen et al., 2015) and the first derivatives of the Laplace approximation obtained with automatic differentiation of the negative log-likelihood can be used by other approaches such as hybrid MCMC.

More details on study population

The great tit is 18–20g small passerine bird species widespread throughout European woodlands and gardens. As a cavity nester, it readily accepts nest-boxes for breeding, which allows monitoring of the whole population if a surplus of nest-boxes is provided (Harvey, Greenwood, & Perrins, 1979). The study area consists of mixed pine-deciduous woodland on poor sandy soils. From 1955 to 2015, more nest boxes than required were placed in the study area at approximately constant availability. On average the ratio of nest boxes to breeding females was around $3:1$ in a typical year. During the breeding season from April to June/July, nest boxes were visited once per week. At each visit, the number of eggs or nestlings was counted and nestlings were given metal leg rings on day 7 and the parents caught on the nest using a spring trap. For some years clutch or brood size manipulation experiments were carried out, which possibly affected fledgling production or recruitment probability, therefore, manipulated broods were excluded from our analysis. We also deleted 35 third clutch observations for simplifying the comparison between the different brood types. We also deleted the records with uncertainty of the brood type, and clutch size being smaller than number of fledglings. Unknown females were not included in our analyses, as their mother effects as random effects in the model could not be determined. Eventually, 5892 out of 6353 records were kept for our analysis.

Simulation study

A simulation study was carried out to test the power of our method in identifying the best model. We simulated laying dates z which stabilizing selection acts on with a mixture of normal distribution $0.7N(23, 7.5) + 0.3N(62, 10.5)$, which is close to the reality of the Dutch great tit population. We considered 50 years and for each year the sample size was drawn from a Poisson distribution with a mean of $n = 100$ individuals. To simplify the simulation study, we considered stabilizing selection via the expected number of fledglings (episode W) while the zero-inflated probability (episode P) was kept as a fixed parameter (set to 0.12). In terms of the parameters in equation (3) and (4) in the main text, vector $(\bar{\alpha}, \bar{\theta}, \bar{\omega})$ was set to $(2, 18, log(45))$ and the vector of standard deviation of the random effects $(\sigma_\alpha, \sigma_\theta, \sigma_\omega)$ was set to $(0.2, 18, 0.2)$. For brevity the variance-covariance matrix $\mathbf{\Sigma}$ was set diagonal and only $\phi_{\alpha,\alpha}$ and $\phi_{\theta,\theta}$ in the transition matrix Φ were considered as non-zero. They were set to be equal ($\phi_{\alpha,\alpha} = \phi_{\theta,\theta}$) and took values from $(0, 0.1, 0.25, 0.5, 0.75, 0.9)$. The standard deviation of random mother effects was set to 0.05 and added only to episode W.

Since there is a potentially long list of candidate models, we did not fit all the possible models and instead considered, in addition to the true model, five models that can help us to test if our model selection procedure has the power to: identify the zero-inflation probability as a parameter of a selection episode; distinguish models with and without fluctuation in ω_t; identify the auto-correlation parameters in $\mathbf{\Phi}$; distinguish models with and without off-diagonal parameters in $\mathbf{\Phi}$; identify random mother effects in the 'true' model. Specifically, based on the true model we fitted (i) a model with zero-inflation probability regressed against laying dates with random intercepts but without random slopes; (ii) a model with fixed ω_t; (iii) a model with all entries in $\mathbf{\Phi}$ equal to zero; (iv) a model with 2×2 upper-left non-zero entries in $\mathbf{\Phi}$; (v) a model without random mother effects. For each value of $\phi_{\alpha,\alpha}$ and $\phi_{\theta,\theta}$, we ran 100 simulations and for each simulation we compared the reported AIC between the true model and each of the alternative models respectively. The true model was selected against the alternative model only when the AIC of it is at least two points lower than that of the alternative model.

Fig. S1 shows the simulation result. The left plot shows the percentage of cases for which the true model was selected over each of the alternative models against the actual auto-correlation values used in the simulations. It is clear that when zero-inflation probability is only a fixed parameter in the model, the model selection procedure never wrongly favours the model with fluctuating zero-inflation probability. When ω_t was set to fixed in an alternative model, the true model with random ω_t was detected in approximately 80% of the simulations. If $\phi_{\alpha,\alpha}$ and $\phi_{\theta,\theta}$ were excluded from the true model, it then reduced to an alternative model with α_t, θ_t and ω_t following iid processes. The true model (including auto-correlation) is rarely selected as best over the alternative model when the auto-correlation value is as small as 0.1. However, when the

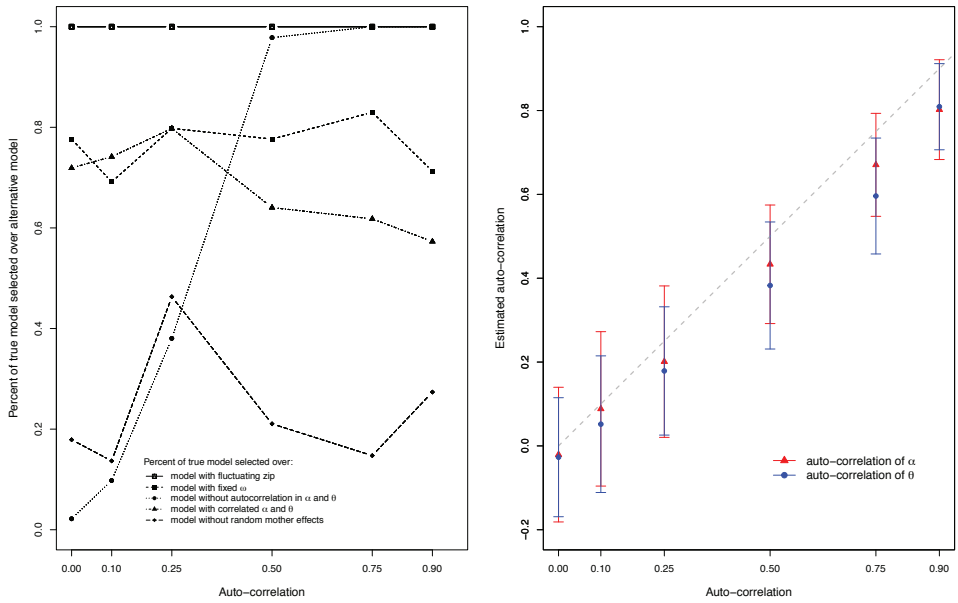

Figure S1: Left: test the power of our method. Each of the line in the plot shows the percentage of our true model was selected against an alternative model out of total 100 simulations. The x axis is the actual values of $\phi_{\alpha,\alpha} = \phi_{\theta,\theta}$ used in simulations. The five lines represent five alternative models that the true model were compared with and the true model was chosen by at least two points lower in AIC than the alternative model. The five alternative models are described in the legend. Right: estimated auto-correlation ($\phi_{\alpha,\alpha}$ and $\phi_{\theta,\theta}$) in all the simulations. The red triangles represent the mean of $\hat{\phi}_{\alpha,\alpha}$ under each setting of the auto-correlation, with error bars representing $\pm$ one standard deviation of the estimates over 100 simulations. The similar explanation applies to $\hat{\phi}_{\theta,\theta}$, which is shown with blue color. The dashed grey line plots the expected value if the MLEs are unbiased.

auto-correlation magnitude increased to 0.5, in over 90% of the simulations the AR(1) structure in α_t and θ_t can be detected. When cross-correlation between α_t and θ_t ($\phi_{\alpha,\theta}$, $\phi_{\theta,\alpha}$) was added to the true model, only in around 60% of the simulations was the true model selected against the more complex alternative model. It is even more challenging when the random mother effects were excluded from the true model, that in only around 20% of the simulations that the true model with random mother effects was chosen.

The right plot in Fig. S1 shows the estimated auto-correlation against the true auto-correlation used in the simulations. Red and blue color corresponds to $\phi_{\alpha,\alpha}$ and $\phi_{\theta,\theta}$ respectively. The triangles and round dots show the mean estimate of $\phi_{\alpha,\alpha}$ and $\phi_{\theta,\theta}$ respectively with error bars representing one standard deviation of all the estimates over 100 simulations. The dashed grey line represents the expected value if the MLEs are unbiased and it goes across all the error bars of $\hat{\phi}_{\alpha,\alpha}$. Estimating $\phi_{\theta,\theta}$ accurately turns more difficult than that for $\phi_{\alpha,\alpha}$ indicated by the larger deviation from the unbiased MLEs.

To sum up, our model fitting and model selection procedure has promising power to capture the basic structure (fixed zero-inflation probability, fluctuated ω_t and auto-correlation in α_t and θ_t) of the true model. However, it also shows that the cross-correlation between the fitness parameters might be overestimated and therefore wrongly included in the selected model. In addition, cautions should be made when excluding random mother effects from the model especially when the models with and without random mother effects report similar AIC values since the random mother effects might be too small to be detected with AIC. At last, both our simulation study and the one in Chevin, Visser, and Tufto (2015) shows that the auto-correlations in the fitness parameters are potentially underestimated.

Supplementary model selection procedure

In the main text we have shown the model selection procedure only for the best model and the models around it. The updating procedure from a null model to the best model is supplemented in Table S1. Model 1 is consistent with stabilizing selection via episode W and episode P and the fitness function parameters remain unchanged across years but vary across episode W and P. Based on the estimates of the parameters in model 1, we changed stabilizing selection into directional selection for episode W (model 2, 2a, 2b, 2c) or for episode P (model 3, 3a, 3b, 3c). The models with correlated random intercepts and slopes (model 2c and 3c) perform best in each situation. Next, from model 4 to model 8b, we updated each model (model 1, 2c, 3c) such that α_t, θ_t and ω_t are either white noise (model 4 to model 4e, note that model 4a, 4c, 4e are hard to get converged, thus they were updated through model 4, 4b and 4d respectively), or AR(1) (model 5 to model 5b), or VAR(1) (model 6 to model 6b) processes. Model 7, 7a, 7b, 7c were updated with only significant entries of Φ kept. Auto-correlations between errors of α_t, θ_t and ω_t were introduced into model

8, 8a and 8b. So far, model 8 reports the smallest AIC, therefore, mother effect was added to it (model 9), and model 9 was eventually confirmed to be the best model, as have shown in the main text.

It is worth to mention that our candidate models were generally updated from the simple ones to the complicated ones and therefore the subsequent models are subject to the choice of the initial models. The choice should be made carefully especially when the initial models report similar AIC values. In this case, one suggestion is that the subsequent models can be updated simultaneously based on the competitive initial models and another suggestion is the neighbor models of the selected model should be carefully tested to ensure it is indeed the best one.

Table S1: Supplementary Model selection procedure of phenotypic selection on breeding time of great tits. The order of models listed below is accordance with the order of models fitting, from model 1 to 9. The following model selection procedure can be found in the main text. ΔAIC and Δp is the difference in AIC and number of parameters p between each model and the best model (model 9). The column of description gives the details of updating model based on the previous ones. For simplification, the probability of successful-brooding component is denoted as episode P and the mean number of fledglings as episode W.

Model	**ΔAIC**	**Δp**	**Description**
1	1246.99	-12	$\eta_{s,t}^{(\alpha)}$, $\eta_{s,t}^{(\theta)}$, $\eta_{s,t}^{(\omega)}$ fixed across t, vary across s
based on model 1, change stabilizing selection via episode P into directional selection			
2	1246.01	-13	only with fixed intercept and slope
2a	1011.41	-12	add random intercepts on model 2
2b	919.21	-11	add random slopes on model 2a
2c	877.37	-10	add covariance to random intercepts and slopes on model 2b
based on model 1, change stabilizing selection via episode W into directional selection			
3	1247.54	-13	only with fixed intercept and slope
3a	708.48	-12	add random intercepts on model 3
3b	509.98	-11	add random slopes on model 3a
3c	437.33	-10	add covariance to random intercepts and slopes on model 3b
change fixed α_t, θ_t and ω_t into white noise			
4	241.24	-10	based on model 1, white noise α_t and ω_t, fixed θ_t
4a	114.45	-9	based on model 4, white noise α_t, θ_t and ω_t
4b	114.08	-8	based on model 2c, white noise α_t and ω_t, fixed θ_t
4c	110.11	-7	based on model 4b, white noise α_t, θ_t and ω_t
4d	129.33	-8	based on model 3c, white noise α_t and ω_t, fixed θ_t

Continued on next page

Table S1 – continued from previous page

Model	ΔAIC	Δp	Description
4e	96.48	-7	based on model 4d, white noise α_t, θ_t and ω_t
change random α_t, θ_t and ω_t into AR(1)			
5	81.74	-6	based on model 4a, AR(1) α_t, θ_t and ω_t
5a	40.84	-4	based on model 4c, AR(1) α_t, θ_t and ω_t
5b	74.57	-4	based on model 4e, AR(1) α_t, θ_t and ω_t
change random α_t, θ_t and ω_t into VAR(1)			
6	89.02	0	based on model 4a, VAR(1) α_t, θ_t and ω_t
6a	88.83	2	based on model 4c, VAR(1) α_t, θ_t and ω_t
6b	80.59	1	based on model 4e, VAR(1) α_t, θ_t and ω_t
keep only significant (at significance statistics 0.05) entries in Φ			
7	82.17	-7	update based on model 6, AR(1) α_t and θ_t
7a	39.13	-5	no significant entries in Φ in model 6a, so update based on model 5a, AR(1) α_t and θ_t
7b	76.48	-5	update based on model 6b, AR(1) α_t and θ_t
7c	76.1	-6	update based on model 6b, AR(1) α_t
add correlations to the errors of α_t, θ_t and ω_t			
8	57.8	-3	update based on model 5, which is the best model so far for stabilizing selection for both episode P and W
8a	19.1	-2	update based on model 7a, which is the best model so far for directional selection via P
8b	74.82	-1	update based on model 5b, which is the best model so far for directional selection via episode W
add mother effect			
9	0	0	update based on model 8a, which is the best model so far (directional selection via episode P and stabilizing selection via episode W)

Supplementary model evaluation

In addition to the model evaluation in the main text, we here further illustrate the performance of our selected model in predicting successful-brooding indices and non-zero number of fledglings. Each panel in Fig. S2 shows the observed indices and the predicted probability of successful-brooding against laying date for a specified year (from 1955 to 2015). Our analyzed data includes three brood types. The red, green and blue dots represent the observed indices of successful-brooding for first broods, replacements broods (first broods failed) and second broods (first broods succeeded) respectively. The solid grey curve represents nonparametric loess regression through the points with the dashed grey lines being associated 95% confidence band. The dark curve shows the predicted probability of successful-brooding at laying dates along the whole breeding season and conditional on zero random mother effects. It can be shown that it is a function of both the zero inflation probability and the mean number of fledglings:

$$\begin{aligned} P(Y_i > 0 \mid p_i, w_i) &= 1 - P(Y_i = 0 \mid p_i, w_i) \\ &= 1 - P(I_i = 0 \mid p_i) - P(X_i = 0 \mid I_i = 1, w_i)P(I_i = 1 \mid p_i) \\ &= (1 - p_i)(1 - e^{-w_i}), \end{aligned} \tag{S1}$$

where p_i and w_i are zero-inflation probability and mean number of fledglings for brood i and estimated with our selected model. Similarly, each panel in Fig. S3 shows the observed number of fledglings (only nonzero observations plotted) and the expected number of fledglings predicted with our selected model for each year. The dots with different colors illustrate the observed number of fledglings from three brood types and the grey line again indicates the nonparametric loess regression with its 95% confidence band (dashed grey lines). The dark curve is the conditional expectation of number of fledglings ($E(Y_i \mid Y_i > 0)$) as a function of w_i estimated with our selected model with associated 95% confidence band (dashed black lines). Specifically, using the law of total expectation, we know that

$$E(Y_i \mid p_i, w_i) = E(Y_i \mid Y_i > 0, w_i)P(Y_i > 0 \mid p_i, w_i) + E(Y_i \mid Y_i = 0, p_i, w_i)P(Y_i = 0 \mid p_i, w_i).$$

Hence

$$\begin{aligned} E(Y_i \mid Y_i > 0, w_i) &= \frac{E(Y_i \mid p_i, w_i)}{P(Y_i > 0 \mid p_i, w_i)} \\ &= \frac{(1 - p_i)w_i}{(1 - p_i)(1 - e^{-w_i})} \\ &= \frac{w_i}{1 - e^{-w_i}}. \end{aligned} \tag{S2}$$

It is worth noting that p_i and w_i in equation (S1) and equation (S2) were calculated conditional on zero

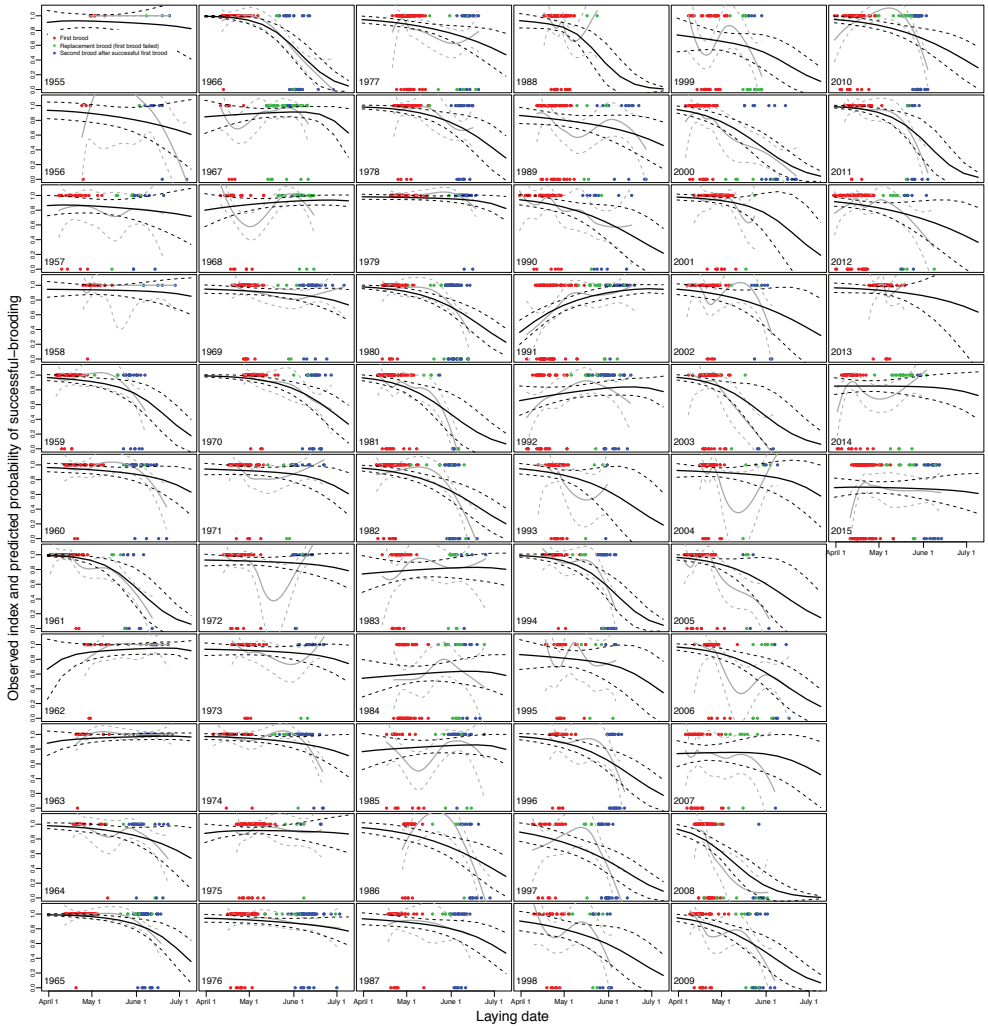

Figure S2: Observed indices and predicted probability of successful-brooding ($P(Y_i > 0 \mid p_i, w_i)$) against the laying date for each year. The blue, red and green dots represent the observed indices of successful-brooding for three different brood types (red dot represents first brood, green dot is replacement brood with first brood failed, and blue dot is second brood with successful first brood). The grey curve is loess regression (with default degree of smoothing = 0.75) through the scatter points with 95% confidence band (dashed grey lines). The black line indicates the probability of successful-brooding predicted with our selected model at laying dates along the whole breeding season and conditional on zero random mother effects and the dashed black lines represent associated 95% confidence band.

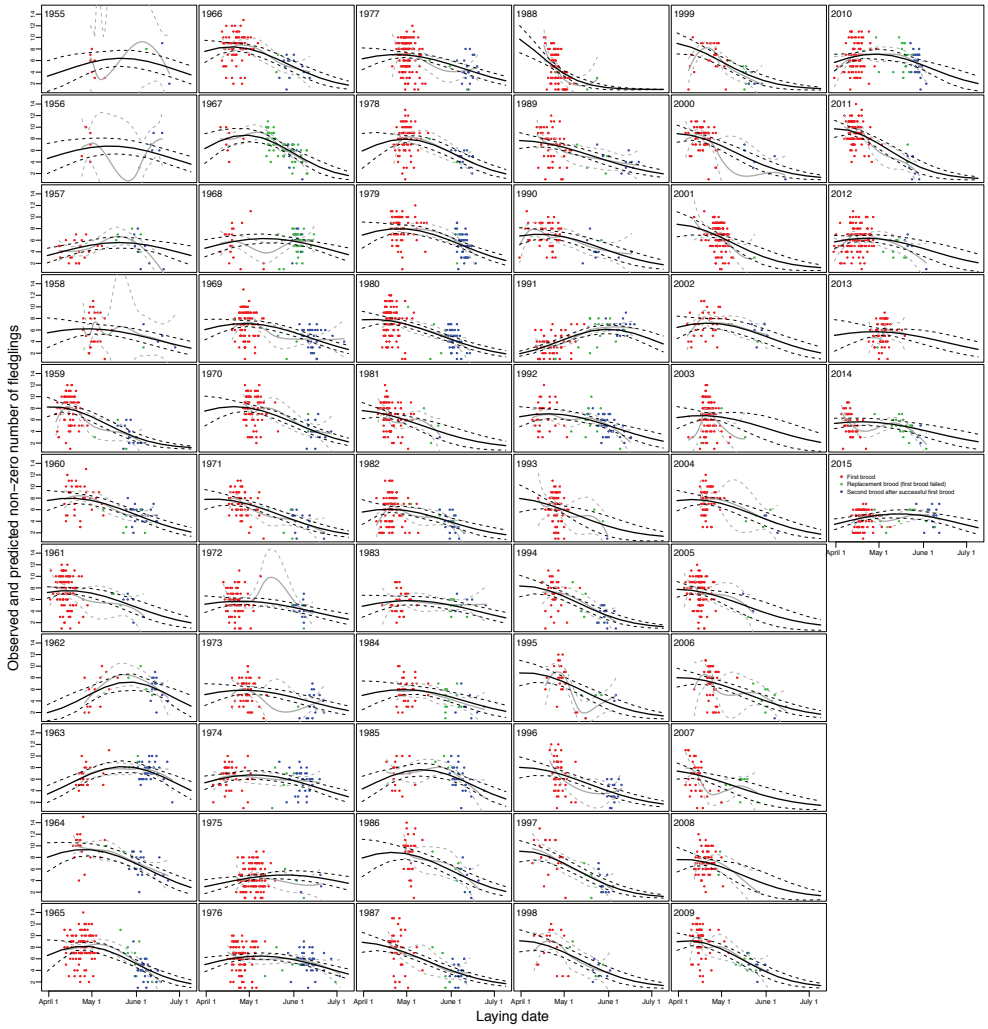

Figure S3: Observed and predicted nonzero number of fledglings ($E(Y_i \mid Y_i > 0, w_i)$) against the laying date for each year. Note that only nonzero number of fledglings are plotted. The blue, red and green dots represent the observed number of fledglings for three different brood types (red dot represents first brood, green dot is replacement brood with first brood failed, and blue dot is second brood with successful first brood). The grey curve is loess regression (with default degree of smoothing = 0.75) through the scatter points with 95% confidence band (dashed grey lines). The black line indicates the number of fledglings predicted with our selected model conditional on zero random mother effects with dashed black lines representing its 95% confidence band.

random mother effects for simplification. From both Fig. S2 and S3 we can see that for most of the years the dark line lies within the 95% confidence band of loess regression, indicating a good fit of our selected model. Moreover, we find from both figures that the replacement broods (first brood failed, green dots) were laid earlier than the second broods (first brood succeed, blue dots). Interestingly, it is hard to see any difference in the probability of successful-brooding between the replacement broods and second broods after successful first broods, but the mean number of fledglings for the second broods after successful first broods are strikingly smaller than that of the replacement broods. This might result from the increasing mistiming between the breeding time and optimal breeding time, and the fitness effects of being mismatched relative to the food peak are stronger at the individual level for the mean number of fledglings compared with the probability of successful-brooding. However, it is interesting to see that for most of the years the second broods suffer higher probability of complete loss than the first broods, as have been discussed in the main text.

Model fitting with partial data

In our study we used the great tit data of 1955-2015 (61 years) from the Hoge Veluwe. However, because a severe storm damaged the pine plantation in the winter of 1972-1973, some of the nest-boxes had to be replaced or relocated. Therefore, some of previous study on HV great tit population treated the HV1 (1955-1972) and HV2 (1973-2004) as two temporally separate populations (see Husby, Kruuk, & Visser, 2009). Other studies only focused on the HV great tit data after 1973 (for example Reed, Jenouvrier, & Visser, 2013; Gamelon et al., 2016). It is of our interest to fit the selected model with the data after 1973 and make a comparison between the estimates with this partial data set and full data set.

Table S2 shows the comparison between the estimates from our selected model with full data (1955-2015, 5892 records) and partial data (1973-2015, 4449 records), and the estimates from the model with fixed ω with partial data. We find from the second and third column that most of the estimates with the full data and with partial data are close to each other, but three differences are worth noting. First, the estimate of $\bar{\theta}$ is smaller (14.95 days) with partial data, which is reasonable and consistent with what can be seen from Fig. S4, where for recent years the estimated optimal laying dates are earlier compared with that in previous years. Second, the estimates of transition ($\phi_{\alpha,\alpha}$ and $\phi_{\theta,\theta}$) are slightly smaller with partial data. At last, the estimates with full data generally have less uncertainty (smaller estimate of standard error). Since the selected model from Chevin et al. (2015) assumed fixed ω_t across the study period from 1973 to 2015, it is interesting to get a flavor that how our result obtained from a candidate model with fixed ω_t and with data after 1973 differ from theirs. The last column in Table S2 therefore lists the estimates of

Table S2: Estimates(standard error) of model parameters from the selected model with full data and partial data, and the model with fixed ω_t and partial data.

Parameter	Estimate(S.E.)		
	Selected model		Model with fixed ω
	Full data	Partial data	Partial data
$\bar{\alpha}$	2.000(0.036)	1.996(0.041)	1.998(0.041)
$\bar{\theta}$	18.227(5.826)	14.950(5.753)	15.841(5.159)
$e^{\bar{\omega}}$ (days)	47.395(3.234)	45.985(3.835)	44.785(2.774)
$\gamma_{\alpha,\alpha}$	0.176(0.024)	0.181(0.031)	0.182(0.029)
$\gamma_{\theta,\theta}$	21.180 (3.422)	18.131(3.330)	19.423(2.838)
$\gamma_{\omega,\omega}$	0.205 (0.049)	0.191(0.056)	NA
$\phi_{\alpha,\alpha}$	0.334(0.122)	0.206(0.173)	0.251(0.161)
$\phi_{\theta,\theta}$	0.524(0.110)	0.386(0.157)	0.338(0.146)
σ_α	0.166(0.023)	0.177(0.032)	0.176(0.029)
σ_θ	18.034(2.808)	16.728(3.095)	18.278(2.694)
σ_ω	0.205(0.049)	0.191(0.056)	NA
$\beta_p^{(0)}$	2.946 (0.220)	2.742(0.233)	2.739(0.234)
$\beta_p^{(1)}$	-0.025(0.005)	-0.028(0.005)	-0.028(0.005)
σ_p^1	0.032(0.004)	0.028(0.004)	0.029(0.005)
ρ_p	-0.827(0.054)	-0.830(0.062)	-0.831(0.061)
β_p^m	0.701(0.092)	0.654(0.103)	0.653(0.103)
β_w^m	0.041(0.013)	0.041(0.016)	0.041(0.016)

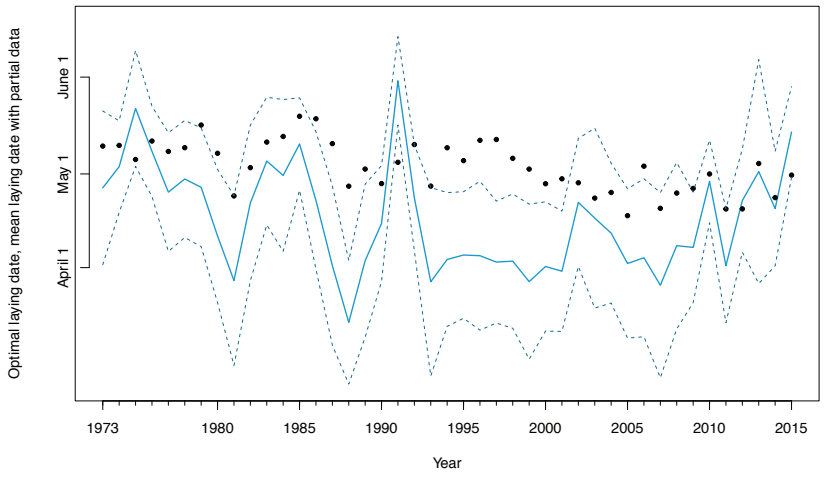

Figure S4: Position of optimal laying date estimated from our selected model with partial data from 1973 to 2015. The estimated movement of optimal laying date from the selected model is shown with solid blue line, along with its 95% confidence interval (dashed blue lines). The black dots are the observed within-year mean laying dates.

parameters in a model with the same formulation as our selected model except for that ω_t is assumed to be constant. We can see that the estimates in the last column are not far from that in the third column and the basic conclusion made from comparison with estimates from Chevin et al. (2015) remain the same, that our result reports larger width of fitness function, larger autocorrelation of the optimum laying dates and larger standard deviation of the fluctuated optimum laying dates.

Fig. S4 shows the movement of optimal laying date estimated from our selected model with partial data from 1973 to 2015. The estimated movement of optimal laying date from the selected model is shown with solid blue line, along with its 95% confidence interval (dashed blue lines). The black dots indicate the observed within-year mean laying dates. The pattern of the optimum movement in Fig. S4 is exactly identical to the movement of optimum in Fig. 2 in the main text from 1973 to 2015. This again implies that the full data set from 1955 to 2015 can be assumed to be generated from the same great tit population without invalidating the general results of our analysis.

Supplementary figures

The estimates of ω_t from our selected model range from 3.47 to 4.04 over the study period, and the corresponding natural exponent e^{ω_t} fluctuates from 32.15 to 56.65 days and the fluctuation can be seen clearly from the top-left plot of Fig. S5, even though the estimate of variance of ω_t is negligible and the candidate model with fixed ω_t does not perform much worse then our selected model. The movement of estimated within-year max fitness α_t (max mean number of fledglings), probability of successful-brooding and mean number of fledglings are shown in the top-right, bottom-left and bottom-right plot respectively, with the colorful lines representing non-parametric local regressions. 1988 is a standing-out year with a narrow width (32.49), large maximum number of fledglings (11.29) and early optimal laying date (14th March), which implies strong stabilizing selection via the mean number of fledglings (episode W) on laying dates. From the bottom plots the good years (1979, for example) with high mean probability of successful-brooding and mean number of fledglings can be differentiated from the bad years (1984, for example). The information obtained from the plots might provide insights for future researches which investigate the potentially abiotic variables driving the selection.

Although our approach offers an advance in the study of phenotypic selection, we believe we have not yet made best use of their full potential. Here, the estimates of random slopes produce order 1 autocorrelation in the annual directional selection as shown in Fig. S6. This implies that our model specification failed to capture the correlation structure of the fluctuated directional selection. While it does not bias the random slopes estimates, the standard deviation of the random slopes tends to be underestimated when the lag 1

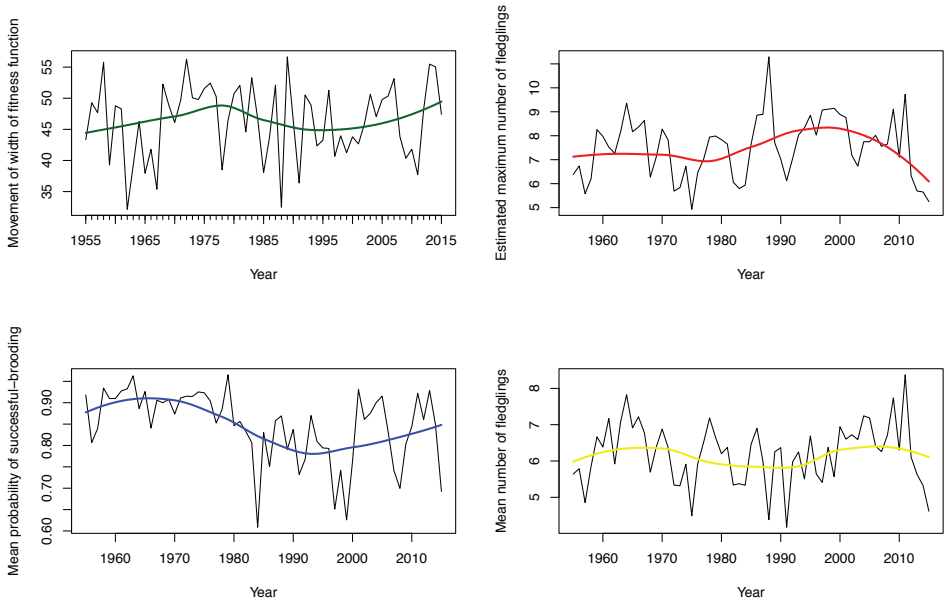

Figure S5: Annual movement of width of fitness function (top-left), maximum fitness (top-right), mean probability of successful-brooding (bottom-left) and mean number of fledglings (bottom-right). The black fluctuated lines are the corresponding estimates from our selected model (the discrete estimates are connected across years) and the colorful lines represent non-parametric local regressions.

autocorrelation of estimates is present.

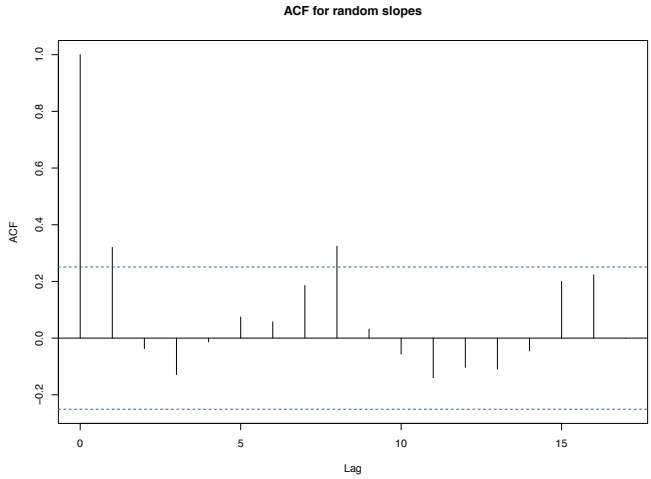

Figure S6: Estimated autocorrelation function of annual random slopes in the selected model for the probability of successful-brooding.

References

Chevin, L.-M., Visser, M. E., & Tufto, J. (2015). Estimating the variation, autocorrelation, and environmental sensitivity of phenotypic selection. *Evolution*, *69*(9), 2319–2332. doi: 10.1111/evo.12741

Fournier, D. A., Skaug, H. J., Ancheta, J., Ianelli, J., Magnusson, A., Maunder, M. N., ... Sibert, J. (2012). AD Model Builder: using automatic differentiation for statistical inference of highly parameterized complex nonlinear models. *Optimization Methods and Software*, *27*(2), 233–249. doi: 10.1080/10556788.2011.597854

Gamelon, M., Grøtan, V., Engen, S., Bjørkvoll, E., Visser, M. E., & Sæther, B. E. (2016). Density dependence in an age-structured population of great tits: Identifying the critical age classes. *Ecology*, *97*(9), 2479–2490. doi: 10.1002/ecy.1442

Harvey, P. H., Greenwood, P. J., & Perrins, C. M. (1979). Breeding Area Fidelity of Great Tits (Parus major). *The Journal of Animal Ecology*, *48*(1), 305.

Husby, A., Kruuk, L. E., & Visser, M. E. (2009). Decline in the frequency and benefits of multiple brooding in great tits as a consequence of a changing environment. *Proceedings of the Royal Society B: Biological Sciences*, *276*(1663), 1845–1854. doi: 10.1098/rspb.2008.1937

Kristensen, K., Nielsen, A., Berg, C. W., Skaug, H., & Bell, B. (2015). TMB: automatic differentiation and Laplace approximation. *arXiv preprint arXiv:1509.00660*. doi: 10.18637/jss.v070.i05

Reed, T. E., Jenouvrier, S., & Visser, M. E. (2013). Phenological mismatch strongly affects individual fitness but not population demography in a woodland passerine. *Journal of Animal Ecology*, *82*(1), 131–144. doi: 10.1111/j.1365-2656.2012.02020.x

Paper II

Evolution of double brooding

Jarle Tufto*†, Yihan Cao*, Marcel E. Visser‡

Thu Jan 30 11:24:02 2020

Abstract

In some populations of birds, females produce a second brood after raising a successful first brood. The proportion of females doing so varies strongly among study populations and years. To understand the adaptive significance of double brooding we consider double brooding jointly with the evolution of onset of breeding in a model with resources limited to a finite window in time. Double versus single brooding is modeled as a threshold character. Onset of breeding and the liability of double brooding follows a binormal phenotypic distribution. Depending on the cost of laying two broods versus one and the delay between the first and second brood relative to the width of the resource window and the phenotypic variance of onset of breeding, the adaptive topography may have single or multiple, purely single- or purely double-brooding adaptive peaks. Despite no frequency-depedence, an adaptive peak at an intermediate frequency of double brooding can exist if double brooding has a sufficiently negative phenotypic correlation with onset of breeding. If the location of the resource windows in time fluctuates between years, double-brooding has an additional adaptive value as a conservative bet-hedging strategy. Climate change, producing a linear trend in the location of the resource window towards earlier dates, may select for a reduced frequency of double brooding. An opposite effect is also possible if the additive genetic covariance between the liability and onset of breeding is negative. Finally, the model is discussed in terms of an empirical example.

*Department of Mathematical Sciences/Centre for Biodiversity Dynamics, Norwegian University of Science and Technology, 7491 Trondheim, Norway.

†Corresponding author. Email:jarle.tufto@ntnu.no

‡Department of Animal Ecology, Netherlands Institute of Ecology (NIOO-KNAW), Post Office Box 50, 6700AB Wageningen, Netherlands

Paper III

Multi-episodic fluctuating selection via fertility and viability in a great tit (*Parus major*) population

Yihan Cao[1], Marcel E. Visser[2], and Jarle Tufto[1]

[1]*Centre for Biodiversity Dynamics, Department of Mathematical Sciences, Norwegian University of Science and Technology, 7491 Trondheim, Norway*
[2]*Department of Animal Ecology, Netherlands Institute of Ecology (NIOO-KNAW), Post Office Box 50, 6700AB Wageningen, Netherlands*

Correspondence
Yihan Cao
E-mail: yihan.cao@ntnu.no

Author contributions
M.E.V. provided the data; J.T. conceived the idea; Y.C. initiated the statistical model, analyzed the data and conducted the analyses; Y.C. wrote the initial draft with input from J.T.; all authors contributed to revisions on later manuscript versions and gave final approval for publication.

Acknowledgments
We warmly thank Marlène Gamelon for her helpful and detailed comments on the initial draft. This work was supported by the Research Council of Norway through its Centres of Excellence funding scheme (project number 223257 to CBD).

Data Accessibility
All the necessary data and source code to carry out the analyses in this study will be available in a Dryad Digital Repository upon publication.

Paper IV

Bayesian inference with tmbstan for a state-space model with VAR(1) state equation

Yihan Cao,* Marcel E. Visser,† Jarle Tufto*

1 Introduction

Both frequentist and Bayesian statistical inference have been used for investigating ecological processes. In the frequentist framework, Template model builder (TMB, Kristensen et al., 2016), an R package developed for fast fitting complex linear or nonlinear mixed models, has gained the popularity recently, especially in the field of ecology which usually involves in modeling complicated ecological processes (for example Cadigan, 2015; Albertsen et al., 2016; Auger-Méthé et al., 2017). The combination of reverse-mode automatic differentiation and Laplace approximation for high-dimension integrals makes parameter estimation with TMB very efficient even for non-Gaussian and complex hierarchical models. TMB provides a flexible framework in model formulation and can be implemented even for statistical models where the predictor is nonlinear in parameters and random effect. However, the lack of capability of working in the Bayesian framework has hindered the adoption of it for Bayesians.

Within the Bayesian framework, the software package *Stan* (Gelman et al., 2015), a probabilistic programming language for statistical inference written in C++ attracts peoples attention. It uses the No-U-Turn Sampler (NUTS) (Hoffman & Gelman, 2014), an adaptive extension to Hamiltonian Monte Carlo (Neal et al., 2011), which itself is a generalization of the familiar Metropolis algorithm, to conduct sampling more efficiently through the posterior distribution by performing multiple steps per iteration. Stan is a valuable tool for many ecologists utilizing Bayesian inference, particularly for problems where BUGS (Lunn et al., 2000) is prohibitively slow (Monnahan et al., 2017). As such, it can extend the boundaries of feasible models for applied problems, leading to a better understanding of ecological processes. Fields that would likely benefit include estimation of individual and population growth rates, meta-analyses and cross-system comparisons, among many others.

Combining the merits of TMB and Stan, the new software package *tmbstan* (Monnahan & Kristensen, 2018) which provides MCMC sampling for TMB models was developed. This package provides ADMB and TMB users a possibility for making Bayesian statistical analysis when prior information on the unknown parameters is available. From the user's perspective, it implements NUTS sampling from a target density proportional to the product of marginal likelihood (computed by TMB or Stan) and the prior density

*Centre for Biodiversity Dynamics, Department of Mathematical Sciences, Norwegian University of Science and Technology, 7491 Trondheim, Norway

†Department of Animal Ecology, Netherlands Institute of Ecology (NIOO-KNAW), Post Office Box 50, 6700AB Wageningen, Netherlands

specified by the user. The user has the flexibility to decide which random effects are integrated out via the Laplace approximation in TMB and then the TMB model is passed to function Stan in the RStan package so that the rest of the parameters are integrated by Stan. This methodology might therefore potentially be more computationally efficient than using MCMC alone to integrate out all parameters. Monnahan and Kristensen (2018) introduced the *tmbstan* package, applied it to simulation studies and compared its capabilities (computational efficiency and the accuracy of Laplace approximation) with other platforms such as ADMB and TMB.

However, it is unclear that if Bayesian inference with arbitrary prior distribution implemented with Stan would perform comparatively with frequentist inference when modeling complex ecological processes. It is also unclear that when using tmbstan, if using the Laplace approximation to integrate latent variables is more computationally efficient than handling all latent variables via MCMC. In the case studies in Monnahan and Kristensen (2018), Laplace approximation turned out to reduce the computational efficiency of MCMC. Another issue arose in the case studies is that the Laplace approximation to the integration of random effects is not accurate to a degree and this could lead to biased parameter estimates or uncertainties in parameter estimation. To gain more insights on these issues, in this paper we conduct simulation studies and a case study in the context of modeling fluctuating and auto-correlated selection with state-space models (SSM). These forms of models are more generally increasingly used in ecology to model time-series such as animal movement paths and population dynamics (for example Cadigan, 2015; Albertsen et al., 2016; Auger-Méthé et al., 2017). Furthermore, following Cao, Visser, and Tufto (2019), we also use order-1 vector autoregressive model (VAR(1)) to model the unobserved states, which in our study are temporally fluctuating and potentially auto-correlated height, width and location of a Gaussian fitness function. This also allows us to make a further investigation into the issue of underestimation of the auto-correlation parameter in auto-regressive models shown in Chevin et al. (2015) and Cao et al. (2019).

Through the simulation and empirical studies, our paper aims to (1) compare estimates between frequentist inference and Bayesian inference under different simulation schemes; (2) investigate how the choice of prior influence Bayesian inference; (3) compare the computational efficiency of MCMC with and without integrating out some of the random effects via Laplace approximation.

2 Methodology

2.1 Model formulation

We consider a typical ecological process, the fluctuating selection in a bird species, the great tit (*Parus major*). We conduct the study in the context of temporally changing selection on the laying date with the number of fledglings as the fitness component, but it can be generalized to any episode of viability or fertility selection, or to overall selection through lifetime fitness. The discrete nonnegative variable, number of fledglings, is best modelled by distributions such as Poisson, or zero-inflated Poisson (for example Chevin et al., 2015; Cao et al., 2019). Within the framework of generalized linear models, the expected value of response variable is commonly linked to the linear predictors of biologically interest by logarithm. When both linear and quadratic effects of the traits are included, this leads to a Gaussian model of stabilizing selection. In this study, the number

of fledglings in a specific brood is assumed to be Poisson distributed, $X_i|w_i \sim \text{Poisson}(w_i)$, where i indicates the breeding event. The fitness (the expected number of fledglings w_i) of individuals with phenotype z_i is then given by

$$\ln w_i = \eta_t^{(\alpha)} - \frac{(z_i - \eta_t^{(\theta)})^2}{2(e^{\eta_t^{(\omega)}})^2}, \tag{1}$$

where $\eta_t^{(\alpha)}$, $\eta_t^{(\theta)}$ and $e^{\eta_t^{(\omega)}}$ (e based to guarantee positive) are parameters determining the logrithm of maximum fitness, optimum laying date and width of the fitness function in year t respectively. We further model $\eta_t^{(\alpha)}$, $\eta_t^{(\theta)}$ and $\eta_t^{(\omega)}$, the three stochastic processes as following:

$$\begin{aligned} \eta_t^{(\alpha)} &= \mu_\alpha + \sigma_\alpha \alpha_t, \\ \eta_t^{(\theta)} &= \mu_\theta + \sigma_\theta \theta_t, \\ \eta_t^{(\omega)} &= \mu_\omega + \sigma_\omega \omega_t. \end{aligned} \tag{2}$$

The elements of vector $\mu = (\mu_\alpha, \mu_\theta, \mu_\omega)^T$ are the means of the three processes. The stochastic processes α_t, θ_t, ω_t are assumed to be multivariate normal distributed $(\alpha_t, \theta_t, \omega_t)^T \sim \mathbf{N}_3(\mathbf{0}, \mathbf{\Gamma_0})$ with $\mathbf{\Gamma_0} = \begin{bmatrix} 1 & \rho_{\alpha,\theta} & \rho_{\alpha,\omega} \\ \rho_{\alpha,\theta} & 1 & \rho_{\theta,\omega} \\ \rho_{\alpha,\omega} & \rho_{\theta,\omega} & 1 \end{bmatrix}$, where $\rho_{\alpha,\theta}$, $\rho_{\alpha,\omega}$ and $\rho_{\theta,\omega}$ indicate the correlations and are assumed to be mutually independent. $(\alpha_t, \theta_t, \omega_t)^T$ are further assumed to follow a first-order vector autoregressive (VAR(1)) process as below:

$$\begin{bmatrix} \alpha_t \\ \theta_t \\ \omega_t \end{bmatrix} = \mathbf{\Phi} \begin{bmatrix} \alpha_{t-1} \\ \theta_{t-1} \\ \omega_{t-1} \end{bmatrix} + \mathbf{w}_t, \tag{3}$$

where $\mathbf{\Phi}$ is 3×3 transition matrix and $\mathbf{w}_t$ is a 3-dimentional vector of white noise. The covariance matrix of $\mathbf{w}_t$ is calculated as $\mathbf{\Gamma_0} - \mathbf{\Phi}\mathbf{\Gamma_0}\mathbf{\Phi}$. Correlations between the elements of $\mathbf{w}_t$ are determined by both $\rho = (\rho_{\alpha,\theta}, \rho_{\alpha,\omega}, \rho_{\theta,\omega})$ and $\mathbf{\Phi}$. If ρ is $\mathbf{0}$ vector and $\mathbf{\Phi}$ is diagonal, then $\mathbf{w}_t$ reduces to be three independent and identically distributed white noise processes. In this case, α_t, θ_t and ω_t simplify to three independent first-order autoregressive (AR(1)) processes. If ρ is $\mathbf{0}$ and all entries of $\mathbf{\Phi}$ are zero, both $(\alpha_t, \theta_t, \omega_t)^T$ and $\mathbf{w}_t$ reduce to three independent and identically distributed white noise processes. In any case, our non-centered parameterization implies that the standard deviation of α_t, θ_t and ω_t is only determined by σ_α, σ_θ and σ_ω respectively. We expect the non-centered parameterization yields simpler posterior geometries (Betancourt & Girolami, 2015) and will be much more efficient in terms of effective sample size when there is not much data (Stan Development Team, 2018b, chapter 20).

It is worth mentioning that one objective of this study is to provide another case study beyond the ones in Monnahan and Kristensen (2018). Therefore, even though α_t, θ_t and ω_t are assumed to be VAR(1) in the model, in the simulation study we consider only AR(1) θ_t and white noise of α_t and ω_t. The alternative simulation studies in which α_t, θ_t and ω_t are formulated as other possible stochastic processes can be conducted similarly and exhaustively, but that is an enormous amount of work in one single study. When α_t, θ_t and ω_t are assumed to be VAR(1), one caution to be taken is that all the eigenvalues of $\mathbf{\Phi}$ must lie in the unit circle to guarantee the VAR (1) process to be stationary (Wei, 2006). At last, in the simulation study, we assume that the model structure is known, which means that we already know θ_t is AR(1) process since the aim of the study is not to explore the structure of the true model.

2.2 Prior distribution

The priors are assumed to be independent to each other $\pi(\mu, \mathbf{\Phi}, \mathbf{\Sigma}) = \pi(\mu)\pi(\mathbf{\Phi})\pi(\mathbf{\Sigma})$. We take a normal $N(\mathbf{m}, q\mathbf{I}_3)$ prior distribution for the process mean vector $\mu = (\mu_\alpha, \mu_\theta, \mu_\omega)$ and input weak prior information on the process mean by taking $\mathbf{m} = \mathbf{0}$ and $q = 100$. Since in this study we assume constant $\eta_t^{(\alpha)}$ and $\eta_t^{(\omega)}$, $\phi_{\theta,\theta}$ is the only non-zero entry in $\mathbf{\Phi}$. We used truncated normal prior on $\phi_{\theta,\theta}$ since it outperforms Jeffreys' prior (Jeffreys & Jeffreys, 1961), g prior (Zellner, 1986) and natural conjugate prior (Schlaifer & Raiffa, 1961) in terms of posterior sensitivity using Highest Posterior Density Region (HPDR) criterion concluded from the simulation study in Karakani et al. (2016). Lei et al. (2011) also uses truncated normal distribution as subjective prior for the auto-regressive parameter in its AR (1) model. The mean and standard deviation of the truncated normal distribution are arbitrarily set to be 0 and 0.5 respectively.

For the variance of the error term σ_θ^2 (σ_α^2 and σ_ω^2 are assumed to be zero), two priors are used:
(1) half-Cauchy (0, 10) prior on σ_θ (Prior1);
(2) lognormal (1, 0.5) prior on σ_θ (Prior2).
These two priors are referred to Prior1 and Prior2 respectively in the rest of this paper. It is worth mentioning that we also tested uniform prior on $log(\sigma_\theta)$ (non-informative improper prior which equals to $1/\sigma$ prior on σ (Gelman et al., 2006)) and inverse-gamma (1, 1) prior on σ_θ^2 (non-informative proper prior, also illustrated in (Gelman et al., 2006)), but both of them render an issue that the sampler traps in a subspace of the whole parameter space of $log(\sigma_\theta)$ and results in numerous divergent transitions. It was potentially caused by the posterior becoming improper and consisting of a mode and an infinite low-posterior-density ridge extending to infinity as illustrated in Tufto et al. (2012). We thus in this study only consider the two proper informative priors (Prior1 and Prior2), while more information on the MCMC with inverse-gamma (1, 1) prior on σ_θ^2 is given in Supporting Information.

Note also that the scale parameters $\log(\sigma_\theta)$ is declared in the TMB template in the logarithmic format, but the half-Cauchy prior and lognormal prior contributed to the total likelihood with the log density in terms of σ_θ and for inverse-gamma prior, it is in terms of σ_θ^2, where σ_θ is a positive transform $\sigma = e^{log\sigma}$. Therefore, Jacobian adjustment (see chapter 20.3 in Stan Development Team (2018b) for Jacobian adjustment) was conducted by adding $log\sigma_\theta$ to the total likelihood when half-Cauchy prior and lognormal prior are used. When testing inverse-gamma prior, it was $\log 2 + 2\log\sigma_\theta$ added to the total likelihood.

2.3 Software implementation

The model is formulated with C++ and passed to TMB for frequentist inference. The model objective (fn) and gradient (gr) functions are fed to optimization function *nlminb* with default setting to optimize the objective function.

For Bayesian inference, the TMB model objective and gradient functions are passed to *tmbstan* which uses the *stan* function and executes the No-U-Turn sampler (NUTS) algorithm by default to sample. Currently the other options are "HMC" (Hamiltonian Monte Carlo), and "Fixed_param". We ran the simulation study on a multicore computing server with enough RAM to avoid swapping to disk. The number of warmup iterations to be excluded when computing the summaries is set to 1000 and for total sample length, it is 3000. We thin each chain to every second sample and set the value

adapt_delta to 0.95, which is the average proposal acceptance probability Stan aims for during the adaption (warmup) period. We set a seed for each simulation including data set and tmbstan to make sure all the simulation results are reproducible.

Divergent transitions during sampling may occur due to a large step size in the sampler or a poorly parameterized model, meaning that the iteration of the MCMC sampler runs into numerical instabilities (Carpenter et al., 2017) and thus inferences will be biased. RStan team suggested that the problem may be alleviated by increasing the adapt_delta parameter (gives a smaller step size), especially when the number of divergent transitions is small (Stan Development Team, 2018a). In our simulation studies, we find it difficult to completely avoid divergent transitions across all data sets even though adapt_delta is increased to 0.95. Similar to Fuglstad, Hem, Knight, Rue, and Riebler (2019), we thus removed simulations where 0.1% or more divergent transitions in the iterations after warmup occur during the inference to avoid reporting biased results.

It is worth mentioning that the execution of Markov chains can be done in parallel. While the default of RStan is to use 1 core, the RStan team recommended to set it to as many processors as the hardware and RAM allow and at most one core per chain (Stan Development Team, 2018a). The simulations we run are done with a server that has 28 available cores. We thus set the number of cores to be 4 for the 4 Markov chains. However, since for frequentist inference, optimization algorithm used in R function "nlminb" makes the best use of all available cores of CPU, we thus only compare the computational efficiency between tmbstan with and without Laplace approximation and ignore the computational efficiency with "nlminb" to ensure fair comparisons.

3 Simulation scheme and results

3.1 Simulation scheme

All the data simulated are in natural units and considered to be biologically realistic according to the empirical studies of natural birds populations (e.g. Grant & Grant, 2002; Vedder et al., 2013). Samples were modeled from a population undergoing stabilizing selection with AR(1) θ_t, fixed $\eta_t^{(\alpha)}$ and $\eta_t^{(\omega)}$. Vector $\mu = (\mu_\alpha, \mu_\theta, \mu_\omega)^T$ is set to $(2, 20, 3.5)$. The autocorrelation $\phi_{\theta,\theta}$ is set to 0.1, 0.4 and 0.7 (only positive values considered since the estimate of auto-correlation in temporal optimal laying date is positive, for example 0.3029 in Chevin et al. (2015) and 0.524 in Cao et al. (2019)), the variance of fluctuating optimal laying date σ_θ is set to 20.

For each value of $\phi_{\theta,\theta}$, $tmax = 25$ or 50 time points were simulated and for each time point the sample size was drawn from a Poisson distribution with mean $n = 25$, 50 or 100 individuals. We considered four combinations of $tmax$ and n, which are $(tmax = 25, n = 50)$, $(tmax = 25, n = 100)$, $(tmax = 50, n = 25)$ and $(tmax = 50, n = 100)$. These four combinations are refered as simulation setting 1, 2, 3, 4 respectively in the following sections. Similar to Cao et al. (2019), we neglected response to selection and used the same normal distribution for simulating individual phenotype each year. The phenotypic standard deviation before selection σ_z was set to 20, such that the strength of stabilizing selection $S = \sigma_z^2/(e^{\eta_t^{(\omega)}})^2 + \sigma_z^2$ (e.g. Chevin et al., 2015) was 0.267. For each individual, its fitness was computed from its phenotype using equation (1), and its actual number of offspring was then drawn from a Poisson distribution with mean $w_t(z)$.

3.2 Frequentist vs. Bayesian estimates

The results of one single simulation obtained from maximum likelihood in the frequentist framework are compared with those from *tmbstan*. The summaries of the estimates with tmbstan are computed after dropping the warmup iterations and merging the draws from all the four chains. The frequentist and Bayesian estimates with different sample sizes and $\phi_{\theta,\theta} = 0.4$ are shown in Table 1, the estimates with other values of auto-correlation in θ_t ($\phi_{\theta,\theta}$ =0.1 and 0.7) can be found in Supporting Information.

From Table 1 we find that both frequentist and Bayesian inferences show good estimates for μ_α and μ_ω. It is interesting to see that the auto-correlation for θ_t is not always under-estimated under all settings (for example ($tmax = 25, n = 50$)), this can be also seen from the tables for parameter estimates in Supporting Information. Bayesian inference with Prior1 (half-Cauchy prior) generally reports smaller estimates of μ_θ than MLE and Prior2 (lognormal prior) but larger estimates of $\phi_{\theta,\theta}$ and $log\sigma_\theta$. The estimates with MLE and Prior2 are close to each other while the estimates with Prior2 show fewer uncertainties for $\phi_{\theta,\theta}$ and $log\sigma_\theta$ implied by the smaller standard errors in the brackets. Prior2 also reports smaller estimates for $log\sigma_\theta$ compared with MLE and Prior1 since it puts very large weight on small values of the variance, as will be graphically demonstrated in section 3.4. We also find that $\phi_{\theta,\theta}$ and $\log \sigma_\theta$ are difficult parameters to estimate since none of these three techniques can estimate them accurately across all the cases. However, the estimates are based on one realization of simulation, the discrepancy between estimates to the true value would vary from simulation to simulation.

We also compare the estimates across the different sample sizes. We typically compare the estimates between setting ($tmax = 25, n = 50$) and ($tmax = 25, n = 100$), ($tmax = 50, n = 25$) and ($tmax = 50, n = 100$), ($tmax = 25, n = 100$) and ($tmax = 50, n = 100$). We find that increasing the mean sample size at each time point does not necessarily increase the certainty of the estimates, but the data set with increased time points ($tmax = 50, n = 100$) contains more information on the parameters of interest and thus reports more certain estimates compared with the data set with ($tmax = 25, n = 100$). The same conclusion can be also drawn by making similar comparisons among the estimates in Table S1 and S2 in Supporting Information.

We can also find from Table 1, Table S1 and S2 from Supporting Information that the Bayesian inference with Prior1 in some cases report 1 or 2 divergent transitions while with Prior2 there are no divergent transitions reported. This implies that the geometric shape of posterior likelihood with Prior1 is more challenging for sampling probably due to light tails and thus potentially leads to an incomplete exploration of the target distribution.

3.3 Bias Plot

The comparison between the estimates in the last section is based on one realization of the simulation. To make comparisons of estimates over more realizations, the simulation was repeated 50 times under the setting of ($tmax = 50, n = 25$). Due to divergent transitions, only 44 out of 50 replicates were kept and the replications with more than 0.1% divergent transitions (in 2000 iterations) were excluded from the analysis. For the estimate of $\phi_{\theta,\theta}$ and $log\sigma_\theta$ in each replication, the bias was calculated in a frequentist framework as the absolute difference between the true value and the mean estimate from each inference technique. The absolute bias for $\phi_{\theta,\theta}$ and $log\sigma_\theta$ are graphically displayed in the upper and lower plot in Fig. 1 respectively. From the upper plot we find that in most replications, Bayesian inference with Prior1 slightly outperforms the frequentist

Table 1: Frequentsit and Bayesian estimates (standard errors) from the model with AR(1) θ_t, autocorrelation in θ_t $\phi_{\theta,\theta} = 0.4$, and different sample sizes ($(tmax = 25, n = 50)$, $(tmax = 25, n = 100)$, $(tmax = 50, n = 25)$ and $(tmax = 50, n = 100)$) from one realization of the simulation. For each sample size setting, the number of divergent transitions in the MCMC is also reported and is used as a measure of stability of the inference scheme. MLE stands for maximum likelihood estimate, Prior1 and Prior2 represent half-Cauchy (0, 10) and lognormal (1, 0.5) prior respectively.

$\phi_{\theta,\theta} = 0.4$, $tmax = 25$, $n = 50$				
Parameters	True value	MLE	Prior1	Prior2
no. divergent transitions	NA	NA	1	0
μ_α	2	2.017(0.015)	2.017(0.015)	2.016(0.015)
μ_θ	20	18.5(3.7)	18.3(5.1)	18.5(3.7)
μ_ω	3.5	3.472(0.028)	3.475(0.028)	3.469(0.028)
$\phi_{\theta,\theta}$	0.4	0.14(0.20)	0.23(0.23)	0.16(0.18)
$log\sigma_\theta$	2.996	2.77(0.15)	2.88(0.19)	2.70(0.14)
$\phi_{\theta,\theta} = 0.4$, $tmax = 25$, $n = 100$				
Parameters	True value	MLE	Prior1	Prior2
no. divergent transitions	NA	NA	2	0
μ_α	2	1.995(0.011)	1.995(0.012)	1.995(0.012)
μ_θ	20	20.2(8.7)	18.3(17.5)	20.1(7.4)
μ_ω	3.5	3.506(0.022)	3.508(0.022)	3.504(0.021)
$\phi_{\theta,\theta}$	0.4	0.50(0.17)	0.59(0.18)	0.46(0.13)
$log\sigma_\theta$	2.996	3.25(0.18)	3.43(0.28)	3.13(0.14)
$\phi_{\theta,\theta} = 0.4$, $tmax = 50$, $n = 25$				
Parameters	True value	MLE	Prior1	Prior2
no. divergent transitions	NA	NA	0	0
μ_α	2	1.974(0.015)	1.974(0.015)	1.973(0.015)
μ_θ	20	20.0(3.8)	19.8(4.9)	20.1(4.2)
μ_ω	3.5	3.520(0.032)	3.523(0.032)	3.515(0.031)
$\phi_{\theta,\theta}$	0.4	0.42(0.14)	0.48(0.15)	0.42(0.13)
$log\sigma_\theta$	2.996	2.84(0.13)	2.92(0.16)	2.79(0.13)
$\phi_{\theta,\theta} = 0.4$, $tmax = 50$, $n = 100$				
Parameters	True value	MLE	Prior1	Prior2
no. divergent transitions	NA	NA	0	0
μ_α	2	1.9865(0.0076)	1.9864(0.0076)	1.9861(0.0076)
μ_θ	20	20.7(3.9)	20.0(5.0)	20.7(4.1)
μ_ω	3.5	3.512(0.015)	3.513(0.015)	3.510(0.015)
$\phi_{\theta,\theta}$	0.4	0.41(0.13)	0.47(0.15)	0.41(0.12)
$log\sigma_\theta$	2.996	2.89(0.12)	2.97(0.17)	2.85(0.11)

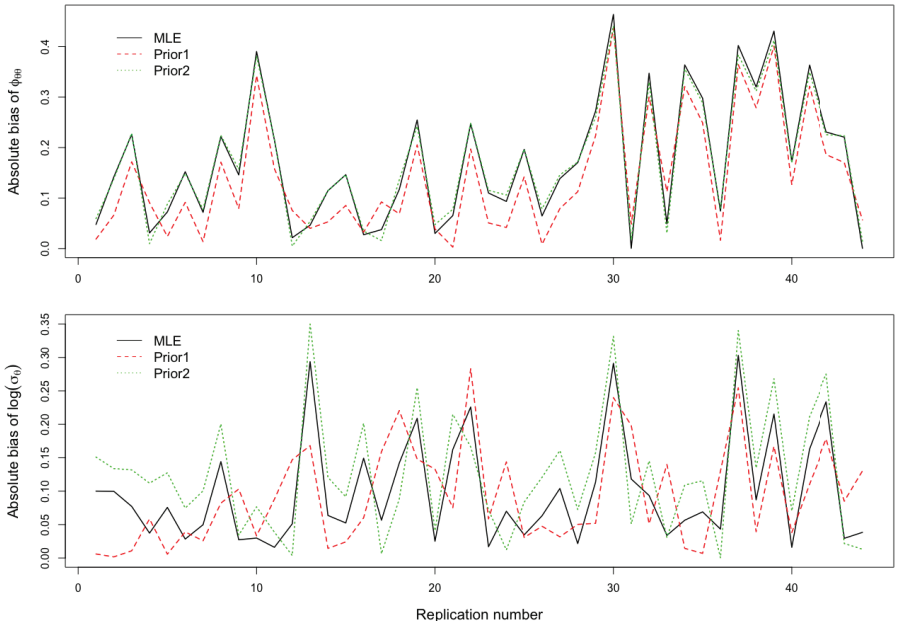

Figure 1: Bias plots for the auto-regressive parameter $\phi_{\theta,\theta}$ (the upper plot) and for the scale parameter logσ_θ (the lower plot) respectively under the setting with time series length $tmax = 50$, average annual sample size $n = 25$, autocorrelation in θ_t $\phi_{\theta,\theta} = 0.4$ and 44 replications (50 replications were conducted, among which 6 replications report 3 or more divergent transitions for the MCMC of Bayesian inference and thus are removed from the analysis).

inference and Bayesian inference with Prior2, the latter two reported very close estimates for $\phi_{\theta,\theta}$. One striking thing is that the bias is close to or even larger than 0.4 for some replications, this suggests that the inferences report even negative estimates of $\phi_{\theta,\theta}$ and it again turns out to be a difficult parameter. In the lower plot, we can see no single inference technique stands out in estimating the scale parameter $log\sigma_\theta$.

3.4 Prior-posterior distribution

Fig. 2 shows histograms of posterior samples of the scale parameter σ_θ from models with the two different prior distributions: half-Cauchy (0, 10) and log-normal (1, 0.5), which are represented by solid lines in the left and right plot on each subplot respectively. The true value of σ_θ is indicated by a solid red line. Plot (a), (b), (c) and (d) correspond to setting $(tmax = 25, n = 50)$, $(tmax = 25, n = 100)$, $(tmax = 50, n = 25)$ and $(tmax = 50, n = 100)$ respectively. We can see from plot (a) that the priors are quite informative and pull the posteriors towards small values away from the true value and this prior-domination is more clear with log-normal prior where the prior distribution sharply peaks at 2. The domination is not mitigated even though the mean annual sample size is increased to 100 as shown in plot (b). With the same total sample size in plot (c) $(tmax = 50, n = 25)$ as that in plot (a) $(tmax = 25, n = 50)$, the posterior likelihoods in plot (c) are, however, not dominated by the priors. The prior-domination is also mitigated in plot (d) compared with plot (b) by increasing the time points from

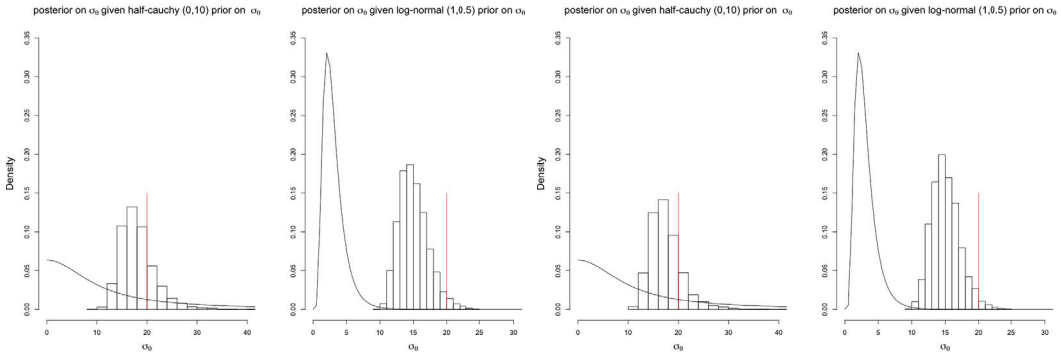

(a) $(tmax = 25, n = 50)$.

(b) $(tmax = 25, n = 100)$.

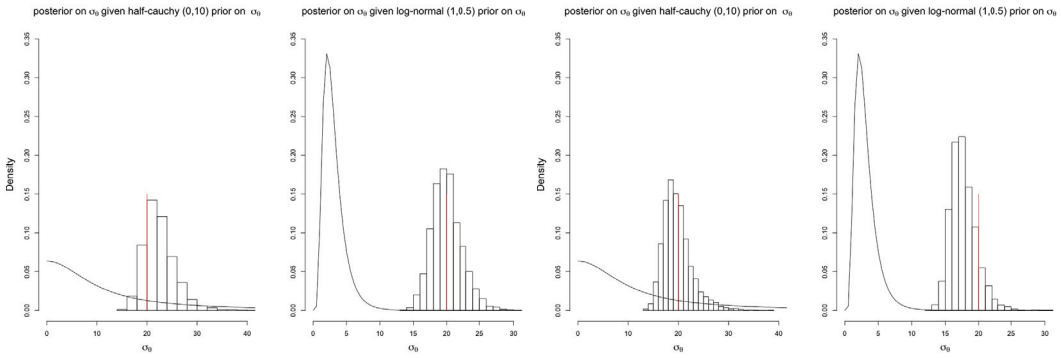

(c) $(tmax = 50, n = 25)$.

(d) $(tmax = 50, n = 100)$.

Figure 2: Histograms of posterior samples of the scale parameter σ_θ from models with two different prior distributions. Plot (a), (b), (c) and (d) correspond to sample size setting $(tmax = 25, n = 50)$, $(tmax = 25, n = 100)$, $(tmax = 50, n = 25)$ and $(tmax = 50, n = 100)$ respectively. On each subplot, the left one shows the histogram of posterior samples given half-Cauchy (0, 10) prior on σ_θ and similarly, the right one displays the histogram of posterior samples given log-normal (1, 0.5) prior on σ_θ. Overlain on each subplot (the solid black lines) is the corresponding prior density function. The red lines indicate the true value of σ_θ. Only $\phi_{\theta,\theta} = 0.4$ was considered in the simulations.

25 to 50.

Altogether, the informative log-normal prior pulls more of the posterior towards a narrower range of smaller parameter values especially when the number of time points in the data is small. The posterior samples are less dominated by the half-Cauchy prior in this case. Increasing the annual mean sample size does not necessarily lead to better identification of the small region of parameter space. Only the amount of time points is the matter for the likelihood to overwhelm the prior distribution and to dominate the posterior distribution.

3.5 Computational efficiency with and without Laplace approximation

In *tmbstan*, sampling can be performed with or without Laplace approximation for the random effects. It is possible to mix the Laplace approximation with MCMC by specifying *laplace=TRUE*, such that the random effects are integrated with the Laplace approximation in TMB and other parameters (such as fixed effects and hyperparameters specifying the distribution of the random effects) are handled by the NUTS in Stan. In the case studies in Monnahan and Kristensen (2018), the Bayesian inference algorithms with Laplace approximation is less computationally efficient than without Laplace approximation, where the efficiency is defined as the minimum effective sample size per second. Following that definition, we calculated the efficiency of tmbstan with and without Laplace approximation with simulated data. Different from Monnahan and Kristensen (2018), we did not consider the computational efficiency of Frequentist inference with the Laplace approximation, as explained in the last section.

In Fig. 3, plot (a) displays violin plots of computational efficiency without (orange) and with (green) Laplace approximation (la) of Bayesian inference with Prior1 under different sample size settings. The setting 1, 2, 3, 4 on x axis stand for setting ($tmax = 25, n = 50$), ($tmax = 25, n = 100$), ($tmax = 50, n = 25$) and ($tmax = 50, n = 100$) respectively. Only $\phi_{\theta,\theta} = 0.4$ was considered and the divergent transitions were not taken into account. Inside the violin plots are box plots showing the quantiles of 50 realized computational efficiencies. Similarly, the violin plots of computational efficiency with Prior2 are shown on plot (b). We find from both plot (a) and (b) that Bayesian inference without Laplace approximation generally is more efficient under setting 1, 2, and 3, the outperformance is more manifest when the sample size is small ($tmax = 25, n = 50$). However, when the sample size is increased to ($tmax = 50, n = 100$), inference with Laplace approximation turns out to be slightly more efficient than that without Laplace approximation, the boxplots and violin plots also tend to be more compact under this setting.

Even though the technique in which the random effects are integrated out by Laplace approximation in TMB turns out to be less efficient in most settings, we still provide a counterexample from Monnahan and Kristensen (2018) in which the enabling of Laplace approximation is always less computationally efficient in the case studies.

3.6 Laplace approximation check

By comparing the Bayesian posteriors with and without Laplace approximation, we are allowed to check how well the Laplace approximation works. Fig. 4 shows pair plots of posterior samples with and without Laplace approximation done by TMB under different sample size settings with Prior2. Only autocorrelation in θ_t $\phi_{\theta,\theta} = 0.4$ was considered.

(a) Computational efficiency with Prior1.

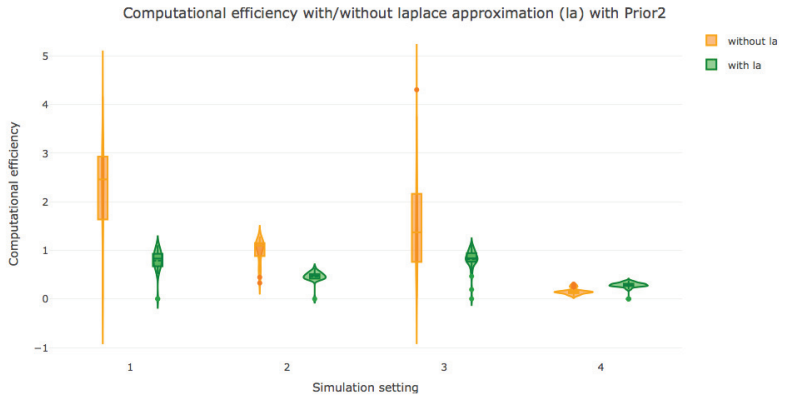

(b) Computational efficiency with Prior2.

Figure 3: Violin plots of computational efficiency (minimum effective sample size per second) without (orange) and with (green) Laplace approximation (la). The four settings on x axis correspond to sample size setting ($tmax = 25, n = 50$), ($tmax = 25, n = 100$), ($tmax = 50, n = 25$) and ($tmax = 50, n = 100$) respectively. Plot (a) shows the computational efficiency of Bayesian inference with Prior1 and plot (b) with Prior2. Only $\phi_{\theta,\theta} = 0.4$ was used in simulations. Inside the violin plots are box plots showing the quantiles of 50 realized computational efficiencies. For each realization among the 50 simulations and across the settings, the same specifications in tmbstan are used.

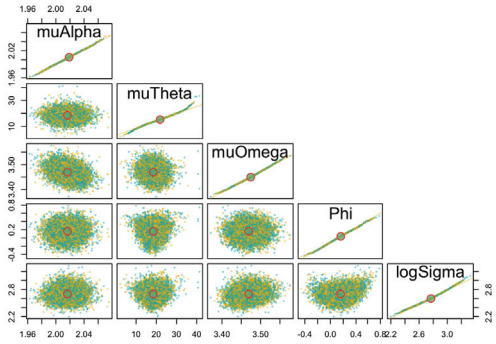

(a) ($tmax = 25, n = 50$) with Prior2.

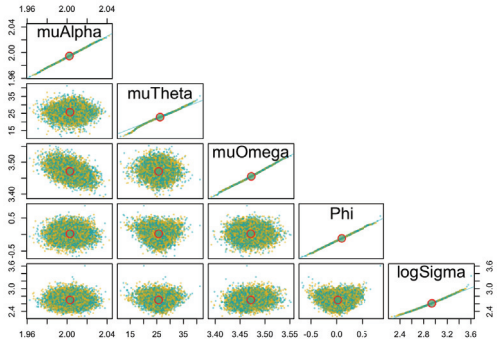

(b) ($tmax = 25, n = 100$) with Prior2.

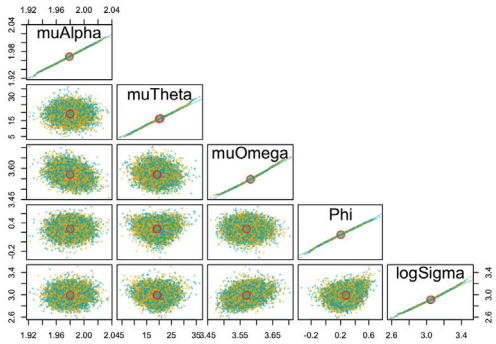

(c) ($tmax = 50, n = 25$) with Prior2.

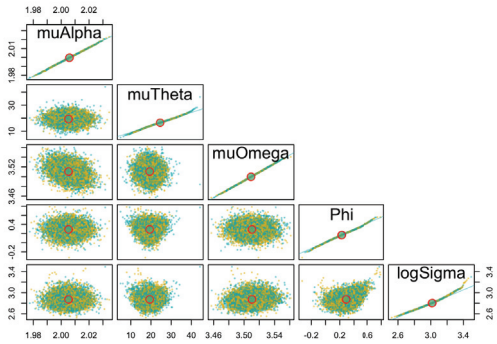

(d) ($tmax = 50, n = 100$) with Prior2.

Figure 4: Pair plots of posterior samples for Laplace approximation check from one realization of the simulation with Prior2. The four plots (a) (b) (c) and (d) correspond to the four settings of sample size in simulation. The random effects in the TMB model can be integrated with two techniques: (1) full MCMC integration via NUTS and (2) Laplace approximation. To check the accuracy of Laplace approximation to the posterior likelihood density, the posterior samples for all the fixed effects in the model without (yellow dots) and with Laplace approximation (green dots) are shown pair-wisely on the same plot. Columns and rows on the lower diagonal correspond to pair-wise parameters, with the diagonal showing QQ-plot of posterior samples from Bayesian inference without (yellow dots) and with (green dots) Laplace approximation for that parameter including a 1:1 line in yellow. The large red circles on the off-diagonal plots represent the pairwise means. On each off-diagonal plot, there are 4000 yellow dots corresponding to 1000 samples retained from each of four chains without Laplace approximation, so as the green dots with Laplace approximation. Posterior rows were randomized to prevent consistent overplotting of one integration technique. Overlaps in the two colored dots suggest that the Laplace approximation is accurate.

Plot (a), (b), (c) and (d) correspond to setting ($tmax = 25, n = 50$), ($tmax = 25, n = 100$), ($tmax = 50, n = 25$) and ($tmax = 50, n = 100$) respectively. On each subplot, the lower diagonal plots contain pairwise parameter posterior points. The green dots represent posterior points from full MCMC integration via NUTS and the yellow points from enabled Laplace approximation of the random effects. The hollow red circles on the off-diagonal plots represent the pairwise means. The diagonal shows QQ-plot of posterior samples from Bayesian inference without (yellow dots) and with (green dots) Laplace approximation for that parameter including a 1:1 line in yellow. Even though the posterior points are densely packed, the overlap of the red circles with each technique shows seemingly good alignment of the two versions of the posterior, and this suggests that the Laplace approximation to the marginal likelihood where random effects are integrated out works well. Similar pair plots for Laplace approximation check with Prior1 can be found in Supporting Information.

4 Real-data case study

Having established the utility of our modeling approach and frequentist and Bayesian inference in the context of simulated data, we also applied the same statistical model to the analysis of a real great tit dataset of practical interest. The observed data were collected from a Dutch great tit (*Parus major*) population at the Hoge Veluwe National Park in the Netherlands (52°02' - 52°07'N, 5°51' - 5°32E). The recorded variables include the number of chicks, number of fledglings, mother ID, brood laying date and so on for each brood. Laying dates are presented as the number of days after March 31 (day 1=April 1, day 31=May 1). Similar to Reed et al. (2013), only the broods with one or more chicks were considered in our analysis due to the high proportion (15.7%) of zero-observations in the number of fledglings among the broods. The number of fledglings was taken as the fitness component and assumed to be Poisson distributed. The analyzed dataset consists of brood records breeding in 61 years from 1955 to 2015 and the sample size in a specific year ranges from 10 to 164 with an average of 81 across the study years. See Reed et al. (2013) for more details on the study population and fieldwork procedures.

The focus of this empirical study is to compare the computational efficiency of Bayesian inference with and without Laplace approximation and to check the accuracy of Laplace approximation. However, since the true structure of the model is unknown, we first conducted model selection under the frequentist framework and the candidate models considered are different from each other only in the model structure of stochastic α_t, θ_t and ω_t. The details of all the candidate models including the best model are given in Supporting Information. We then made Bayesian inference with the two different priors as in the simulation study using the selected model. For each prior distribution, we implemented tmbstan with and without Laplace approximation to check the accuracy of Laplace approximation.

Table 2 lists the reported estimates of model parameters from maximum likelihood (MLE) and Bayesian estimates with half-Cauchy (0, 10) prior (Prior1) and log-normal (1, 0.5) prior (Prior2). The best model indicates VAR(1) structure of α_t and θ_t and non-zero correlation $\hat{\rho}_{\alpha,\theta}$. The width of stabilizing fitness function turned to be constant over the study years implied by zero $\hat{\omega}_t$. Frequentist inference and Bayesian inference with Prior2 report close estimates for $\phi_{\theta,\theta}$ but the estimates with Prior2 show again less uncertainty for most of the estimates except for $\rho_{\alpha,\theta}$. In terms of $\log \sigma_\theta$, Bayesian inference with Prior1

Table 2: Frequentist and Bayesian estimates of parameters in the selected model with great tit dataset. The Bayesian estimates (in column Prior1 and Prior2) are obtained without Lapalace approximation done by TMB.

parameter	**MLE**	**Prior1**	**Prior2**
μ_α	2(0.0369)	2(0.0491)	2(0.0379)
μ_θ	18.5(5.35)	18.8(7.12)	19.4(5.09)
μ_ω	3.88(0.055)	3.89(0.0563)	3.86(0.0522)
$\phi_{\alpha,\alpha}$	0.379(0.12)	0.458(0.13)	0.398(0.124)
$\phi_{\theta,\theta}$	0.48(0.112)	0.545(0.114)	0.477(0.102)
$log\sigma_\alpha$	-1.72(0.14)	-1.63(0.152)	-1.76(0.126)
$log\sigma_\theta$	3.07(0.137)	3.16(0.155)	2.98(0.125)
$\rho_{\alpha,\theta}$	-0.728(0.0825)	-0.715(0.0895)	-0.661(0.0987)

Table 3: Comparison of computational efficiency between Bayesian inference without (in the row "Full MCMC") and with Laplace approximation (in the row "Laplace approximation") for random effects for the great tit case study.

Model	**Inference**	**Time(s)**	**min.ESS**	**Efficiency(ESS/t)**
Prior 1	Full MCMC	1542.215	186.7651	0.1211019
	Laplace approximation	15491.85	1004.643	0.06484975
Prior 2	Full MCMC	1266.096	291.0717	0.229897
	Laplace approximation	7815.218	1111.257	0.1421914

reports the largest estimate and least certainty compared with the other two techniques. The close resemblance between estimates of $\log \sigma_\theta$ based on maximum likelihood and Bayesian inferences suggests that the data contains a good amount of information on $\log \sigma_\theta$ so that the maximum likelihood overwhelms the log-normal prior and dominates the posterior likelihood.

Table 3 shows computational efficiencies of Bayesian inference without and with Laplace approximation. It turns out that the computational efficiency with Laplace approximation is approximately half of that without Laplace approximation in both models with Prior1 and Prior2.

Similar to Fig. 4, Fig. 5 and Fig. 6 display pair plots of posterior samples to check the accuracy of Laplace approximation with Prior1 and Prior2 respectively. Both the figures seemingly suggest a good mix of posterior samples with and without Laplace approximation for all the parameters in the selected model, indicating that the Laplace approximation assumption is met.

5 Conclusions and extensions

In this study, we have investigated frequentist inference and Bayesian inference with two different priors. The inferences were implemented with a state-space model estimating temporal fluctuating selection and with simulated biological data under four different simulation settings. A state-of-the-art R package (tmbstan) for fast fitting statistical models was used for Bayesian inference with Laplace approximation turning on or off. The simulation studies show that the choice of prior can have an important impact on the geometric

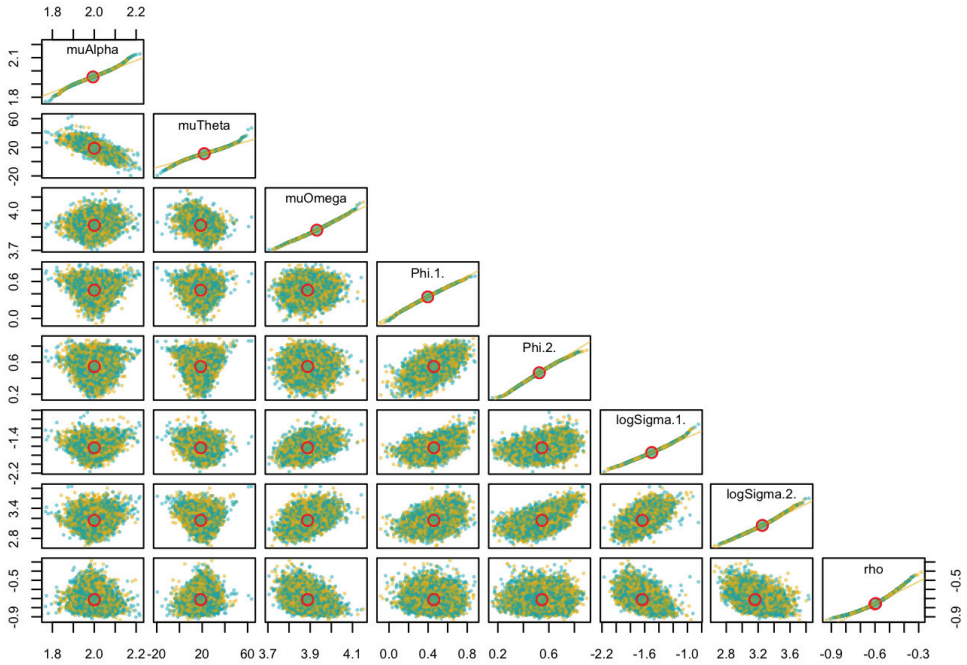

Figure 5: Pair plots of posterior samples for Laplace approximation test for the great tit case study with Prior1. The random effects in the great tit TMB model can be integrated with two techniques: (1) full MCMC integration via NUTS and (2) Laplace approximation. To check the accuracy of Laplace approximation to the posterior likelihood density, the posterior samples for all the fixed effects in the model without (yellow dots) and with Laplace approximation (green dots) are shown pair-wisely on the same plot. Columns and rows on the lower diagonal correspond to pair-wise parameters, with the diagonal showing QQ-plot of posterior samples from Bayesian inference without (yellow dots) and with (green dots) Laplace approximation for that parameter including a 1:1 line in yellow. The large red circles of the off-diagonal plots represent the pairwise means. On each off-diagonal plot, there are 4000 yellow dots corresponding to 1000 samples retained from each of four chains without Laplace approximation, so as the green dots with Laplace approximation. Posterior rows were randomized to prevent consistent overplotting of one integration technique. Overlaps in the two colored dots suggest the Laplace approximation assumption is met.

shape of the posterior distributions of the model parameters and a non-informative prior (in this study uniform prior and inverse-gamma prior on the scale parameter) may lead to unstable inference since the Markov chains may not converge or get stuck in part of the ridge of posterior. With unobserved states following a VAR(1) process, we also found that the autoregressive parameters and the scale parameters in the variance-covariance matrix of the states are difficult and challenging to be estimated accurately. The increased sample size at each time point does not necessarily provide more information for

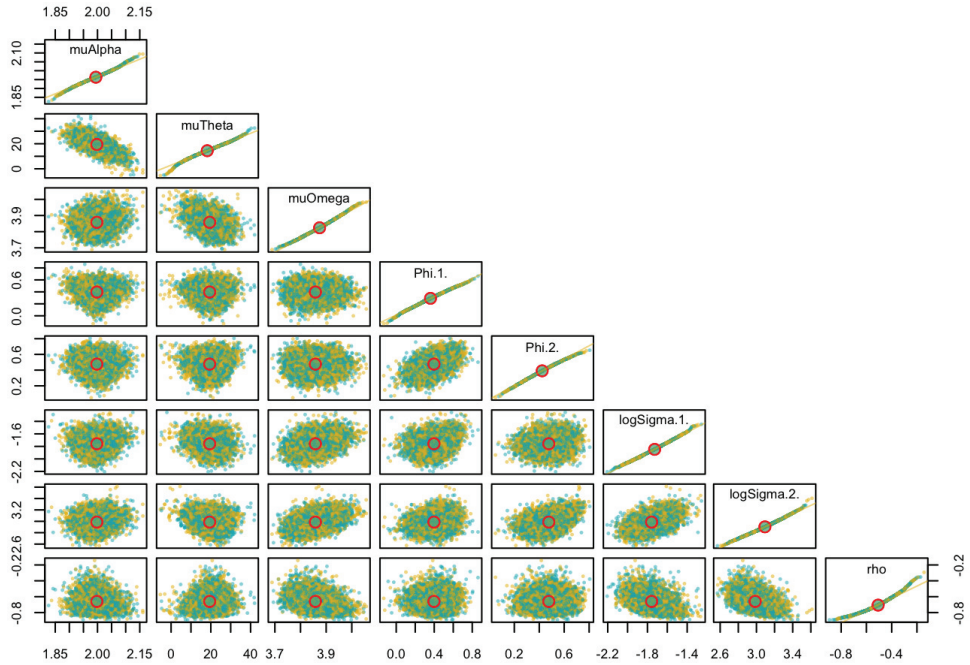

Figure 6: Pair plots of posterior samples for Laplace approximation test for the great tit case study with Prior2. The random effects in the great tit TMB model can be integrated with two techniques: (1) full MCMC integration via NUTS and (2) Laplace approximation. To check the accuracy of Laplace approximation to the posterior likelihood density, the posterior samples for all the fixed effects in the model without (yellow dots) and with Laplace approximation (green dots) are shown pair-wisely on the same plot. Columns and rows on the lower diagonal correspond to pair-wise parameters, with the diagonal showing QQ-plot of posterior samples from Bayesian inference without (yellow dots) and with (green dots) Laplace approximation for that parameter including a 1:1 line in yellow. The large red circles of the off-diagonal plots represent the pairwise means. On each off-diagonal plot, 4000 yellow dots correspond to 1000 samples retained from each of four chains without Laplace approximation, so as the green dots with Laplace approximation. Posterior rows were randomized to prevent consistent overplotting of one integration technique. Overlaps in the two colored dots suggest the Laplace approximation assumption is met.

the transition parameters and scale parameters. Only more time points in the data could make the likelihood dominate the posterior likelihood and thus lead to better estimates of these parameters. Half-Cauchy prior on the scale parameter leads to less stable inference than log-normal prior indicated by the number of divergent transitions in the Markov Chains. Laplace approximation for the random effects turns out to be accurate suggested by the pair plots of the posterior samples with and without Laplace approximation for both the simulation studies and the great tit case study. Turning on Laplace approxi-

mation in tmbstan would probably reduce computational efficiency but it is worth trying when there is a good amount of data, in which case the Laplace approximation is more likely to be accurate and also potentially improve the computational efficiency of MCMC.

In our study, we used arbitrary prior distributions, however, the prior information can be obtained from different sources. For example, in our great tit case study, the timing and width of the caterpillar peak can provide a clue for the time window of optimal laying dates, thus the information can be used to decide the prior for the scale parameter of the optimal laying dates. Prior information can also be generated from previous studies on the same species and more general ecological knowledge coming from other related species (Tufto et al., 2000).

We conducted simulation studies with only AR(1) process of the optimal laying dates, but the model is formulated and coded in a way that can be effortlessly extended to order-1 vector autoregression (VAR(1)). It can be widely used for modeling ecological processes where auto-correlation and cross-correlation in the processes arise due to shared environmental variables at either temporal or spatial scale. We expect more ecologists to adopt these two new estimation methods, TMB, and tmbstan, given its flexibility in either frequentist or Bayesian inference for a wide range of models, including the models where the unobserved ecological processes are treated as latent variables and assumed to be VAR processes. However, the drawback of Bayesian VAR (BVAR) methods is that it usually requires estimation of a large number of parameters and thus the over-parameterization might lead to unstable inference and inaccurate out-of-sample forecasts. Some shrinkage methods (Sims & Zha, 1998; Koop et al., 2010; Giannone et al., 2015; Sørbye & Rue, 2017, for example) were thereby developed, in which Bayesian priors provide a logical and consistent method of imposing parameter restrictions that can be potentially applied to ecological data cases.

References

Albertsen, C. M., Nielsen, A., & Thygesen, U. H. (2016). Choosing the observational likelihood in state-space stock assessment models. *Canadian Journal of Fisheries and Aquatic Sciences*, *74*(5), 779–789.

Auger-Méthé, M., Albertsen, C. M., Jonsen, I. D., Derocher, A. E., Lidgard, D. C., Studholme, K. R., ... Flemming, J. M. (2017). Spatiotemporal modelling of marine movement data using Template Model Builder (TMB). *Marine Ecology Progress Series*, *565*, 237–249.

Betancourt, M., & Girolami, M. (2015). Hamiltonian Monte Carlo for hierarchical models. *Current trends in Bayesian methodology with applications*, *79*, 30.

Cadigan, N. G. (2015). A state-space stock assessment model for northern cod, including under-reported catches and variable natural mortality rates. *Canadian Journal of Fisheries and Aquatic Sciences*, *73*(2), 296–308.

Cao, Y., Visser, M. E., & Tufto, J. (2019). A time-series model for estimating temporal variation in phenotypic selection on laying dates in a dutch great tit population. *Methods in Ecology and Evolution*, *10*(9), 1401–1411.

Carpenter, B., Gelman, A., Hoffman, M. D., Lee, D., Goodrich, B., Betancourt, M., ... Riddell, A. (2017). Stan: A probabilistic programming language. *Journal of statistical software*, *76*(1).

Chevin, L.-M., Visser, M. E., & Tufto, J. (2015). Estimating the variation, autocorrelation, and environmental sensitivity of phenotypic selection. *Evolution*, *69*(9), 2319–2332.

Fuglstad, G.-A., Hem, I. G., Knight, A., Rue, H., & Riebler, A. (2019). Intuitive principle-based priors for attributing variance in additive model structures. *arXiv preprint arXiv:1902.00242*.

Gelman, A., Lee, D., & Guo, J. (2015). Stan: A probabilistic programming language for bayesian inference and optimization. *Journal of Educational and Behavioral Statistics*, *40*(5), 530–543.

Gelman, A., et al. (2006). Prior distributions for variance parameters in hierarchical models (comment on article by Browne and Draper). *Bayesian analysis*, *1*(3), 515–534.

Giannone, D., Lenza, M., & Primiceri, G. E. (2015). Prior selection for vector autoregressions. *Review of Economics and Statistics*, *97*(2), 436–451.

Grant, P. R., & Grant, B. R. (2002). Unpredictable evolution in a 30-year study of Darwin's finches. *science*, *296*(5568), 707–711.

Hoffman, M. D., & Gelman, A. (2014). The No-U-Turn sampler: adaptively setting path lengths in Hamiltonian Monte Carlo. *Journal of Machine Learning Research*, *15*(1), 1593–1623.

Jeffreys, H., & Jeffreys, H. (1961). *Theory of probability (3rd edn)*. Oxford.

Karakani, H. M., van Niekerk, J., & van Staden, P. (2016). Bayesian analysis of AR (1) model. *arXiv preprint arXiv:1611.08747*.

Koop, G., Korobilis, D., et al. (2010). Bayesian multivariate time series methods for empirical macroeconomics. *Foundations and Trends® in Econometrics*, *3*(4), 267–358.

Kristensen, K., Nielsen, A., Berg, C. W., Skaug, H., & Bell, B. M. (2016). TMB: Automatic differentiation and Laplace approximation. *Journal of Statistical Software*, *70*(5), 1–21.

Lei, G., Boys, R., Gillespie, C., Greenall, A., & Wilkinson, D. (2011). Bayesian inference for sparse VAR (1) models, with application to time course microarray data. *Journal of Biometrics and Biostatistics*.

Lunn, D. J., Thomas, A., Best, N., & Spiegelhalter, D. (2000). WinBUGS-a Bayesian modelling framework: concepts, structure, and extensibility. *Statistics and computing*, *10*(4), 325–337.

Monnahan, C. C., & Kristensen, K. (2018). No-U-turn sampling for fast bayesian inference in ADMB and TMB: Introducing the adnuts and tmbstan R packages. *PloS one*, *13*(5), e0197954.

Monnahan, C. C., Thorson, J. T., & Branch, T. A. (2017). Faster estimation of bayesian models in ecology using Hamiltonian Monte Carlo. *Methods in Ecology and Evolution*, *8*(3), 339–348.

Neal, R. M., et al. (2011). MCMC using Hamiltonian dynamics. *Handbook of markov chain monte carlo*, *2*(11), 2.

Reed, T. E., Jenouvrier, S., & Visser, M. E. (2013). Phenological mismatch strongly affects individual fitness but not population demography in a woodland passerine. *Journal of Animal Ecology*, *82*(1), 131–144.

Schlaifer, R., & Raiffa, H. (1961). *Applied statistical decision theory*. Wiley Cambridge.

Sims, C. A., & Zha, T. (1998). Bayesian methods for dynamic multivariate models. *International Economic Review*, 949–968.

Sørbye, S. H., & Rue, H. (2017). Penalised complexity priors for stationary autoregressive processes. *Journal of Time Series Analysis*, *38*(6), 923–935.

Stan Development Team. (2018a). Rstan: the R interface to stan. *R package version 2.17.3*. `http://mc-stan.org`.

Stan Development Team. (2018b). Stan modeling language users guide and reference manual. *Version 2.18.0*. `http://mc-stan.org`.

Tufto, J., Lande, R., Ringsby, T.-H., Engen, S., Sæther, B.-E., Walla, T. R., & DeVries, P. J. (2012). Estimating Brownian motion dispersal rate, longevity and population density from spatially explicit mark–recapture data on tropical butterflies. *Journal of Animal Ecology*, *81*(4), 756–769.

Tufto, J., Sæther, B.-E., Engen, S., Arcese, P., Jerstad, K., Røstad, O. W., & Smith, J. N. (2000). Bayesian meta-analysis of demographic parameters in three small, temperate passerines. *Oikos*, *88*(2), 273–281.

Vedder, O., Bouwhuis, S., & Sheldon, B. C. (2013). Quantitative assessment of the importance of phenotypic plasticity in adaptation to climate change in wild bird populations. *PLoS Biology*, *11*(7), e1001605.

Wei, W. (2006). *Time series analysis: Univariate and multivariate methods* (2nd ed.).

Zellner, A. (1986). On assessing prior distributions and Bayesian regression analysis with g-prior distributions. *Bayesian inference and decision techniques*.

Supporting Information (SI) for

Bayesian inference with tmbstan for a state-space model with VAR(1) state equation

1 Supplementary results of simulation studies

Similar to Table 1 in the main text, we here show the frequentist and Bayesian estimates of the same parameters but with different true values of $\phi_{\theta,\theta}$. Table S1 and Table S2 list the estimates of parameters under different simulation settings with $\phi_{\theta,\theta} = 0.1$ and 0.7 respectively. From these two tables, we find generally similar patterns to the table of estimates in the main text. For example, dataset with more time points ($tmax = 50, n = 100$) leads to more accurate estimates compared with the dataset with shorter time series ($tmax = 25, n = 100$). Increasing the sample size at each time point improves neither the accuracy nor the certainty of the estimates for the parameters of interest, only a bigger sample size is required for this purpose.

In the main text, we only present the pair plots of posterior samples for Laplace approximation check with Prior2. We here supplement the pair plots (Fig. S1) with Prior1 under the four different sample size settings. Fig. S1 also suggests accurate Laplace approximation indicated by the good mix of posterior samples. To further validate this conclusion, we visually inspect the accuracy of Laplace approximation by plotting bivariate contour plots of posterior samples from the Bayesian model with and without Laplace approximation on the same figure, as shown in Fig. S2. Only the joint posterior distribution ($\phi_{\theta,\theta}$ and $\log(\sigma_\theta)$) is considered and other parameters are ignored for simplifying the analysis. The overlap of contours with (yellow) and without (green) Laplace approximation for the random effects suggests again that the Laplace approximation in these cases is accurate.

Table S1: Frequentsit and Bayesian estimates from the model with AR(1) θ_t, autocorrelation in θ_t $\phi_{\theta,\theta} = 0.1$, and different sample sizes.

$\phi_{\theta,\theta} = 0.1$, $tmax = 25$, $n = 50$				
Parameters	True value	MLE	Prior1	Prior2
no. divergent transitions	NA	NA	1	0
μ_α	2	2.006(0.016)	2.005(0.016)	2.006(0.016)
μ_θ	20	19.6(6.4)	19.3(9.3)	19.8(6.1)
μ_ω	3.5	3.475(0.030)	3.479(0.030)	3.472(0.030)
$\phi_{\theta,\theta}$	0.1	0.26(0.19)	0.34(0.22)	0.25(0.16)
$log\sigma_\theta$	2.996	3.21(0.16)	3.34(0.20)	3.11(0.14)
$\phi_{\theta,\theta} = 0.1$, $tmax = 25$, $n = 100$				
Parameters	True value	MLE	Prior1	Prior2
no. divergent transitions	NA	NA	1	0
μ_α	2	1.996(0.010)	1.996(0.010)	1.997(0.010)
μ_θ	20	17.1(3.7)	16.4(5.0)	17.0(3.8)
μ_ω	3.5	3.493(0.021)	3.494(0.022)	3.491(0.022)
$\phi_{\theta,\theta}$	0.1	0.07(0.21)	0.15(0.24)	0.10(0.18)
$log\sigma_\theta$	2.996	2.85(0.15)	2.95(0.18)	2.78(0.13)
$\phi_{\theta,\theta} = 0.1$, $tmax = 50$, $n = 25$				
Parameters	True value	MLE	Prior1	Prior2
no. divergent transitions	NA	NA	0	0
μ_α	2	1.977(0.015)	1.977(0.015)	1.976(0.015)
μ_θ	20	19.8(2.7)	19.7(3.1)	19.9(2.8)
μ_ω	3.5	3.529(0.033)	3.535(0.033)	3.525(0.033)
$\phi_{\theta,\theta}$	0.1	0.04(0.15)	0.07(0.17)	0.06(0.14)
$log\sigma_\theta$	2.996	2.88(0.12)	2.93(0.12)	2.83(0.12)
$\phi_{\theta,\theta} = 0.1$, $tmax = 50$, $n = 100$				
Parameters	True value	MLE	Prior1	Prior2
no. divergent transitions	NA	NA	0	0
μ_α	2	1.9858(0.0076)	1.9857(0.0078)	1.9856(0.0077)
μ_θ	20	20.3(2.8)	20.3(2.9)	20.3(2.9)
μ_ω	3.5	3.515(0.015)	3.515(0.016)	3.513(0.015)
$\phi_{\theta,\theta}$	0.1	0.09(0.14)	0.12(0.16)	0.11(0.14)
$log\sigma_\theta$	2.996	2.89(0.10)	2.93(0.11)	2.86(0.10)

Table S2: Frequentsit and Bayesian estimates from the model with AR(1) θ_t, autocorrelation in θ_t $\phi_{\theta,\theta} = 0.7$, and different sample sizes.

$\phi_{\theta,\theta} = 0.7$, $tmax = 25$, $n = 50$				
Parameters	True value	MLE	Prior1	Prior2
no. divergent transitions	NA	NA	1	0
μ_α	2	2.012(0.015)	2.012(0.015)	2.011(0.014)
μ_θ	20	15.7(4.8)	15.0(8.7)	16.0(5.0)
μ_ω	3.5	3.483(0.031)	3.486(0.031)	3.480(0.031)
$\phi_{\theta,\theta}$	0.7	0.45(0.18)	0.55(0.19)	0.43(0.16)
$log\sigma_\theta$	2.996	2.72(0.18)	2.89(0.27)	2.65(0.16)
$\phi_{\theta,\theta} = 0.7$, $tmax = 25$, $n = 100$				
Parameters	True value	MLE	Prior1	Prior2
no. divergent transitions	NA	NA	NA	0
μ_α	2	1.987(0.011)	1.980(0.014)	1.986(0.011)
μ_θ	20	18.3(9.7)	20(18)	18.4(8.1)
μ_ω	3.5	3.539(0.022)	3.566(0.049)	3.537(0.022)
$\phi_{\theta,\theta}$	0.7	0.70(0.13)	0.60(0.35)	0.63(0.11)
$log\sigma_\theta$	2.996	3.10(0.23)	3.36(0.29)	2.95(0.16)
$\phi_{\theta,\theta} = 0.7$, $tmax = 50$, $n = 25$				
Parameters	True value	MLE	Prior1	Prior2
no. divergent transitions	NA	NA	1	0
μ_α	2	2.021(0.016)	2.021(0.016)	2.021(0.016)
μ_θ	20	19.3(8.9)	20(14)	19.7(7.8)
μ_ω	3.5	3.488(0.031)	3.490(0.030)	3.482(0.030)
$\phi_{\theta,\theta}$	0.7	0.739(0.094)	0.781(0.091)	0.692(0.081)
$log\sigma_\theta$	2.996	3.24(0.18)	3.39(0.25)	3.13(0.14)
$\phi_{\theta,\theta} = 0.7$, $tmax = 50$, $n = 100$				
Parameters	True value	MLE	Prior1	Prior2
no. divergent transitions	NA	NA	1	0
μ_α	2	1.9899(0.0076)	1.9899(0.0076)	1.9896(0.0075)
μ_θ	20	21.1(6.2)	20(12)	21.6(5.5)
μ_ω	3.5	3.511(0.015)	3.511(0.015)	3.510(0.015)
$\phi_{\theta,\theta}$	0.7	0.71(0.10)	0.76(0.10)	0.667(0.086)
$log\sigma_\theta$	2.996	2.93(0.17)	3.09(0.27)	2.84(0.14)

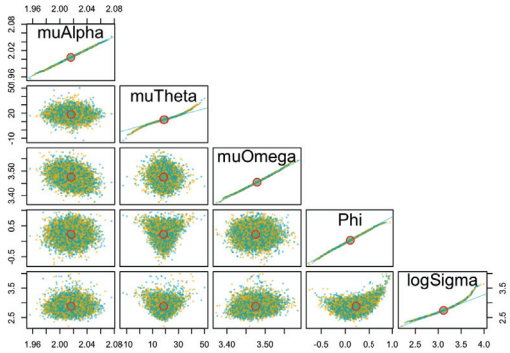

(a) ($tmax = 25, n = 50$) with Prior1.

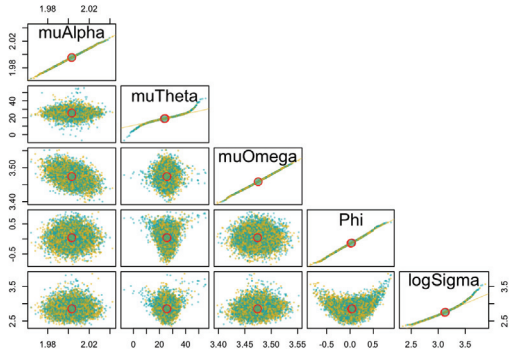

(b) ($tmax = 25, n = 100$) with Prior1.

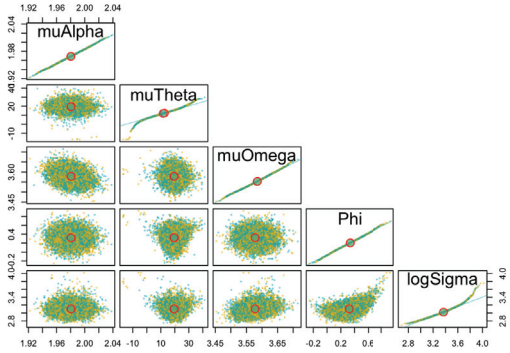

(c) ($tmax = 50, n = 25$) with Prior1.

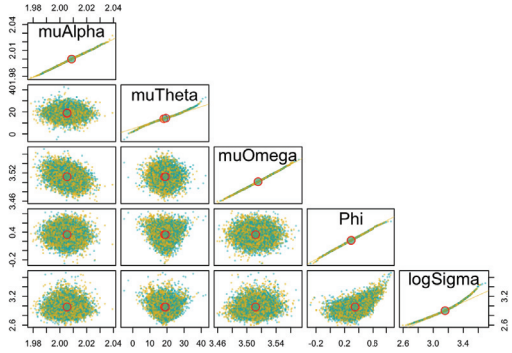

(d) ($tmax = 50, n = 100$) with Prior1.

Figure S1: Pair plots of posterior samples for Laplace approximation check for one realization of the simulation with prior1. The four plots (a), (b), (c), and (d) correspond to the four schemes of simulation. The random effects in the TMB model can be integrated with two techniques: (1) full MCMC integration via NUTS and (2) Laplace approximation. To check the accuracy of Laplace approximation to the posterior likelihood density, the posterior samples for all the fixed effects in the model without (yellow dots) and with Laplace approximation (green dots) are shown pair-wisely on the same plot. Columns and rows on the lower diagonal correspond to pair-wise parameters, with the diagonal showing QQ-plot of posterior samples from Bayesian inference without (yellow dots) and with (green dots) for that parameter including a 1:1 line in yellow. The large red circles of the off-diagonal plots represent the pairwise means. On each off-diagonal plot, there are 4000 yellow dots corresponding to 1000 samples retained from each of four chains without Laplace approximation, so as to the green dots with Laplace approximation. Posterior rows were randomized to prevent consistent overplotting of one integration technique. Overlaps in the two colored dots suggest the Laplace approximation assumption is met.

Prior1

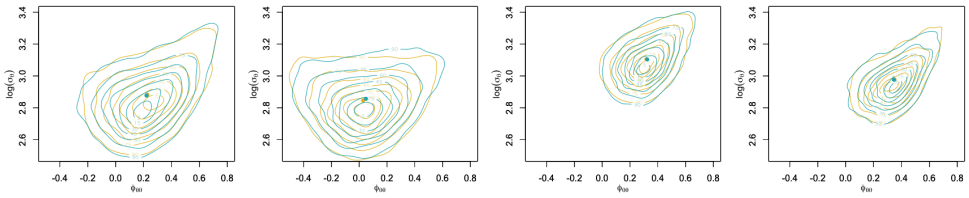

(a) $(tmax = 25, n = 50)$ **(b)** $(tmax = 25, n = 100)$ **(c)** $(tmax = 50, n = 25)$ **(d)** $(tmax = 50, n = 100)$

Prior2

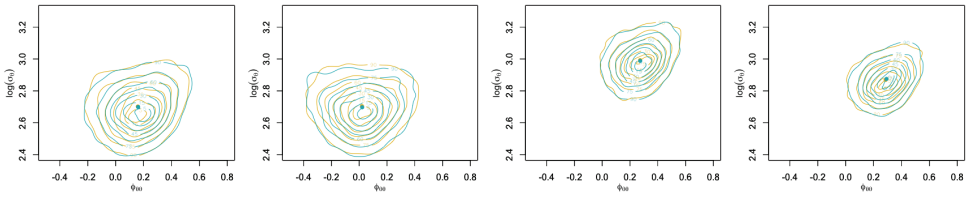

(e) $(tmax = 25, n = 50)$ **(f)** $(tmax = 25, n = 100)$ **(g)** $(tmax = 50, n = 25)$ **(h)** $(tmax = 50, n = 100)$

Figure S2: Bivariate contour plots of posterior samples of $\phi_{\theta,\theta}$ and $\log(\sigma_\theta)$ from one realization of the simulation with Prior1 (the first row) and Prior2 (the second row) for Laplace approximation check. The posterior samples data used are the same as that in Fig. S1 and Figure 4 in the main text. The yellow contours indicate the joint posterior distribution of ($\phi_{\theta,\theta}$, $\log(\sigma_\theta)$) from the estimation technique full MCMC integration via NUTS, and the green contours correspond to the technique that Laplace approximation is used. The yellow and green dots in each plot represent the mean of the bivariate posterior samples in each setting respectively.

Table S3: Model selection for the real data case study. The table lists all the candidate models fitted with the great tit data. Model 7 is selected as the best model due to the smallest AIC value. Column Δp and ΔAIC lists the difference between the selected model and the corresponding candidate model in the number of parameters and reported AIC value respectively. The rightmost column describes the candidate models. The elements in matrix $\mathbf{\Phi}$ and vector ρ are set to 0 if not otherwise specified.

Model	Δp	ΔAIC	Description
1	-5	821.51	$\alpha_t = \theta_t = \omega_t = 0$
2	-4	295.07	$\theta_t = \omega_t = 0$, random α_t
3	-3	34.81	$\omega_t = 0$, random α_t and θ_t
4	-2	176.51	random α_t, θ_t and ω_t
5	-4	265.32	$\alpha_t = \omega_t = 0$, random θ_t
6	2	2.52	$\omega_t = 0$, VAR(1) α_t and θ_t: $\phi_{\alpha,\alpha} \neq \phi_{\theta,\theta} \neq \phi_{\alpha,\theta} \neq \phi_{\theta,\alpha} \neq 0$, $\rho_{\alpha,\theta} \neq 0$
7 (best model)	0	0	$\omega_t = 0$, AR(1) α_t and AR(1) θ_t: $\phi_{\alpha,\alpha} \neq \phi_{\theta,\theta} \neq 0$
8	1	1.92	$\omega_t = 0$, VAR(1) α_t and θ_t: $\phi_{\alpha,\alpha} \neq \phi_{\theta,\theta} \neq \phi_{\theta,\alpha} \neq 0$, $\rho_{\alpha,\theta} \neq 0$
9	1	1.21	$\omega_t = 0$, VAR(1) α_t and θ_t: $\phi_{\alpha,\alpha} \neq \phi_{\theta,\theta} \neq \phi_{\alpha,\theta} \neq 0$, $\rho_{\alpha,\theta} \neq 0$
10	-1	12.93	$\omega_t = 0$, random θ_t, AR(1) α_t: $\phi_{\alpha,\alpha} \neq 0$
11	-1	6.7	$\omega_t = 0$, random α_t, AR(1) θ_t: $\phi_{\theta,\theta} \neq 0$

2 Supplementary info on real data case study

Beside half-Cauchy and lognormal priors for the scale parameters of the great tit model as shown in the main text, we also tested inverse-gamma (1, 1) prior for the scale parameter σ_α^2 and σ_θ^2. To visualize MCMC diagnostics we show trace plots for the two scale parameters along with the prior densities in Fig. S3. The solid black line in plot (a) shows prior density function of σ_α (or σ_θ) given a Inverse-gamma (1, 1) prior density on σ_α^2 (or σ_θ^2). The details on density function transformation are omitted here. The solid red line indicates the density mode. The prior density mode of σ_α at 0.71 translates to density mode of logσ_α at -0.34. However, the left trace plot in plot (b) for logσ_α implies that the posterior likelihood is dominated by the prior so that the sampler gets trapped in the subspace of the parameter, which is a space near -0.34, while the true posterior density mode locates around -1.7.

As mentioned in the main text, the great tit model implemented with Bayesian inference was selected in the frequentist framework with model selection procedure. Table S3 lists all the candidate models fitted with the great tit data. Model 7 is selected as the best model due to the smallest AIC value reported. Colomun Δp and ΔAIC lists the difference between the selected model and the corresponding candidate model in the number of parameters and reported AIC value respectively. The rightmost column describes the candidate models.

We also plot the contours of posterior samples with and without Laplace approximation for a subset

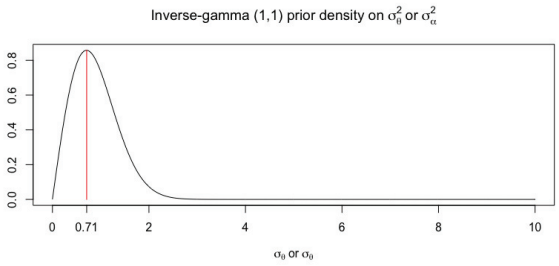

(a) Prior density function on σ_α or σ_θ given Inverse-gamma (1, 1) prior on σ_α^2 or σ_θ^2 respectively.

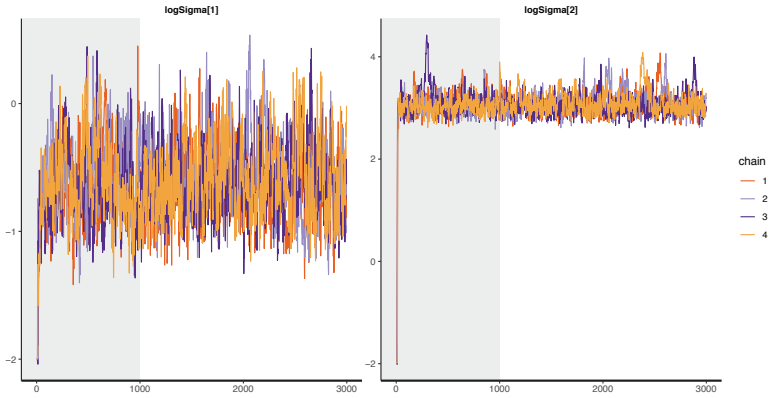

(b) Trace plots for $log\sigma_\alpha$ (left) and for $log\sigma_\theta$ (right).

Figure S3: A prior density and trace plots for the great tit case study. In plot (a), the solid curve indicates an equivalence of the density to inverse-gamma (1, 1) prior on σ_α^2 or σ_θ^2, the equivalent density on σ_α or σ_θ is calculated with rules of density function transformation, which is omitted here. The red solid line indicates the density mode. Plot (b) shows trace plots with the inverse-gamma (1,1) priors for parameter σ_α^2 (left) and σ_θ^2 (right) respectively. The grey areas indicate warm-up iterations.

(a) Bivariate contour plots with Prior1.

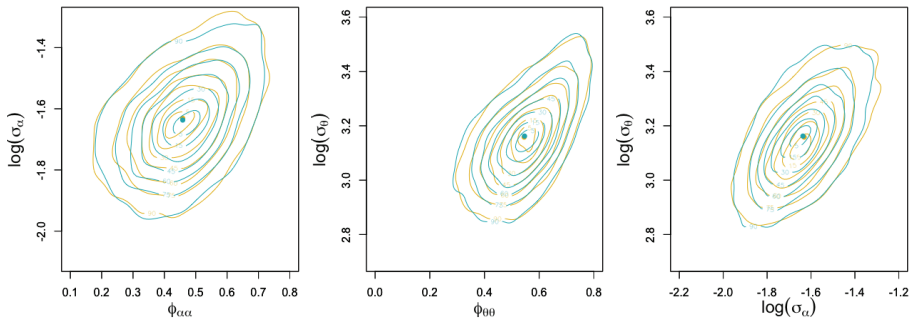

(b) Bivariate contour plots with Prior2.

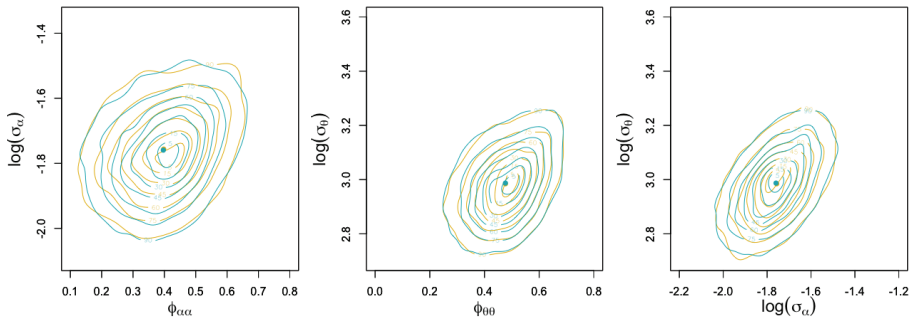

Figure S4: Bivariate contour plots of posterior samples of a subset of the parameters in the selected great tit model for Laplace approximation check. The posterior samples used here are the same as that in Figure 5 and Figure 6 in the main text. The plots in row (a) correspond to the Bayesian model with Prior1, and in row (b) they are with Prior2. Similar to Fig. S2, the yellow contours indicate the joint posterior distribution of the parameters from the estimation technique full MCMC integration via NUTS, and the green contours correspond to the technique that Laplace approximation is used. The yellow and green dots in each plot again represent the mean of the bivariate posterior samples in each plot respectively. Only a subset of the parameters is considered for simplification.

of parameters in the great tit model on the same graph (Fig. S4), to get a clearer visualization of the posteriors' distribution. The first and second row of the contour plots corresponds to the Bayesian great tit model with Prior1 and Prior2 respectively. The round dots on the plots are the mean of posterior samples for each estimation technique. The good amount of overlap of the yellow contours, dots (without Laplace approximation), and green contours, dots (with Laplace approximation) again suggests a good accuracy of Laplace approximation.